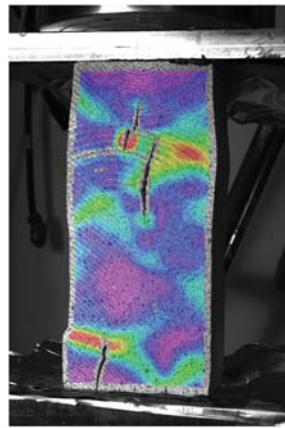
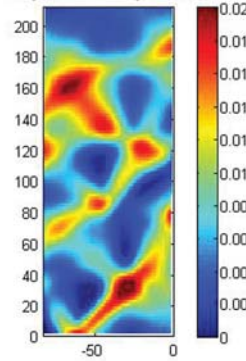




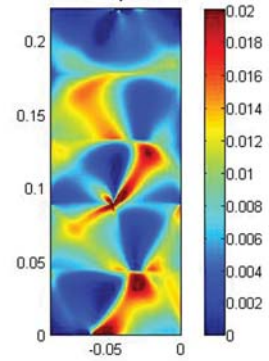
LUND
UNIVERSITY



Experiment Epsilon x



Model Epsilon x



INFLUENCE OF ANNUAL RING ORIENTATION ON COMPRESSION STRENGTH PERPENDICULAR TO GRAIN IN GLULAM

PHILIP WALLIN

Structural
Mechanics

Master's Dissertation

DEPARTMENT OF CONSTRUCTION SCIENCES
DIVISION OF STRUCTURAL MECHANICS

ISRN LUTVDG/TVSM--15/5203--SE (1-104) | ISSN 0281-6679

MASTER'S DISSERTATION

INFLUENCE OF ANNUAL RING ORIENTATION ON COMPRESSION STRENGTH PERPENDICULAR TO GRAIN IN GLULAM

PHILIP WALLIN

Supervisors: Professor **ERIK SERRANO**, Div. of Structural Mechanics, LTH, Lund and
HENRIK DANIELSSON, PhD, Div. of Structural Mechanics, LTH, Lund / Limträteknik AB.
Examiner: Professor **PER JOHAN GUSTAFSSON**, Div. of Structural Mechanics, LTH, Lund.

Copyright © 2015 Division of Structural Mechanics
Faculty of Engineering (LTH), Lund University, Sweden.
Printed by Media-Tryck LU, Lund, Sweden, June 2015 (*PI*).

For information, address:
Div. of Structural Mechanics, LTH, Lund University, Box 118, SE-221 00 Lund, Sweden.
Homepage: <http://www.byggmek.lth.se>

Abstract

This thesis presents an analysis of glued laminated timber (glulam) when loaded in compression perpendicular to the grain. Both theoretical and experimental investigations have been carried out. The main focus was related to the growth ring patterns of the laminations and their influence on the stresses, the strains and the failure mode.

The theoretical part of the work consisted of creating a linear elastic finite element model in 2D of glulam when loaded in compression perpendicular to the grain. Stress and strain plots created by the model were analyzed and the influence of different annual ring patterns were investigated. Considering compression perpendicular to the grain, a common failure mode of the cross section is cracking due to tension perpendicular to the loading direction. The pattern and the curvature of the annual rings have a large impact on this fracture mode. The model shall be able to predict where in the cross section the first crack initiates.

The model was verified by experimental work. Three different geometries of glulam were tested in compression perpendicular to the grain. Measurements of the deformations in the cross sections of the samples were carried out with Digital Image Correlation, DIC. The DIC equipment measured the displacements in 3D of spots in the cross section. A random pattern, called “Speckle pattern”, was created on the cross sectional surface in order to create the spots which the DIC equipment measures. The displacements were computed into strains and the strains were plotted over the surface of the test specimen.

The strain plots from the DIC have been compared to the strain plots computed by the finite element model. The main focus relate to the distribution of the strains and how these seem to be affected by the annual ring pattern.

Sammanfattning

I denna avhandling presenteras en teoretisk och experimentell analys av limträ belastat i tryck vinkelrätt fiberriktningen. Analysen är inriktad mot årsringarnas krökning och orientering i lamellerna och deras inverkan på spänningar, töjningar och brottmoder.

Den teoretiska delen i arbetet var att skapa en linjärelastisk finita element modell i 2D av limträ i tryck vinkelrätt fiberriktningen. De beräknade spänningarna och töjningarna analyserades och påverkan från årsringarnas krökning och orientering undersöktes. En brottmod för limträ i tryck vinkelrätt fiberriktningen är uppsprickning i tvärsnittet. Denna uppsprickning påverkas till stor del av årsringarnas orientering och krökning i de olika lamellerna. Modellen ska kunna beräkna var i limträtvärsnittet som första sprickan uppstår.

Modellens riktighet verifierades med provningar. Tre olika geometrier av limträ testades för tryck vinkelrätt fiberriktningen. Mätningar av deformationerna i tvärsnittsytan hos provkropparna utfördes med Digital Image Correlation, DIC. DIC- utrustningen uppmätte förskjutningen i 3D av punkter i tvärsnittet. Med ett så kallat "speckle mönster" skapades ett slumpässigt mönster för att DIC utrustningen skulle kunna urskilja olika mätpunkter. Förskjutningarna räknades sedan om till töjningar och en töjningsplot över tvärsnittet skapades.

Töjningsplotar från DIC jämfördes med töjningsplotar från finita element modellen. Jämförelsen var främst avseende fördelningen av töjningarna och hur dessa påverkades av årsringarna.

Notations

D	Constitutive matrix in the global coordinate system.
<i>R</i>	Radial direction.
<i>T</i>	Tangential direction.
<i>L</i>	Longitudinal direction.
C	Material compliance matrix.
<i>E</i>	Young's modulus (modulus of elasticity).
G	Transformation matrix 3D.
<i>x</i>	x-direction in global coordinate system.
<i>y</i>	y-direction in global coordinate system.
<i>z</i>	z-direction in global coordinate system.
f	Load vector.
<i>t</i>	Thickness.
t	Traction vector.
b	Body force.
v	Arbitrary weight function.
u	Displacement vector.
N	Element shape functions.
a	Nodal point displacements.
S	Stress tensor.

\mathbf{n}	unit normal vector.
\mathbf{K}	Stiffness matrix.
\mathbf{f}_b	Boundary vector.
\mathbf{f}_l	Load vector.
$f_{c,90}$	Compressive strength perpendicular to the grain
$E_{c,90}$	Modulus of elasticity perpendicular to the grain
$F_{c,90,max}$	Maximum load level
$F_{c,90,max,est}$	Estimated value of maximum load level
h_0	Gauge length
$k_{c,90}$	Increase factor in Eurocode 5
\mathcal{L}_h	Part of the boundary \mathcal{L}
\mathcal{L}_g	Part of the boundary \mathcal{L}
$\sigma_{c,90,d}$	Design compressive stress
ε	Strain vector.
\mathcal{L}	Boundary of surface.
γ	Shear strain.
ν	Poisson's ratio.
σ	Stress vector.
φ	Angle in polar coordinate system.
τ	Shear stress.

$\tilde{\square}$	Denotes quantity in local coordinate system.
$\tilde{\nabla}$	Matrix differential operator.
$\mathbf{0}$	Zero vector.
∂	partial derivative.
\int_V	Integration over volume.
\int_S	Integration over surface.
\int_A	Integration over area.
$\oint_{\mathcal{L}}$	Integration over boundary \mathcal{L} .
$\int_{\mathcal{L}_h}$	Integration over boundary \mathcal{L}_h
$\int_{\mathcal{L}_g}$	Integration over boundary \mathcal{L}_g
\square^T	Transpose.
\square^{-1}	Inverse.

Contents

Abstract	i
Sammanfattning	iii
Notations	v
1 Introduction	1
1.1 Background	1
1.2 Aim	2
1.3 Method	3
1.4 Limitations	4
2 Wood as a construction material	5
2.1 Orthotropy	5
2.2 Glued laminated Timber (Glulam)	6
2.3 Linear Elasticity	7
2.4 Compression perpendicular to the grain in glulam	9
2.5 Strength- and stiffness properties	13
2.6 Norris failure criteria	14
3 Design codes	15
3.1 Determination of some physical and mechanical properties according to EN 408	15
3.2 Comparison of strength properties of Eurocode 5 and BKR	17
3.3 Compression perpendicular to the grain in Eurocode 5	18
4 Laboratory Work	21
4.1 Experimental equipment- Digital Image Correlation (DIC)	21
4.2 Limitations	22
4.3 Implementation	22
4.4 Specimen data	26
5 The finite element method	29
5.1 General	29

5.2	Weak form of two dimensional elasticity	30
5.3	The finite element formulation of two dimensional elasticity	31
5.4	Quadrilateral elements	34
6	Model	35
6.1	Limitations	35
6.2	General	36
6.3	Elements	37
6.4	Loading and boundary conditions	39
6.5	Evaluation of parameters and annual rings	41
7	Results and analysis	43
7.1	Illustration of the laboratory results	43
7.2	Results and analysis	48
7.2.1	Sample 21 - 3 Lamellae	48
7.2.2	Stress- Deformation plot	49
7.2.3	Strains	51
7.2.4	Norris failure criteria	53
7.3	Sample 11 - 4 Lamellae	55
7.3.1	Stress- Deformation plot	56
7.3.2	Strains	57
7.3.3	Norris failure criteria	59
7.4	Sample 16 - 5 Lamellae	61
7.4.1	Stress- Deformation plot	62
7.4.2	Strains	63
7.4.3	Norris failure criteria	65
8	Discussion	67
8.1	Improvements of model	67
8.2	The Eurocodes	67
9	Conclusions	71
	References	73
	Appendices	75
	Appendix A	77
	Appendix B	97
	Appendix C	101

Chapter 1

Introduction

1.1 Background

Wood is the oldest building material and it is still today one of the most common materials used in constructional work. In Sweden, approximately 90 % of all single family houses are built in wood. Since wood is cheap and renewable it has become more popular as a building material in recent years. Today around 20 % of all apartment buildings in Sweden are built with timber frames [24], [25].

Glued laminated timber, glulam, are wood elements constructed by several wood lamellae glued together. Each wood lamella is controlled with respect to strength properties and defects. Glulam has in general greater strength than timber and it can be produced with large cross sections and longer lengths. Glulam is often used in construction of residential buildings, bridges and schools.

In 2011 Eurocode was adopted as a standard in structural design in Sweden. Considering wood, one of the differences between the old Swedish standard “BKR” and the new “Eurocode” is the strength values of glulam loaded in compression perpendicular to the grain. According to BKR, “Boverkets konstruktionsregler”, the characteristic strength of glulam when loaded in compression perpendicular to the grain was 7- 8 MPa. The strength of glulam used in Eurocode, considering the same loading condition, is 2.5 MPa. In Eurocode there is also an increase factor, $k_{c,90}$, which is multiplied by the strength value. This increase factor accounts for influence of support conditions and load distribution effects.

In this thesis, the in-plane distribution of stresses and strains in a glulam cross section loaded perpendicular to the grain will be examined. These distributions are to a large extent influenced by the growth ring pattern of the individual laminations. A finite element model will be created in order to compute the behavior of the stresses and strains in a plane perpendicular to the grain of glulam. The model shall be able to evaluate where the first crack initiates. The accuracy of the model will be confirmed by laboratory work.

1.2 Aim

The aims of this thesis are the following:

- Gain knowledge about wood as an orthotropic building material.
- Create a finite element model, of the cross sectional surface of glulam, that describes the behavior of wood when loaded in compression perpendicular to the grain. The model shall be able to evaluate in which region of the cross section the first crack initiates.
- By experimental work learn about the behavior of stresses and strains in cross sections of glulam when loaded in compression perpendicular to the grain.
- Discuss how well the test standard EN 408 captures the risk of rupture in a cross section of glulam when loaded in compression perpendicular to the grain.

1.3 Method

A literature study is made to gain information of wood as a construction material. The main focus in the literature study is regarding the features of wood when loaded perpendicular to the grain. Knowledge gained from the study is used to decide how to create the FE- model.

The model is created in Matlab as a linear elastic finite element model. The material is considered orthotropic and plane stress is assumed. The input data in the model are the stiffness in radial direction, stiffness in tangential direction, shear stiffness, annual ring pattern, width and height of the cross section and the number of lamellae. All input data can easily be changed to fit different conditions. Quadrilateral elements are used and the strength and the stiffness properties are estimated from previous research work in the field made by others.

In order to validate the model and learn more about the behavior of glulam when loaded in compression perpendicular to the grain, some laboratory work will be carried out. In the experimental work, three different geometries of glulam cross sections will be loaded perpendicular to the grain. The strains in the cross sectional surface will be computed by a DIC equipment. From the DIC equipment the strains computed over the cross section will be exported into Matlab and can be compared to the strains predicted by the model.

The results from the model and the experiments will be used to discuss the approach of designing wood structures loaded in compression perpendicular to the grain in the Eurocodes. The strength values of wood in compression perpendicular to the grain, in EN 408, will also be discussed.

1.4 Limitations

The following limitations apply for the work in this thesis:

- Plane stress is considered in the cross section perpendicular to the grain
- The annual rings are assumed to be cylindrical
- The material is assumed to be homogeneous, i.e. knots, initial cracks, resin pockets etcetera are not taken into consideration.
- The moisture content is assumed to be constant in the whole cross section.
- The material behavior is assumed to be linear elastic up until the first crack occurs.
- The same strength and stiffness properties are used for all lamellae.

Chapter 2

Wood as a construction material

2.1 Orthotropy

Wood is a biological material which is designed to meet the needs of the living tree. The loads acting on a tree are mainly gravity loads and wind loads, giving stress mostly in the direction parallel to the stem. To resist these loads, wood has its greatest strength and stiffness in this direction. The strength and stiffness perpendicular to the longitudinal direction of the stem is much lower [1].

Wood is an anisotropic material with large differences in structural properties related to the three principal directions of the growth. The three principal directions are called the longitudinal direction (L), radial direction (R) and tangential direction (T), see Figure 2.1. The longitudinal direction is parallel to the fibre direction. Both the radial and tangential directions are in a plane of the stem perpendicular to the fibre direction. The radial direction being radial to the annual rings and the tangential direction being tangential to the annual rings [2]. Due to the three directions, all perpendicular to one another, wood can be considered as an orthotropic material.

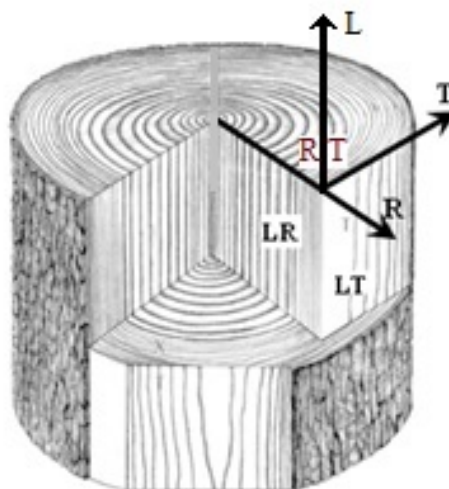


Figure 2.1: Cross-section of log with material principal directions L, R, T [8]

The annual rings can easily be seen in a cross section of a stem. These growth rings occur since the tree is growing with different rates throughout the year. The lighter rings are formed during spring and early summer and are named earlywood. The darker wood is named the latewood and is formed during summer [2]. The properties of wood are related to the longitudinal, radial and tangential directions and the pattern of the annual rings also influences the properties. In the cross section of all wood elements, the radial and tangential directions vary in every point in the cross section because of the curvature of the annual rings. In this thesis the curvature of the annual rings will have a great significance in the modeling of glued laminated timber in compression perpendicular to the fibre direction.

2.2 Glued laminated Timber (Glulam)

Glulam was invented in Germany in the late 19th century. In the early 1900's it came to Sweden. Up until the 1960's, the production of glulam was quite modest, but in the recent decades the production has increased. Most of the glulam in Scandinavia is used for construction of industrial buildings, schools and residential buildings.

Glulam is made of several wood lamellae glued together, see Figure 2.2. The benefits of this technique are several. The lamellae are sorted based on strength grades and the strongest lamellae are placed at the extremities of the beam, where the stresses are generally greatest. Multiple laminated timber sections also minimize the risk of defects ending up together, called homogenisation effect. These properties of glulam makes it stronger than solid timber of the same dimensions and is called the "Laminating effect". Glulam beams can be produced with large spans thanks to its high strength/weight ratio [4]. The size and length of glulam beams are often limited by the transportation capabilities.



Figure 2.2: Cross- section of glulam. Four Lamellae

In practical design situations glulam is normally treated as a homogenous, orthotropic elastic material. Furthermore, it is considered a transverse isotropic material meaning that the fibre direction is in the longitudinal direction and the properties are assumed to be the same in all directions perpendicular to the grain. In the design of glulam structures the consideration of size/volume effects and instability problems are often of greater importance than of ordinary wood elements, as a result of the usually large dimensions. In compression perpendicular to the grain, the different pattern of growth rings in the cross section has a larger influence on the behavior compared to conventional timber [5]. The effect of the curvature of the growth rings on the stresses and strength of a glulam cross section will be studied in more detail in Chapter 2.4.

2.3 Linear Elasticity

For linear elastic materials in three dimensions considering orthotropy with the material directions defined by longitudinal, radial and tangential directions and assuming small strains, the stresses are proportional to the strains according to Hooke's generalized law:

$$\tilde{\boldsymbol{\sigma}} = \tilde{\mathbf{D}}\tilde{\boldsymbol{\varepsilon}} \quad (2.1)$$

where $\tilde{\boldsymbol{\sigma}}$ is the stress vector, $\tilde{\boldsymbol{\varepsilon}}$ is the strain vector and $\tilde{\mathbf{D}}$ is the material stiffness matrix given by:

$$\tilde{\boldsymbol{\sigma}} = [\sigma_{LL} \quad \sigma_{RR} \quad \sigma_{TT} \quad \tau_{LR} \quad \tau_{LT} \quad \tau_{RT}]^T \quad (2.2)$$

$$\tilde{\boldsymbol{\varepsilon}} = [\varepsilon_{LL} \quad \varepsilon_{RR} \quad \varepsilon_{TT} \quad \gamma_{LR} \quad \gamma_{LT} \quad \gamma_{RT}]^T \quad (2.3)$$

$$\tilde{\mathbf{D}} = \tilde{\mathbf{C}}^{-1} \quad (2.4)$$

$$\tilde{\mathbf{C}} = \begin{bmatrix} \frac{1}{E_L} & \frac{-\nu_{RL}}{E_R} & \frac{-\nu_{TL}}{E_T} & 0 & 0 & 0 \\ \frac{-\nu_{LR}}{E_L} & \frac{1}{E_R} & \frac{-\nu_{TR}}{E_T} & 0 & 0 & 0 \\ \frac{-\nu_{LT}}{E_L} & \frac{-\nu_{RT}}{E_R} & \frac{1}{E_T} & 0 & 0 & 0 \\ 0 & 0 & 0 & \frac{1}{G_{LR}} & 0 & 0 \\ 0 & 0 & 0 & 0 & \frac{1}{G_{LT}} & 0 \\ 0 & 0 & 0 & 0 & 0 & \frac{1}{G_{RT}} \end{bmatrix} \quad (2.5)$$

The compliance matrix, $\tilde{\mathbf{C}}$, consists of nine independent coefficients since wood is assumed to be an orthotropic material. The subscript L , R and T refer to the three orthogonal material directions of wood. In the expressions there are three moduli of elasticity, E_i , three moduli of shear, G_{ij} and six Poisson's ratios, ν_{ij} [3]. The first subscript refers to the direction of the applied stress and the second subscript to the direction of the lateral deformation. These expressions are valid for wood when considering the material in its local coordinate system. Hooke's law may also be expressed in a global coordinate system, according to:

$$\boldsymbol{\sigma} = \mathbf{D}\boldsymbol{\varepsilon} \quad (2.6)$$

$$\boldsymbol{\sigma} = [\sigma_{xx} \quad \sigma_{yy} \quad \sigma_{zz} \quad \tau_{xy} \quad \tau_{xz} \quad \tau_{yz}]^T \quad (2.7)$$

$$\boldsymbol{\varepsilon} = [\varepsilon_{xx} \quad \varepsilon_{yy} \quad \varepsilon_{zz} \quad \gamma_{xy} \quad \gamma_{xz} \quad \gamma_{yz}]^T \quad (2.8)$$

Where $\boldsymbol{\sigma}$, $\boldsymbol{\varepsilon}$ and \mathbf{D} are the stress vector, the strain vector and the stiffness matrix respectively. The stress-strain relations in the global- and local coordinate systems are related by the direction

cosines between the respective coordinate axes, a_{local}^{global} . The transformation from local to global directions may be written as:

$$\boldsymbol{\sigma} = \mathbf{G}^T \tilde{\boldsymbol{\sigma}} \quad (2.9)$$

$$\tilde{\boldsymbol{\varepsilon}} = \mathbf{G} \boldsymbol{\varepsilon} \quad (2.10)$$

$$\mathbf{D} = \mathbf{G}^T \tilde{\mathbf{D}} \mathbf{G} \quad (2.11)$$

where \mathbf{G} is the transformation matrix [2]:

$$\mathbf{G} = \begin{bmatrix} a_L^x a_L^x & a_L^y a_L^y & a_L^z a_L^z & a_L^x a_L^y & a_L^z a_L^x & a_L^y a_L^z \\ a_R^x a_R^x & a_R^y a_R^y & a_R^z a_R^z & a_R^x a_R^y & a_R^z a_R^x & a_R^y a_R^z \\ a_T^x a_T^x & a_T^y a_T^y & a_T^z a_T^z & a_T^x a_T^y & a_T^z a_T^x & a_T^y a_T^z \\ 2a_L^x a_R^x & 2a_L^y a_R^y & 2a_L^z a_R^z & a_L^x a_R^y + a_L^y a_R^x & a_L^z a_R^x + a_L^x a_R^z & a_L^y a_R^z + a_L^z a_R^y \\ 2a_T^x a_L^x & 2a_T^y a_L^y & 2a_T^z a_L^z & a_T^x a_L^y + a_T^y a_L^x & a_T^z a_L^x + a_T^x a_L^z & a_T^y a_L^z + a_T^z a_L^y \\ 2a_R^x a_T^x & 2a_R^y a_T^y & 2a_R^z a_T^z & a_R^x a_T^y + a_R^y a_T^x & a_R^z a_T^x + a_R^x a_T^z & a_R^y a_T^z + a_R^z a_T^y \end{bmatrix} \quad (2.12)$$

The assumption of plane stress is common in modeling of wood loaded in compression perpendicular to the grain. In plane stress, the only stress components different from zero are in the same plane. Assuming plane stress in the RT - plane reduces Hooke's law to 2D. Hooke's law then becomes:

$$\tilde{\boldsymbol{\sigma}} = \tilde{\mathbf{D}} \tilde{\boldsymbol{\varepsilon}} \quad (2.13)$$

$$\tilde{\boldsymbol{\sigma}} = [\sigma_{RR} \quad \sigma_{TT} \quad \tau_{RT}]^T \quad (2.14)$$

$$\tilde{\boldsymbol{\varepsilon}} = [\varepsilon_{RR} \quad \varepsilon_{TT} \quad \gamma_{RT}]^T \quad (2.15)$$

$$\tilde{\mathbf{D}} = \tilde{\mathbf{C}}^{-1} \quad (2.16)$$

$$\tilde{\mathbf{C}} = \begin{bmatrix} \frac{1}{E_R} & \frac{-\nu_{TR}}{E_T} & 0 \\ \frac{-\nu_{RT}}{E_R} & \frac{1}{E_T} & 0 \\ 0 & 0 & \frac{1}{G_{RT}} \end{bmatrix} \quad (2.17)$$

In modeling it is assumed that wood behaves as a linear elastic orthotropic material below the yielding point. When the magnitude of the stresses in the material reaches the yielding point the behavior enters the plastic zone and it no longer behaves as a linear elastic orthotropic material.

2.4 Compression perpendicular to the grain in glulam

The analysis of compression perpendicular to the grain is in this thesis carried out with the assumption of plane stress. The mean stiffness in the radial direction is typically 10-15 times lower than the stiffness in the fibre direction. In the tangential direction the stiffness is 1.5-2 times lower than in the radial [9].

In most timber engineering design codes, the difference between radial and tangential stiffness is neglected. According to [9], theoretical investigations show that assuming both the radial and the tangential stiffness in the range of the tangential, neglecting the pattern of the annual rings and assuming plane stress, may lead to extreme mistakes for the in-plane stresses and strains along the depth and width of the cross section when loaded perpendicular to the grain. The reason for the poor results when assuming the in-plane stiffness in the range of the tangential stiffness, is according to [9] a poor approximation of the cylindrical anisotropy. Eurocode 5 uses an increase factor, $k_{e,90}$, which shall take different phenomena into account. One of the main goals of this thesis is to describe the behavior of glulam and estimate the risk of rupture when loaded in compression perpendicular to the grain. It is therefore very essential to take into account the radial and tangential stiffness as well as the heterogeneous orientation of the material directions.

The material directions are given by the pattern of the annual rings in a cross section, see Figure 2.3. Due to this cylindrical shape a rectangular Cartesian coordinate system cannot be used and the material principal directions of wood may instead be defined by a polar coordinate system [9].

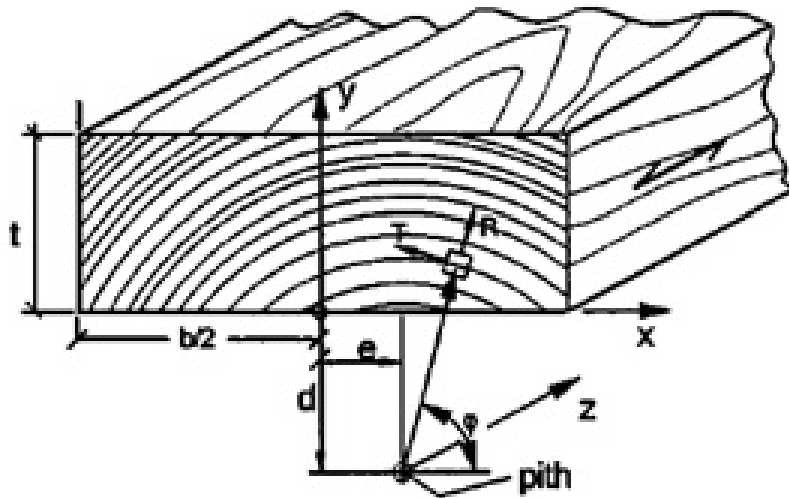


Figure 2.3: Polar coordinate system [11]

The pith location defines the origin of a polar coordinate system. Thus, each lamella has its own coordinate system. Each material point in a lamella is in the polar coordinate system described by the distance from the origin and the angle between the straight line from the origin to the point and the x -axis [14]. In Figure 2.3 this angle is denoted φ . The radial direction in a point expressed in the polar coordinate system has the same direction as the vector from the origin to the specific material point. The tangential direction is perpendicular to the radial direction. For each and every material point the stiffness properties are assumed to be known and the stiffness matrix becomes [10]:

$$\tilde{\mathbf{D}} = \tilde{\mathbf{C}}^{-1} \quad (2.18)$$

Where $\tilde{\mathbf{C}}$ is given in equation (2.17). The transformation from the local coordinate system, i.e. coordinate axes coincide with the material directions, into the global coordinate system can be done by the transformation matrix in equation (2.12), but in two dimensions. In this thesis, transformation matrices stated for plane stress, taking advantage of the relation between the cosine and sine functions, are used. According to [10] these matrices may be written as:

$$\mathbf{A} = \begin{bmatrix} c^2 & s^2 & -2cs \\ s^2 & c^2 & 2cs \\ sc & -sc & c^2 - s^2 \end{bmatrix} \quad (2.19)$$

$$\mathbf{B} = \begin{bmatrix} c^2 & s^2 & -cs \\ s^2 & c^2 & cs \\ 2sc & -2sc & c^2 - s^2 \end{bmatrix} \quad (2.20)$$

where

$$c = \cos(\varphi) \quad (2.21)$$

$$s = \sin(\varphi) \quad (2.22)$$

$$\boldsymbol{\sigma} = \begin{bmatrix} \sigma_{xx} \\ \sigma_{yy} \\ \sigma_{xy} \end{bmatrix} \quad (2.23)$$

$$\tilde{\boldsymbol{\sigma}} = \begin{bmatrix} \sigma_{rr} \\ \sigma_{tt} \\ \sigma_{rt} \end{bmatrix} \quad (2.24)$$

$$\boldsymbol{\varepsilon} = \begin{bmatrix} \varepsilon_{xx} \\ \varepsilon_{yy} \\ \varepsilon_{xy} \end{bmatrix} \quad (2.25)$$

$$\tilde{\boldsymbol{\varepsilon}} = \begin{bmatrix} \varepsilon_{rr} \\ \varepsilon_{tt} \\ \varepsilon_{rt} \end{bmatrix} \quad (2.26)$$

$$\boldsymbol{\sigma} = \mathbf{A}\tilde{\boldsymbol{\sigma}} \quad (2.27)$$

$$\boldsymbol{\varepsilon} = \mathbf{B}\tilde{\boldsymbol{\varepsilon}} \quad (2.28)$$

and

$$\mathbf{C} = \mathbf{B}\tilde{\mathbf{C}}\mathbf{A}^{-1} \quad (2.29)$$

An important feature of the stiffness matrix in the global coordinate system is the so called ‘‘Shear coupling effect’’. For instance, considering the strains, due to the shear coupling effect an applied off-axis uniaxial load in the x -direction leads to, apart from ε_x and ε_y , to shear deformation γ_{xy}

[9]. The shear coupling effect has great impact in the distribution of the stresses and strains in a cross section of wood if the material directions differ significantly from the loading direction [12]. The low value of the shear modulus, G_{RT} , compared to the radial and tangential stiffness is the reason for the strong influence of the shear coupling effect in wood.

Since the difference in tangential and radial stiffness is roughly a factor 2, the contribution of E_T and E_R transformed into the global system is also strongly dependent on the orientation of the annual rings [10]. In a cross section of glulam, for instance Figure 2.2, each lamellae has its own pith. This may result in great differences in the orientation of the annual rings considering the whole cross section. An analysis of the stresses in material directions considering the influence of different width and height of the cross section and varying pattern of growth rings is presented in [13]. In Figure 2.5, the variation in magnitude of the radial and tangential stresses is illustrated for a certain cross section. Figure 2.4 shows the test specimen with six lamellae, double symmetric with respect to geometry and annual ring pattern. In the work by T. Astrup et. al, the glulam cross section was loaded in tension perpendicular to the grain. However because of the assumption of linear elastic behavior, the stress distribution in Figure 2.5 is the same as for compression perpendicular to the grain, if the sign of the stresses is changed. The specimen was glued to stiff steel plates in the upper and lower side and the steel plates were prevented from rotation. An FE-model of the test specimen was created by the FE-program COSMOS.

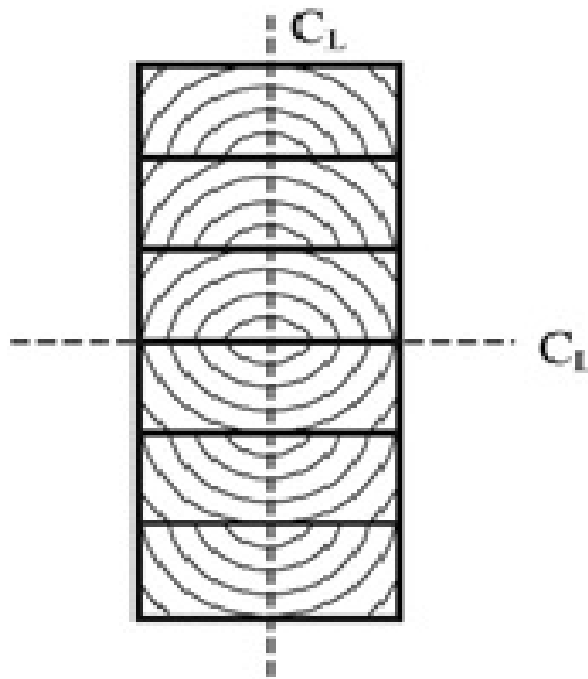


Figure 2.4: Cross section of glulam, double symmetric, exposed to tension perpendicular to the grain [13]

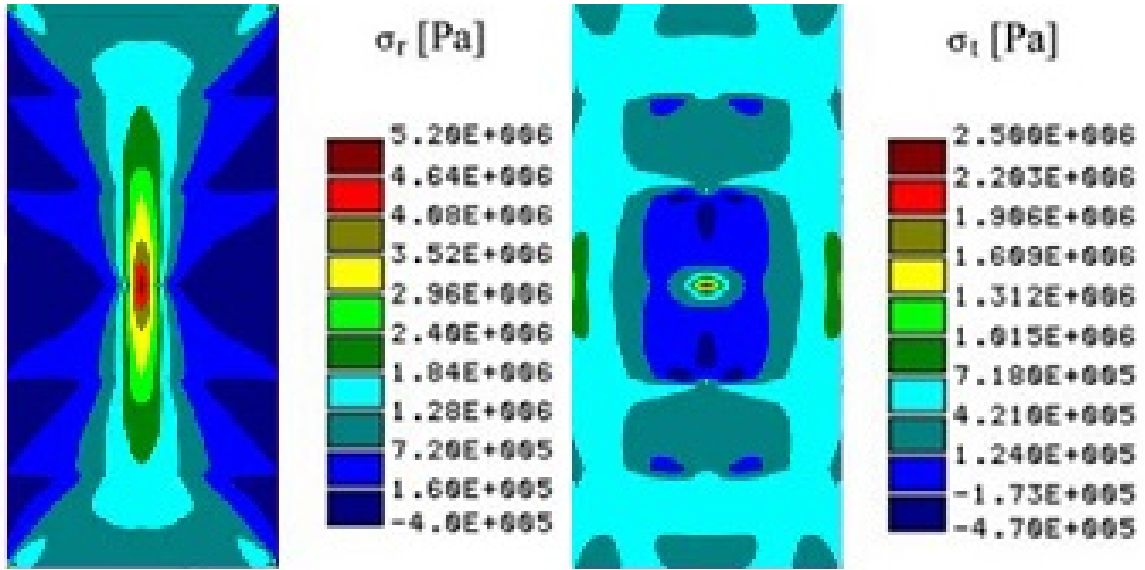


Figure 2.5: Radial stresses (left) and tangential stresses (right), [13]

In Figure 2.5 it should be noted that in a point between the third and fourth lamella the stresses in tension are maximum for the cross section in Figure 2.4 considering tension perpendicular to the grain. The magnitude and location of the maximum stresses in radial and tangential directions depend on the width, number of lamellae and the annual ring pattern [13]. The occurrence of large tensile stresses in the cross section may lead to tensile fracture, i.e. crack initiation and propagation. To determine whether the stresses cause fracture of the material different failure criteria are useful.

2.5 Strength- and stiffness properties

The strength properties of wood are generally depending on the size of the wood specimen. A small piece of clear wood without any natural defects such as knots and cracks has usually higher strength than larger pieces (with knots and cracks). When considering the strength- and the stiffness properties it is therefore important to take the uncertainties regarding the volume effect into account [1]. The influence on strength properties, due to this effect, is however depending upon mode of loading. The variability of the strength of structural timber is greater in tension than compression and in bending the variability is even greater than in pure tension [1].

The stiffness of wood is also dependent on moisture content, temperature, density, angle of load to fibre direction, time under loading, microfibril angle etcetera. Some strength- and stiffness properties for Spruce at 12% moisture content can be seen in Table 2.1 and Table 2.2.

Table 2.1: Strength properties for Spruce at 12 % moisture content in [MPa], [3]

	$f_{t,L}$	$f_{c,L}$	$f_{t,R}$	$f_{c,R}$	$f_{t,T}$	$f_{c,T}$	$f_{v,LR}$	$f_{v,LT}$	$f_{v,RT}$
<i>Norway spruce</i>	63	29	4.9	3.6	2.8	3.8	6.1	4.4	1.6
<i>Spruce</i>	75	50	4.9	7.0			8.6		

Table 2.2: Modulus of Elasticity and Poisson's ratios for Spruce at 12 % moisture content in [MPa], [2]

<i>Spruce</i>	[MPa]
E_L	13500 – 16700
E_R	700 – 900
E_T	400 – 650
G_{LR}	620 – 720
G_{LT}	500 – 850
G_{RT}	29.0 – 39.0
ν_{RL}	0.018 – 0.030
ν_{TL}	0.013 – 0.021
ν_{TR}	0.24 – 0.33

Because of the anisotropy, both the strength and the stiffness properties vary in the three principal directions. In Table 2.1 the first subscripts denotes t for tension, c for compression and v for shear. The second subscripts L , R and T denote the three principal directions of wood. The shear strengths are for the LR , LT and RT planes respectively.

2.6 Norris failure criteria

Commonly used failure criteria for wood are the ones presented by Norris [15]. In three dimensions one of the criteria may be expressed as:

$$\begin{aligned}
 \left(\frac{\sigma_{LL}}{f_{Li}}\right)^2 + \left(\frac{\sigma_{RR}}{f_{Ri}}\right)^2 + \left(\frac{\tau_{LR}}{f_{LR}}\right)^2 - \left(\frac{\sigma_{LL}}{f_{Li}}\right)\left(\frac{\sigma_{RR}}{f_{Ri}}\right) &< 1 \\
 \left(\frac{\sigma_{LL}}{f_{Li}}\right)^2 + \left(\frac{\sigma_{TT}}{f_{Ti}}\right)^2 + \left(\frac{\tau_{LT}}{f_{LT}}\right)^2 - \left(\frac{\sigma_{LL}}{f_{Li}}\right)\left(\frac{\sigma_{TT}}{f_{Ti}}\right) &< 1 \\
 \left(\frac{\sigma_{RR}}{f_{Ri}}\right)^2 + \left(\frac{\sigma_{TT}}{f_{Ti}}\right)^2 + \left(\frac{\tau_{RT}}{f_{RT}}\right)^2 - \left(\frac{\sigma_{RR}}{f_{Ri}}\right)\left(\frac{\sigma_{TT}}{f_{Ti}}\right) &< 1
 \end{aligned} \tag{2.30}$$

Norris failure criteria says that if any of the three functions exceeds 1, failure will occur. In the above equations expressed by Norris in 1962 the letter f denotes the strength properties. The subscripts L , R and T refer to the three principal directions of the material. If the tensile and compression strength differ in the above expression, the equation must be applied in a piecewise manner. In the case of the same magnitude of strength in tension and compression each function expresses a closed ellipsoid in the respective stress spaces with its center in the origin. The three ellipsoids occupy a six dimensional space. Any stress state in the material is represented by a point in this space. If the point representing a certain stress lies within the closed space created by the three ellipsoids the material is assumed not to fail. A point lying on the border of any of the ellipsoids represents a condition of stress which is assumed to lead to failure. For the case of plane stress in the RT-plane, equation (2.30) is reduced to:

$$\left(\frac{\sigma_{RR}}{f_{Ri}}\right)^2 + \left(\frac{\sigma_{TT}}{f_{Ti}}\right)^2 + \left(\frac{\tau_{RT}}{f_{RT}}\right)^2 - \frac{\sigma_{RR}}{f_{Ri}} \frac{\sigma_{TT}}{f_{Ti}} < 1 \tag{2.31}$$

A combined stress state will not lead to failure as long as the point representing the stress state lies within the surface of equation (2.31).

Chapter 3

Design codes

In 2011, Eurocode was adopted as a standard for structural design in Sweden. The Eurocodes are standards in construction works in the EU developed by the European Committee for Standardisation. The Eurocodes were developed with the aim to encourage constructional work between nations in the EU which may lead to lower costs for building projects. A main purpose of the Eurocodes is to ensure a high quality in the design of constructional work [20]. Every nation bound to implement the Eurocodes adapts the standards to fit their own specific conditions such as geology, climate and level of safety. In Chapter 3.1, methods to determine strength in compression perpendicular to the grain according to the European standards are presented.

3.1 Determination of some physical and mechanical properties according to EN 408

Laboratory investigations of different parameters, for instance strength- and stiffness properties, should be carried out by an accredited laboratory. Considering compression perpendicular to the grain and determination of the strength- and stiffness parameters, $f_{c,90}$ and $E_{c,90}$ respectively, the procedure according to the European standard EN 408 is as follows:

- The loaded surfaces shall be prepared to ensure that they are plane, perpendicular to the loading axis and parallel to each other.
- For glulam the test specimen shall have the dimensions given in Table 3.1. Permitted deviation of the values given in Table 3.1 is 1%.

Table 3.1: Dimensions of glulam test specimen

$b \times l$ [mm ²]	b minimum [mm]	h [mm]
25000	100	200

- The load shall be applied perpendicular to the grain and the load axis shall be in the center of the test specimen.
- The loading equipment shall be able to measure the load with an accuracy of 1% in the case of applied load exceeding 10 % of the maximum load.
- After an initial load has been applied, the loading heads shall be locked in order to prevent rotation or angular movement during the test.

- The load shall be applied as a cross head movement with constant rate.
- The estimated maximum compressive load perpendicular to the grain in newtons, $F_{c,90,max,est}$, shall be reached in the range of (300 ± 120) seconds.

The test setup is shown in Figure 3.1. The test specimen is mounted vertically between the compression heads and the load is applied concentrically. The gauge length, h_0 , shall be located centrally in the test specimen and not closer than $b/3$ to the loaded end of the test specimen. h_0 is approximately $0.6h$ and defines the length over which the deformation is measured.

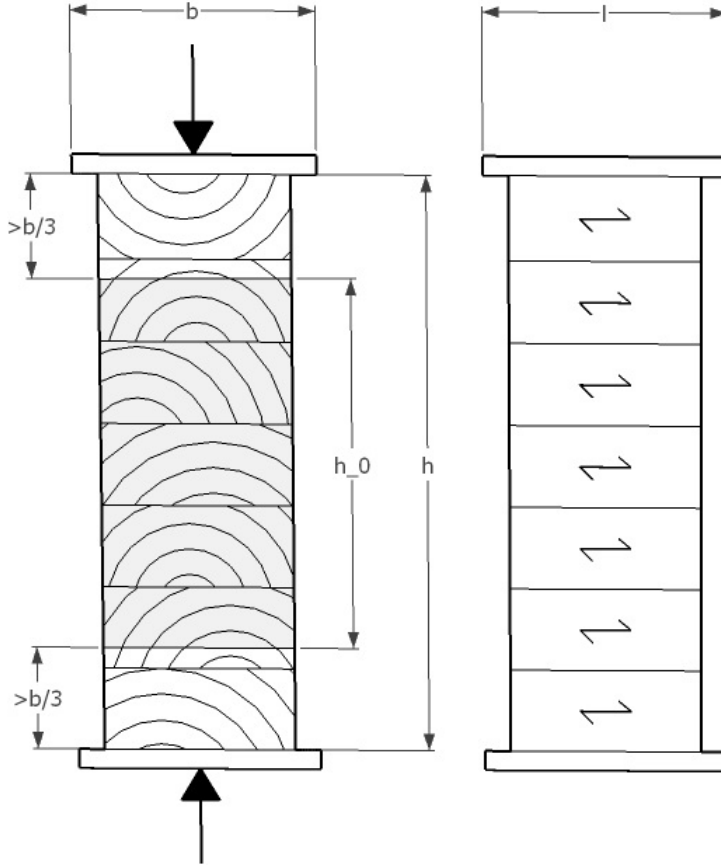


Figure 3.1: Test setup

The compressive strength, $f_{c,90}$, shall be determined according to:

$$f_{c,90} = \frac{F_{c,90,max}}{bl} \quad (3.1)$$

Where b is the width and l is the length of the loaded surface. The maximum load level $F_{c,90,max}$ is determined using an iterative process. First an estimation of $F_{c,90,max}$ is made, the estimated value is called $F_{c,90,max,est}$. Using the test results, plot the load-deformation plot, Figure 3.2. Calculate $0.1F_{c,90,max}$ and $0.4F_{c,90,max}$. Determine where these two values intersect the load-deformation curve. Draw a straight line between the two points, line 1. Line 2 is then drawn parallel to line 1 and through the point defined by $F = 0$ and $0.01h_0$. At the point where line 2 intersects the load-deformation curve the $F_{c,90,max}$ value is found. If the determined value of $F_{c,90,max}$ is within the range of 5% of $F_{c,90,max,est}$ then the value of $F_{c,90,max}$ may be used to determine the compressive strength. Otherwise, the mentioned procedure shall be repeated until $F_{c,90,max}$ is within the tolerance.

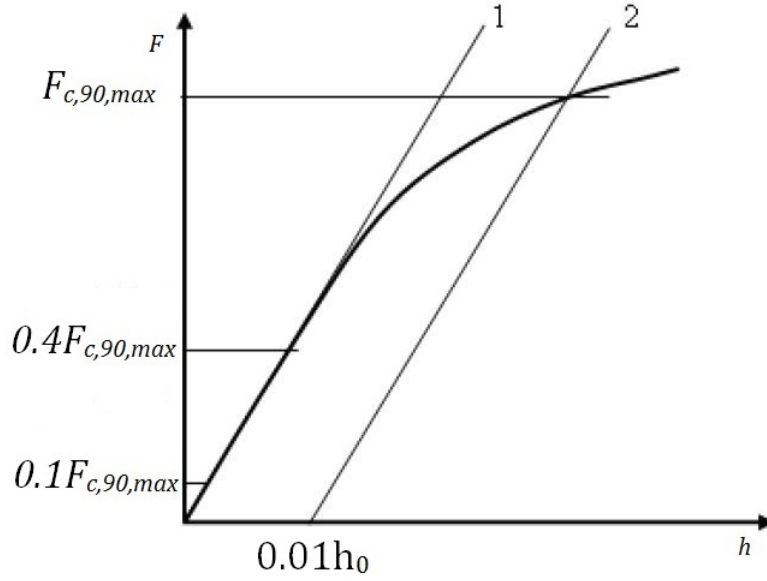


Figure 3.2: Load- deformation curve

The modulus of elasticity, $E_{c,90}$, may then be calculated according to:

$$E_{c,90} = \frac{(F_{40} - F_{10})h_0}{(w_{40} - w_{10})bl} \quad (3.2)$$

$$F_{10} = 0.1F_{c,90,max} \quad (3.3)$$

$$F_{40} = 0.4F_{c,90,max} \quad (3.4)$$

Where w_{10} and w_{40} are the deformations corresponding to the forces F_{10} and F_{40} .

3.2 Comparison of strength properties of Eurocode 5 and BKR

In 1989 Sweden adopted a new design code, called Nybyggnadsregler NR, BFS 1988:18 [22]. Considering compression perpendicular to the grain of solid timber, a new strength value was introduced for all strength classes. The characteristic strength value in compression perpendicular to the grain was increased from 2.0 MPa to 7.0 MPa. As a complement to the new design codes a series of guidance documents, “Byggvägledning, 1990”, were presented. Not until 1998, when BKR 3 (Boverkets konstruktionsregler) was adopted, a new way of calculating the strength value of compression perpendicular to the grain was presented. The new code used a coefficient, k_{c90} , to calculate the strength. The characteristic strength values, regarding compression perpendicular to the grain, were still 7.0 MPa.

In 2011 the latest version of BKR, called BKR 13, was replaced by the Eurocodes. The strength in compression perpendicular to the grain for solid timber and glulam, according to BKR 13 and Eurocode, can be seen in Table 3.2 and Table 3.3. There is a large difference in the strength properties of glulam between BKR 13 and Eurocode.

Table 3.2: Strength in compression perpendicular to the grain according to BKR 13, [MPa]

Solid timber	C24	C27	C30	C35	C40
$f_{c,90,k}$	2.5	2.6	2.7	2.8	2.9
Glulam	LK20	LK30	L30	L40	
$f_{c,90,k}$	7	7	7	8	

Table 3.3: Strength in compression perpendicular to the grain according to EN 338 and EN 14080, [MPa]

Solid timber	C24	C27	C30	C35	C40
$f_{c,90,k}$	2.5	2.6	2.7	2.8	2.9
Glulam (homogeneous)	GL 24h	GL 28h	GL 32h		
$f_{c,90,g,k}$	2.5	2.5	2.5		

3.3 Compression perpendicular to the grain in Eurocode 5

According to Eurocode 5, (EN 1995-1-1:2004), considering compression perpendicular to the grain the following equation shall be fulfilled:

$$\sigma_{c,90,d} \leq k_{c,90} f_{c,90,d} \quad (3.5)$$

Where:

$$\sigma_{c,90,d} = \frac{F_{c,90,d}}{A_{ef}} \quad (3.6)$$

And:

$\sigma_{c,90,d}$ Design compressive stress.

$F_{c,90,d}$ Design compressive force perpendicular to the grain.

A_{ef} Effective contact surface area

$f_{c,90,d}$ Design compression strength perpendicular to the grain.

$k_{c,90}$ Factor taking into account the effects of the load configuration, risk of splitting and the degree of compressive deformation.

Note the subscript $,d$, in equation (3.5) and equation (3.6), indicating that the compressive force, the compressive stress and the compressive strength refer to design values. This means that their values have been modified from characteristic values according to safety factors accounting for duration of load and climate effects.

The effective contact surface, A_{ef} , is calculated as the effective length multiplied by the width of the contact surface. A method to calculate the effective length is by adding 30 mm to the actual length, l , of the wood sample parallel to the grain that is supported [19]. However, the value added to the length, l , may not be larger than a , l or $l_1/2$ see Figure 3.3. By calculating the effective contact surface, a load spreading effect in the grain direction is taken into consideration.

The value of the factor, $k_{c,90}$, shall be taken as 1.0 unless the following conditions are fulfilled:

1. In the case of a member on continuous supports, see Figure 3.3 (a), and $l_1 \geq 2h$ the factor $k_{c,90}$ may be chosen as:
 - $k_{c,90}=1.25$ (Solid Timber)
 - $k_{c,90}=1.5$ (Glulam)
2. In the case of a member on discrete supports, see Figure 3.3 (b), and $l_1 \geq 2h$ the factor $k_{c,90}$ may be chosen as:
 - $k_{c,90}=1.5$ (Solid Timber)
 - $k_{c,90}=1.75$ (Glulam, when $l \leq 400$)

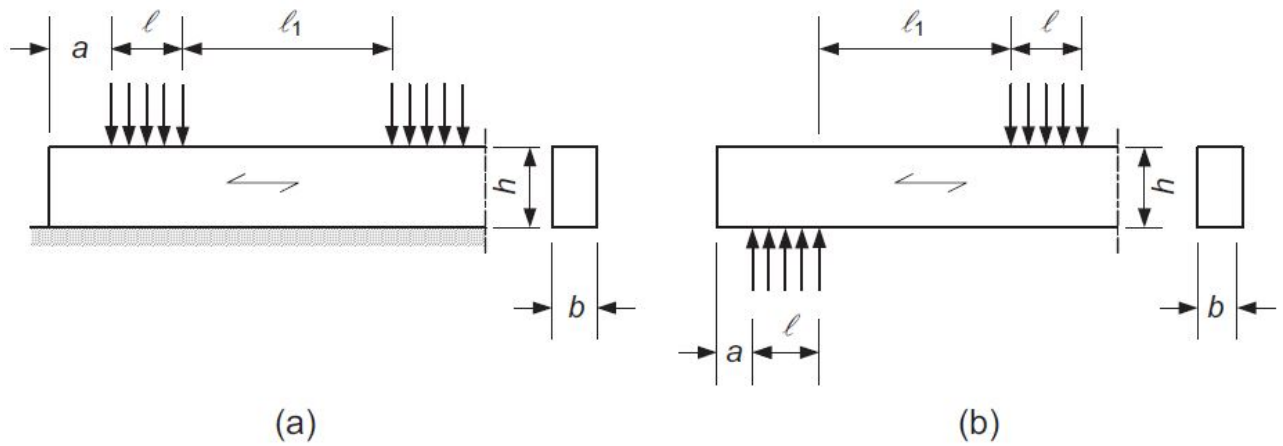


Figure 3.3: Structural element on continuous support (a) and discrete support (b), [19]

Chapter 4

Laboratory Work

4.1 Experimental equipment- Digital Image Correlation (DIC)

Digital Image Correlation is a non-contact optical technique for measuring strain and displacement [17]. The equipment works by comparing digital photos of the test specimen at different stages of deformation. The surface, which is to be analyzed, is prepared with a layer of random and unique pixel blocks. The system tracks the pixel blocks and measures the surface displacement. Then 2D or 3D deformation vector fields and strain maps are created. In many cases the material surface of the test specimen has enough image texture and the layer of pixel blocks are not needed. The images from the testing may be obtained from several different sources, e.g. consumer digital cameras, high speed video, macroscopes and microscopes including scanning electron and atomic force microscopes. The sources delivering the images are different in different applications. DIC is useful in many fields of science. It has been used by for instance Airbus, AWE and British Energy and even for analysis of strains development during the processing of chocolate. Figure 4.1 shows how Adidas uses DIC in the development of their new running shoes.

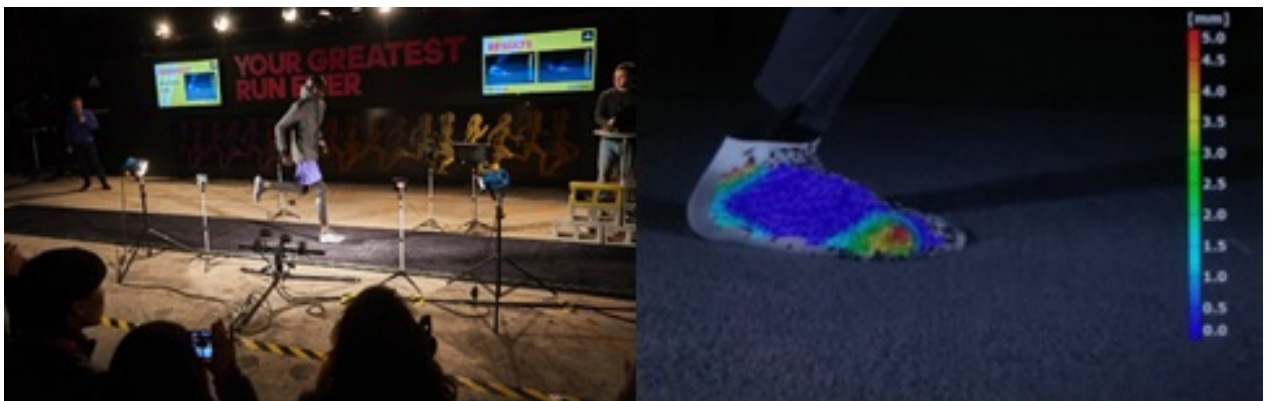


Figure 4.1: DIC used for examine the strains of a foot during running [18]

4.2 Limitations

To achieve very good results from the experimental work, many preparations and measurements of the wood samples would be necessary. Because of the biological nature of wood many features differ between the samples. Some differences between the samples can be measured, for instance the moisture content and density, whereas many other differences are nearly impossible to measure. A list of the most important limitations in this laboratory work is presented below.

- Moisture content is not measured.
- Boundaries between wood surface and steel plates are not ideally friction free.
- The accuracy in the measurements by the DIC is dependent of the quality of the speckle pattern.
- The speckle pattern is hand made. The same pattern can not be repeated for each and every sample.

4.3 Implementation

The measurements of the surface strains and 3D-displacements for the glulam specimens in compression perpendicular to the grain were carried out with a DIC equipment from Correlated Solutions. Two cameras, each 29 Megapixel, were controlled by the DIC system, see Figure 4.2. The light source was manually controlled. During the tests, one image pair was taken every five seconds. The size of the facets, the rectangular surfaces in which a mean value of the strains and displacements are computed, were carefully chosen. The size of the facets have a large impact on the results. The DIC measures the displacements of each facet in comparison to the neighboring facets. Small facets leads to more accurate results, as long as the facets are large enough to contain a unique speckle pattern. If the facets are too small some facets will not have a unique speckle pattern and the DIC will not be able to separate these facets from the others. In addition to the measurements recorded by the DIC-system, the load applied to the test specimen and the load point displacement were measured and logged.

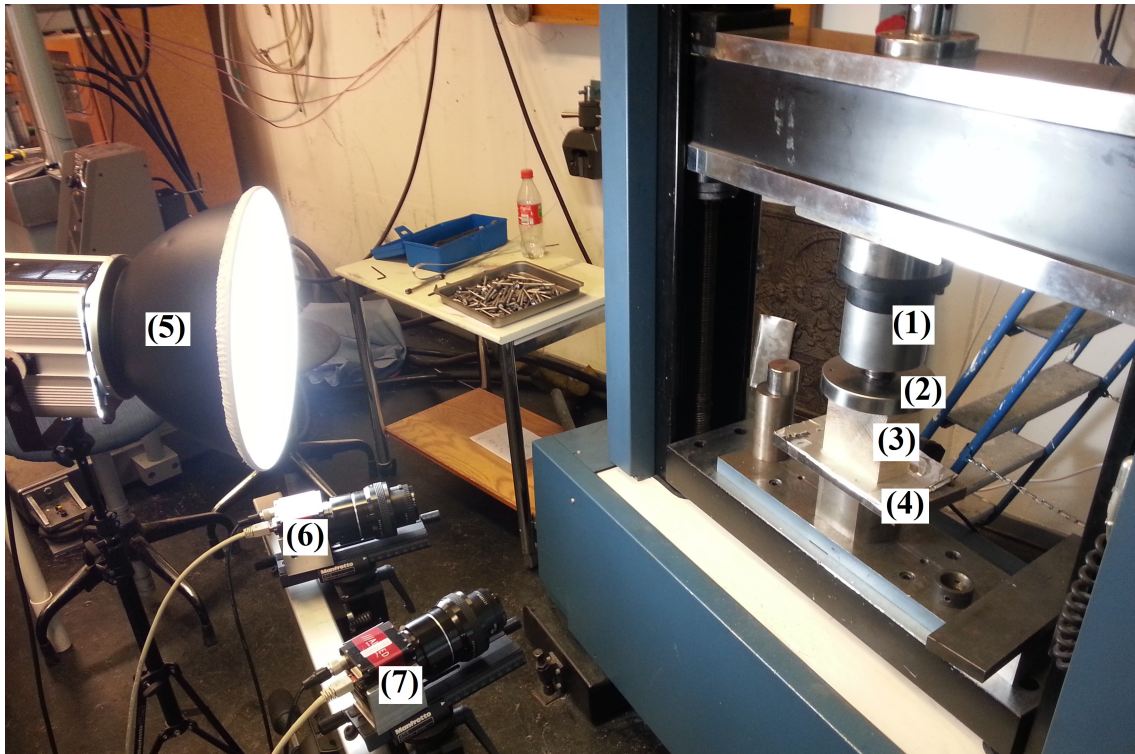
The specimens were before any experimental tests grinded at their load bearing surfaces. The specimens were grinded in order to establish smooth and plane contact areas to the applied load. The dimensions and weight were measured and photos were taken of each of the six sides of the specimen.

Next part of the experimental work was to create a speckle pattern at the surface which was about to be measured. The most important features of the speckle pattern is that it is random and has a high contrast. The glulam samples were therefore first painted with white spray paint and then sprayed with black paint, to create randomly located black spots. The reason for the white and black paint was to create a high contrast, e.g. the contrast would be lower with only the black spots on the naked wood surface.

After the speckle pattern was created it was checked by the DIC, since the randomness and contrast of the pattern has great impact on the capacity of the DIC to track facets and calculate the strains. In those cases the pattern was poor, it was remade. With a functional speckle pattern the final preparation for the DIC setup was to adjust the lamp to give as much light as possible without giving any disturbing reflections.

The boundary conditions were chosen to reflect the situation of no friction at the interfaces between the wood and the stiff steel plates. Several layers of aluminum foil with graphite grease

in between were used. The layers of aluminum foil and grease, at the interfaces of the wood and the steel plates, made it possible for the wood to expand in the direction perpendicular to the applied load. The steel plate in the bottom was fixed and rotation was prevented whereas the steel plate at the top was allowed to rotate. The test setup can be seen in Figure 4.2. Figure 4.3 shows the setup with the speckle pattern and boundary conditions right before the compression test starts. During the test the wood sample is loaded in compression at the rate of approximately five percent strain per minute. The experiment is over when there are large deformations in the wood.

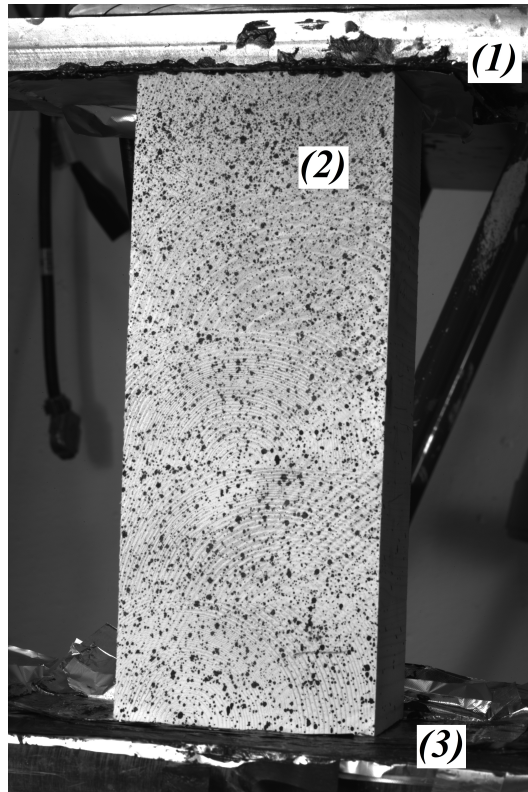


- | | |
|------------------|------------------------|
| (1) Piston | (2) Top steel plate |
| (3) Sample | (4) Bottom steel plate |
| (5) Light source | (6) Camera 1 |
| (7) Camera 2 | |

Figure 4.2: The DIC setup

Figure 4.2 shows the test setup and the setup of the DIC equipment. The test specimen was placed on the rigid steel plate in the testing machine. The stress was applied at the top of the sample by the piston head (Top steel plate). Rotation was allowed in the joint of the piston and the top steel plate. The two cameras of the DIC were calibrated to measure the movements in the surface of the samples from a fixed distance, i.e. the cameras were fixed and the samples were placed at the same place each time. The light source was manually adjusted to achieve the best possible light conditions.

Figure 4.3 shows a close-up of the test setup. Both the steel plate in the bottom and the steel plate at the top are shown. Note the aluminum foil with grease in between in both the bottom and the top interfaces.



- (1) Top steel plate,
aluminum foil and grease
- (2) Sample
- (3) Bottom steel plate,
aluminum foil and grease

Figure 4.3: Test setup

4.4 Specimen data

Table 4.1: Dimensions and densities for the samples

Sample	Nr Lamellae	Dimensions, ($l \times b \times h$)	Density, [kg/m ³]
1	5	57x89x220	440.0
2	4	57x139x138	474.2
3	3	60x114x113	449.2
4	5	55x89x221	431.4
6	3	57x115x113	468.7
8	4	53x139x137	534.2
9	3	58x115x113	452.2
10	5	54x90x220	463.0
11	4	56x139x138	521.3
12	3	54x115x112	452.5
13	5	56x89x221	448.8
14	4	58x139x138	496.5
16	5	54x89x221	462.4
17	4	58x139x137	493.4
18	4	56x140x137	507.4
19	4	53x139x138	525.8
20	4	55x139x138	511.8
21	3	56x114x113	433.2
22	4	56x139x138	502.7
27	5	58x89x221	424.7

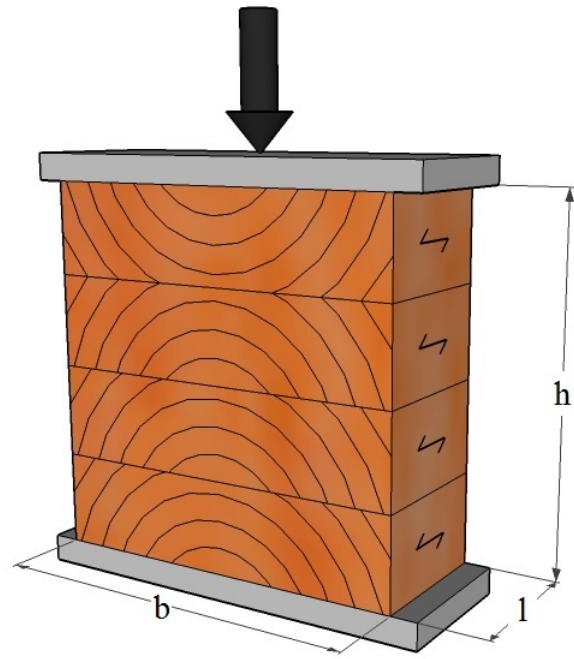


Figure 4.2: The definition of $(l \times b \times h)$ in the test setup

Chapter 5

The finite element method

5.1 General

In engineering mechanics many problems are described by differential equations. These equations are in general too complicated to solve analytically and a numerical approach is then necessary. The finite element (FE) method is a very common numerical technique.

The finite element method is based on the assumption that solution of the differential equation or equations hold over a certain region. In most applications this is not the case, but in the finite element method the characteristic feature is that for a certain region divided into smaller parts, so called finite elements, it is assumed that solution of the differential equations holds for a whole element. The calculations are then carried out over each element. The whole group of elements of a body is called a finite element mesh. The numerical solution gets closer to the real analytical solution with increasing number of elements.

When an approximation which is to be applied over each element is determined, the calculations for each and every element can be carried out. The approximation of how the variables changes over an element is often a polynomial. The polynomial is an interpolation function for the variables between points within the elements. The value of the variables are assumed to be known at the nodal points of the element. The numerical solutions for the elements are then patched together to form an approximate solution for the entire body. The FE method is a powerful tool which can be applied to arbitrary differential equations.

5.2 Weak form of two dimensional elasticity

In the case of two dimensional elasticity the elements of the body are considered as thin disks. For thin disks, the stresses and body forces are acting in the plane, see Figure 5.1, where \mathbf{b} is the body force of the disk, e.g. gravity, \mathbf{t} is the traction vector on its boundary and “ t ” is the thickness of the disk. In Figure 5.1 the vectors \mathbf{b} and \mathbf{t} are acting in the xy -plane. For the disk to be in equilibrium, the equilibrium equation given by (5.1) must be fulfilled.

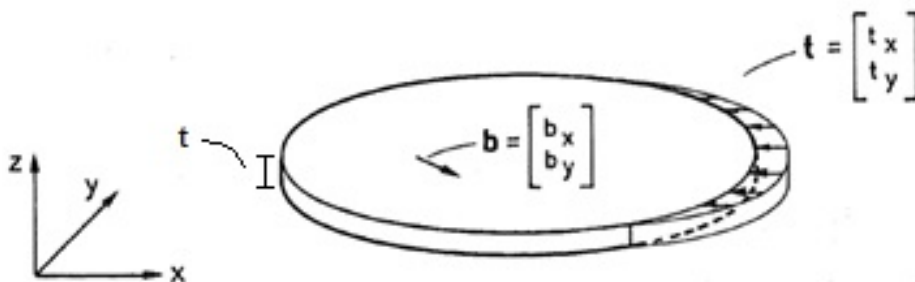


Figure 5.1: Thin disk loaded in plane stress [6]

$$(\tilde{\nabla})^T \boldsymbol{\sigma} + \mathbf{b} = \mathbf{0} \quad (5.1)$$

$$(\tilde{\nabla})^T = \begin{bmatrix} \frac{\partial}{\partial x} & 0 & \frac{\partial}{\partial y} \\ 0 & \frac{\partial}{\partial y} & \frac{\partial}{\partial x} \end{bmatrix} \quad (5.2)$$

$$\boldsymbol{\sigma} = \begin{bmatrix} \sigma_{xx} \\ \sigma_{yy} \\ \sigma_{xy} \end{bmatrix} \quad (5.3)$$

$$\mathbf{b} = \begin{bmatrix} b_x \\ b_y \end{bmatrix} \quad (5.4)$$

$$\mathbf{t} = \begin{bmatrix} t_x \\ t_y \end{bmatrix} \quad (5.5)$$

From equation (5.1) the weak form of the equilibrium equation can be established. The weak formulation is necessary to be able to later on derive the FE formulation. To create the weak form, the equilibrium equation (5.1) is multiplied by an arbitrary weight function \mathbf{v} . By writing out equation (5.1) and multiplying by \mathbf{v} , some terms will become zero and the expression turns out to be:

$$(\tilde{\nabla} \mathbf{v})^T \boldsymbol{\sigma} = \frac{\partial v_x}{\partial x} \sigma_{xx} + \frac{\partial v_y}{\partial y} \sigma_{yy} + \left(\frac{\partial v_x}{\partial y} + \frac{\partial v_y}{\partial x} \right) \sigma_{xy} \quad (5.6)$$

$$\mathbf{v} = \begin{bmatrix} v_x \\ v_y \end{bmatrix} \quad (5.7)$$

$$v_x = v_x(x, y); v_y = v_y(x, y); v_z = 0 \quad (5.8)$$

With equations (5.2) and (5.3) and by the definitions of \mathbf{t} and \mathbf{b} in Figure 5.1, equation (5.6) can after use of the Green-Gauss theorem be written as:

$$\int_V (\tilde{\nabla} \mathbf{v})^T \boldsymbol{\sigma} dV = \int_S \mathbf{v}^T t dS + \int_V \mathbf{v}^T \mathbf{b} dV \quad (5.9)$$

For a thin region, e.g. Figure 5.1 and noticing that $\sigma_{xz} = \sigma_{yz} = 0$, equation (5.9) may be written as:

$$\boxed{\int_A (\tilde{\nabla} \mathbf{v})^T \boldsymbol{\sigma} t dA = \oint_{\mathcal{L}} \mathbf{v}^T t t d\mathcal{L} + \int_A \mathbf{v}^T \mathbf{b} t dA} \quad (5.10)$$

This is the weak form for two dimensional problems, also called the virtual work principle [6]. It is important to notice that the letter t , differs from \mathbf{t} in equation (5.10). The letter t is the thickness of the region, whereas the vector \mathbf{t} is the traction vector.

5.3 The finite element formulation of two dimensional elasticity

The displacement vector \mathbf{u} , is given by equation (5.11):

$$\mathbf{u} = \begin{bmatrix} u_x \\ u_y \end{bmatrix} \quad (5.11)$$

The displacement is to be approximated by equation (5.12). In equation (5.12), \mathbf{N} is the element shape functions and \mathbf{a} is the nodal point displacement vector. The shape functions are approximations of the variation of the variables over an element. There are several such approximations depending upon what sort of elements that are used. Linear, quadratic, cubic and quartic polynomials are some possible approximations.

$$\mathbf{u} = \mathbf{N} \mathbf{a} \quad (5.12)$$

According to the Galerkin method an arbitrary weight vector is chosen as:

$$\mathbf{v} = \mathbf{N} \mathbf{c} \quad (5.13)$$

Since \mathbf{v} is arbitrary, \mathbf{c} is also arbitrary and it can be written:

$$\tilde{\nabla} \mathbf{v} = \mathbf{B} \mathbf{c}; \mathbf{B} = \tilde{\nabla} \mathbf{N} \quad (5.14)$$

Equation (5.14) is then inserted into the weak formulation, equation (5.10):

$$\mathbf{c}^T \left(\int_A \mathbf{B}^T \boldsymbol{\sigma} t dA - \oint_{\mathcal{L}} \mathbf{N}^T t t d\mathcal{L} - \int_A \mathbf{N}^T \mathbf{b} t dA \right) = 0 \quad (5.15)$$

From equation (5.15) it can be seen that since \mathbf{c} is arbitrary equation (5.15) can be written as:

$$\int_A \mathbf{B}^T \boldsymbol{\sigma} t dA = \oint_{\mathcal{L}} \mathbf{N}^T \mathbf{t} t d\mathcal{L} + \int_A \mathbf{N}^T \mathbf{b} t dA \quad (5.16)$$

Equation (5.16), states the balance principle for the body [6]. It is emphasized that equation (5.16) applies irrespectively of the constitutive model. The equation of (5.16) therefore holds for elasticity theory, as well as for instance for plasticity theory. Next step in creating the FE formulation is to choose the constitutive relation, i.e. the assumption of the material behavior. Assuming linear elasticity:

$$\boldsymbol{\sigma} = \mathbf{D}\boldsymbol{\varepsilon} \quad (5.17)$$

$$\boldsymbol{\sigma} = \begin{bmatrix} \sigma_{xx} \\ \sigma_{yy} \\ \sigma_{xy} \end{bmatrix} \quad (5.18)$$

$$\boldsymbol{\varepsilon} = \begin{bmatrix} \varepsilon_{xx} \\ \varepsilon_{yy} \\ \gamma_{xy} \end{bmatrix} \quad (5.19)$$

The matrix \mathbf{D} in equation (5.17) takes different forms depending on whether plane stress or plane strain is considered. The strains given by $\boldsymbol{\varepsilon}$ are on the other hand irrespectively of whether plane strain or plane stress is assumed. The strains in $\boldsymbol{\varepsilon}$ are derived from the displacements using the kinematic relation:

$$\boldsymbol{\varepsilon} = \tilde{\nabla} \mathbf{u} \quad (5.20)$$

From equations (5.12) and (5.14) equation (5.20) becomes:

$$\boldsymbol{\varepsilon} = \mathbf{B}\mathbf{a} \quad (5.21)$$

And equation (5.17) may be written:

$$\boldsymbol{\sigma} = \mathbf{D}\mathbf{B}\mathbf{a} \quad (5.22)$$

Using equation (5.20) in the expression for the balance principle for the body, i.e. equation (5.16), yields:

$$\left(\int_A \mathbf{B}^T \mathbf{D}\mathbf{B} t dA \right) \mathbf{a} = \oint_{\mathcal{L}} \mathbf{N}^T \mathbf{t} t d\mathcal{L} + \int_A \mathbf{N}^T \mathbf{b} t dA \quad (5.23)$$

For the two dimensional body expressed in equation (5.23), considering linear elasticity, the natural boundary condition is given by the traction vector \mathbf{t} along the boundary, \mathcal{L}_h . The essential boundary condition is given by the displacements in \mathbf{u} along the boundary, \mathcal{L}_g , see Figure 5.2

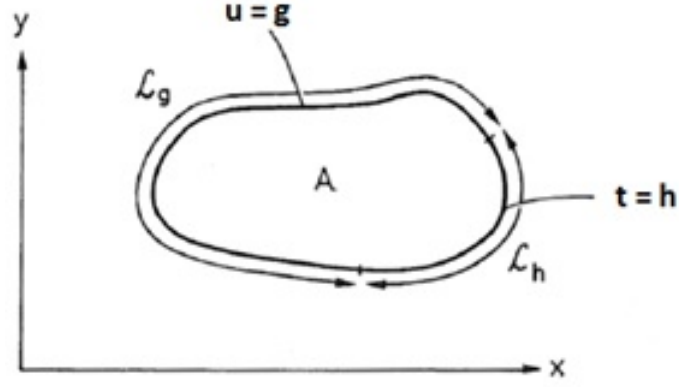


Figure 5.2: Natural and essential boundary conditions

The natural boundary condition given by \mathbf{t} , may be written:

$$\mathbf{t} = \mathbf{S}\mathbf{n} \quad (5.24)$$

Where:

$$\mathbf{S} = \begin{bmatrix} \sigma_{xx} & \tau_{xy} \\ \tau_{yx} & \sigma_{yy} \end{bmatrix} \quad (5.25)$$

$$\mathbf{n} = \begin{bmatrix} n_x \\ n_y \end{bmatrix} \quad (5.26)$$

In equations (5.25) and (5.26), \mathbf{n} is the unit normal vector in the xy -plane normal to \mathcal{L} . The boundary conditions of the body can be given in the form:

$$\mathbf{t} = \mathbf{S}\mathbf{n} = \mathbf{h} \quad \text{on } \mathcal{L}_h; \quad \mathbf{u} = \mathbf{g} \quad \text{on } \mathcal{L}_g \quad (5.27)$$

Where \mathbf{h} and \mathbf{g} are known vectors. Using the boundary conditions of (5.27) in (5.23) finally yields [6]:

$$\left(\int_A \mathbf{B}^T \mathbf{D} \mathbf{B} t \, dA \right) \mathbf{a} = \int_{\mathcal{L}_h} \mathbf{N}^T \mathbf{h} t \, d\mathcal{L} + \int_{\mathcal{L}_g} \mathbf{N}^T \mathbf{t} t \, d\mathcal{L} + \int_A \mathbf{N}^T \mathbf{b} t \, dA \quad (5.28)$$

The above equation, (5.28), is the finite element formulation for two dimensional elasticity. Equation (5.28) may also be written in a more compact form according to:

$$\mathbf{K} = \int_A \mathbf{B}^T \mathbf{D} \mathbf{B} t \, dA \quad (5.29)$$

$$\mathbf{f}_b = \int_{\mathcal{L}_h} \mathbf{N}^T \mathbf{h} t \, d\mathcal{L} + \int_{\mathcal{L}_g} \mathbf{N}^T \mathbf{t} t \, d\mathcal{L} \quad (5.30)$$

$$\mathbf{f}_l = \int_A \mathbf{N}^T \mathbf{b} t \, dA \quad (5.31)$$

Where \mathbf{K} is the stiffness matrix, \mathbf{f}_b is the boundary vector, \mathbf{f}_l is the load vector. Using the format in equations (5.29), (5.30) and (5.31), the FE formulation becomes:

$$\mathbf{K}\mathbf{a} = \mathbf{f}_b + \mathbf{f}_l \quad (5.32)$$

5.4 Quadrilateral elements

In the model of glulam in compression perpendicular to the grain the stresses and strains are in this thesis computed with quadrilateral elements. The quadrilateral elements are four node elements, see Figure 5.3. In order to later on calculate the element stiffness matrix for the element, two more degrees of freedom are introduced. This new node is located in the center of the element and its coordinates are calculated as the mean value of the coordinates of the corner nodes. The element is then considered as four triangular elements and the element stiffness matrix, one for each triangle, is provided by evaluating linear displacement approximations over the four triangular regions, see Figure 5.4. The stresses and strains are computed according to the four element stiffness matrices. The stresses and strains for the whole quadrilateral element are then computed as weighted mean values from the values of the four triangular elements [7].

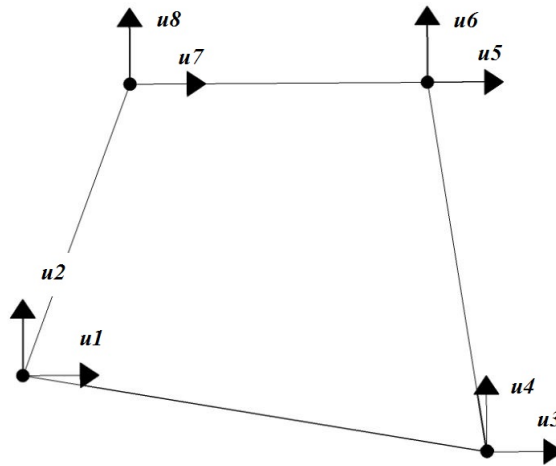


Figure 5.3: Quadrilateral Elements [6]

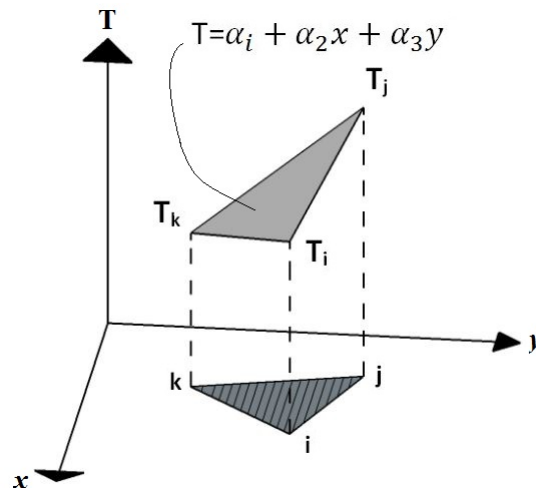


Figure 5.4: Linear displacement approximation, for considered triangular element

Chapter 6

Model

6.1 Limitations

The model is based on some assumptions and simplifications that are listed below. Wood is a heterogeneous material with a large variety in the material structure and simplifications are needed.

- Variation in moisture content is neglected.
- The annual rings are assumed to be cylindrical.
- Clear wood is considered, i.e. no knots, cracks or resin pockets.
- The moduli of elasticity are constant in the three principal directions, i.e. not affected by the distance from the pith.
- Linear elastic material behavior is assumed, i.e. no plasticity.
- Glue lines are not modeled explicitly, i.e. no difference in moduli of elasticity and Poisson's ratios in the interfaces between the lamellae compared to the rest of the cross section.
- Plane stress is considered.

6.2 General

A linear elastic finite element model was created in Matlab considering assumptions of plane stress. The geometry was created in a general manner, i.e. the model is not specific for any given geometry or annual ring orientation. Width, height and number of lamellae are input variables that are easily chosen. The locations of the piths for each lamellae are also input values to the model, which allows every lamella to have its own annual ring pattern. Within each lamella the annual ring pattern is then assumed to be cylindrical.

For each and every element, the radial and tangential directions are computed with respect to the annual ring orientation of the actual lamella. This means that the local coordinate system is known for every element in the geometry. The global coordinate system is chosen, the direction cosines are calculated and the transformation matrices, two for each element, are established according to equations 2.19-2.29. The transformation matrices are then used to transform the local $\tilde{\mathbf{D}}$ -matrices into the global \mathbf{D} -matrices and the stiffness matrices are computed for quadrilateral elements.

The moduli of elasticity, Poisson's ratios, shear modulus and strength properties are input parameters to the model. The strength properties are chosen for clear wood since the model is for research purposes on a material level, e.g. not on a structural element scale. Both the strength properties and the moduli of elasticity show significant variation in magnitude between different wood species. Density and number of annual rings are other factors affecting the magnitude and ratio of stiffness and strength properties.

Some stiffness parameters for glulam according to EN 14080 and Poisson's ratios for different wood species [3] are presented in Table 6.1. In Table 6.2 some strength properties for clear wood are presented [3]. These tables show examples of stiffness and strength properties that can be used as input data to the model.

Table 6.1: Stiffness properties in [MPa] and Poisson's ratios

Wood species	E_R	E_T	G_{RT}	ν_{RT}	ν_{RT}
Norway spruce	790	340	30	0.84	0.34
Spruce	710	430	23	0.51	0.31
Scots Pine	1000	500	70	0.61	0.31
Structural elements	$E_{90,g,mean}$		$G_{g,mean}$		
Glulam, GL 24h	300		650		
Glulam, GL 32h	300		650		

Table 6.2: Material strength properties in [MPa]

Sort of wood	f_{Rt}	f_{Rc}	f_{Tt}	f_{Tc}	f_{RT}
Norway spruce	4.9	3.6	2.8	3.8	1.6
Spruce	4.9	7.0			

6.3 Elements

Quadrilateral elements were chosen in the model. As described in Chapter 5.4, the stresses and strains for a quadrilateral element are computed as mean values of the stresses and strains in four triangular elements. To improve the accuracy of the model it was taken advantage of the parameters being computed in four triangles in each element. Instead of calculating the mean values for stresses and strains of a whole element the values from the triangles were weighted according to their area of the whole element. Thus each element delivers four values of output, one output in each node, instead of one mean value holding for the whole element.

To examine how sensitive the model is to the size of the finite element mesh a plot of the ratio $\frac{\sigma_x}{\sigma_c}$ (Stress in horizontal direction of the cross section divided by the applied compressive stress) in a vertical cut in the middle of the width as function of the height was carried out. The plot can be seen in Figure 6.1. The plot was made for a glulam cross section with three lamellae, see Figure 6.2. The numbers in the label of the figure gives the number of elements/width. In the height of the cross section the ratio elements/height is as close as possible to the elements/width. The size of the finite element mesh has a modest impact on the result when the stresses in the nodes are close to the applied stress. In the regions where the stresses are large, the size of the finite element mesh has a greater impact on the result. The reason for the large stresses in some areas is related to the pattern of the annual rings. Because of the difference in stiffness in radial and tangential directions, the stresses can be very large in those areas where the pattern of the annual rings is disadvantageous considering stiffness. In these regions, the estimation of the radial and tangential directions has a larger impact and the size of the finite element mesh is of greater importance.

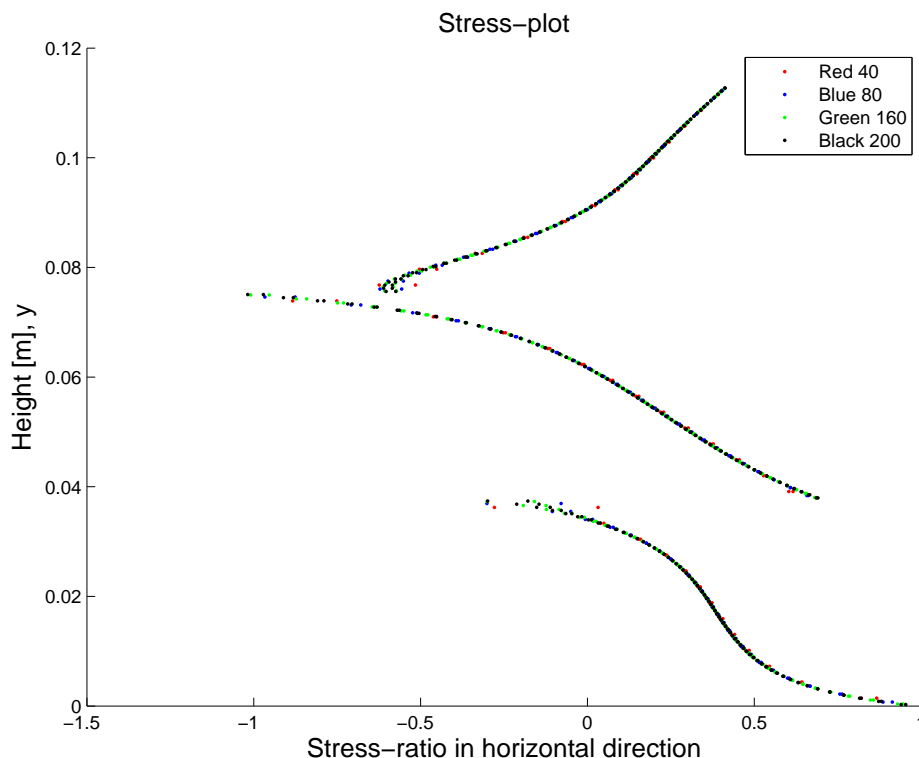


Figure 6.1: The effect of the size of finite element mesh on the stress-ratio, $\frac{\sigma_x}{\sigma_c}$. The stresses are plotted in the nodes. The applied stress is 1 MPa in compression.

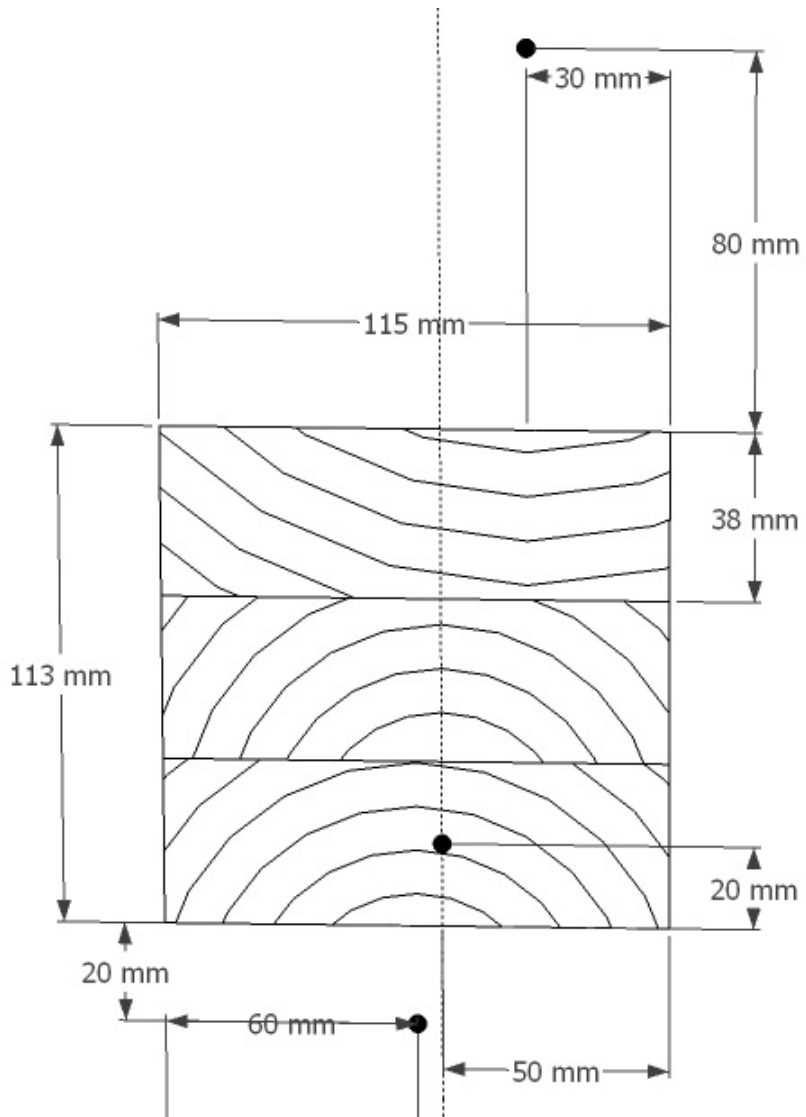


Figure 6.2: Dimensions of the cross section. Black dots marks the piths. The stresses are calculated along the dotted line.

6.4 Loading and boundary conditions

The loading and boundary conditions in the model shall correspond to the conditions in the experiment. In the experimental work the glulam cross sections were exposed to compression perpendicular to the grain by two very stiff steel plates, see Chapter 4.3. The upper stiff steel plate was allowed to rotate. In the laboratory work, aluminum foil and grease were used at the interfaces of the wood and the steel plates in an attempt to create the condition of no friction. In fact there is still some friction at the boundaries and the boundaries in the model may therefore be chosen as either friction free or friction. Since the upper steel plate was not prevented from rotating in the experiment, the upper boundary in the model can be given a small rotation.

The load applied in the experiments is modeled as displacement control. Displacement control means that the nodes in the upper segment are given a displacement in the vertical direction. In the model, three different boundary conditions were investigated.

Boundary condition 1

- The nodes in the lower segment of the test specimen are locked in the vertical direction and one node is locked in both vertical and horizontal direction.
- The nodes in the upper segment are given a displacement in the vertical direction and are free to move in the horizontal direction.
The displacement is constant along the whole width of the specimen.

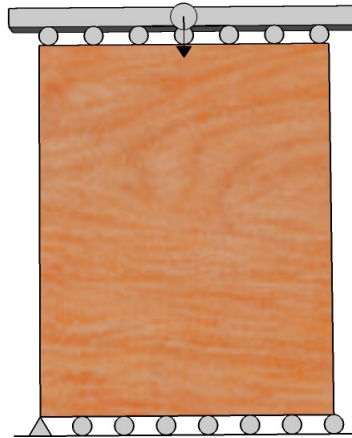


Figure 6.3: Boundary condition 1

Boundary condition 2

- The nodes in the lower segment are locked in both vertical direction and horizontal direction.
- The nodes in the upper segment are displaced in the vertical direction and prevented from movement in the horizontal direction.

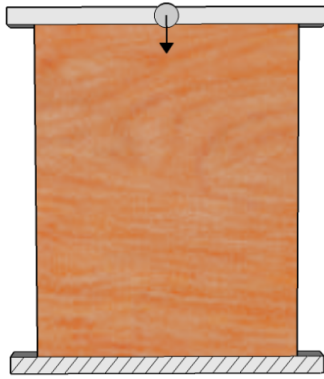


Figure 6.4: Boundary condition 2

Boundary condition 3

- Boundary condition 1 or boundary condition 2 and in addition the upper segment is given a small rotation.

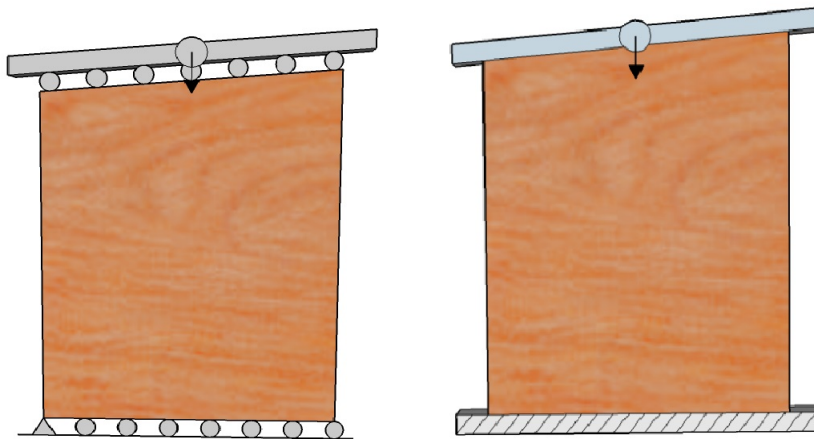


Figure 6.5: Boundary condition 3

6.5 Evaluation of parameters and annual rings

In order to be able to compare the model and the laboratory results, a set of stiffness and strength properties were chosen. These estimated properties were then assumed to hold for all test specimens.

The mean density of all test specimens, see Table 4.1, was calculated and used as a guideline value for determination of the moduli of elasticity in the model. The strength values were chosen for clear wood pieces of spruce at 12 % moisture content, see Table 6.4.

Table 6.3: Modulus of Elasticity in the model [MPa]

E_R	E_T	G_{RT}	ν_{TR}
750	462.5	31.5	0.26

Table 6.4: Strength properties in the model [MPa]

$f_{t,R}$	$f_{t,T}$	$f_{c,R}$	$f_{c,T}$	f_{RT}
4.9	2.8	7.0	3.8	1.6

As an attempt to recreate the best possible annual ring pattern of the samples, the tangential direction for each element in the model was plotted over an image of the respective sample, see Figure 6.6. From the images of the samples, the location of each pith in the cross section can be calculated. The locations of the piths are then input data to the model. The plot of the tangential directions in the model, see Figure 6.6, shows if the model captures the right pattern.

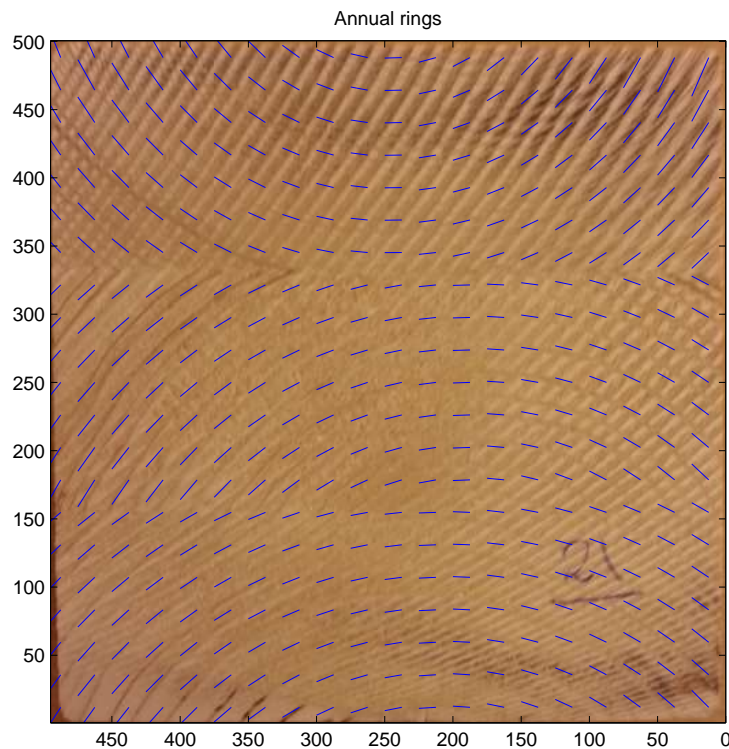


Figure 6.6: Annual rings

Chapter 7

Results and analysis

In order to estimate the accuracy of the model, a comparison of the results from the FE-model and the experimental results will be presented in this Chapter. The main focus of the comparison is considering the strain distribution rather than the exact strain magnitudes. The stiffness parameters differ for each sample and their values can only be estimated. In the model, the stiffness parameters are constant for all samples and are based on the mean density as a guideline. Unlike the estimated set of stiffness values, the material structure for each and every sample is simulated in the model. Results and analysis for three samples, one for each geometry, are presented. For further results see Appendices.

7.1 Illustration of the laboratory results

The experimental work was carried out for all samples in Table 4.1. An example of the results for a test specimen will be presented to illustrate what type of data and results that were obtained during testing.

The stress plotted as a function of the deformation for Sample 4 can be seen in Figure 7.1. The material behavior is fairly linear elastic up until roughly 2.3 MPa. After the fairly linear elastic part the material enters the nonlinear zone. Images by the DIC shows that the first crack initiates at the stress of approximately 2.5 MPa. The first crack is marked by a red dot in Figure 7.1. Once the material has entered its nonlinear zone, the behavior will be plastic when the applied stress of the sample is increased. For the present work, the part of most interest in the graph is up to the point where the first crack occurs.

In Figure 7.1 six different stress states are marked. An image of the deformed sample corresponds to each stress state. Thus, Figure 7.2 - Figure 7.4 show the deformation of the sample during testing.

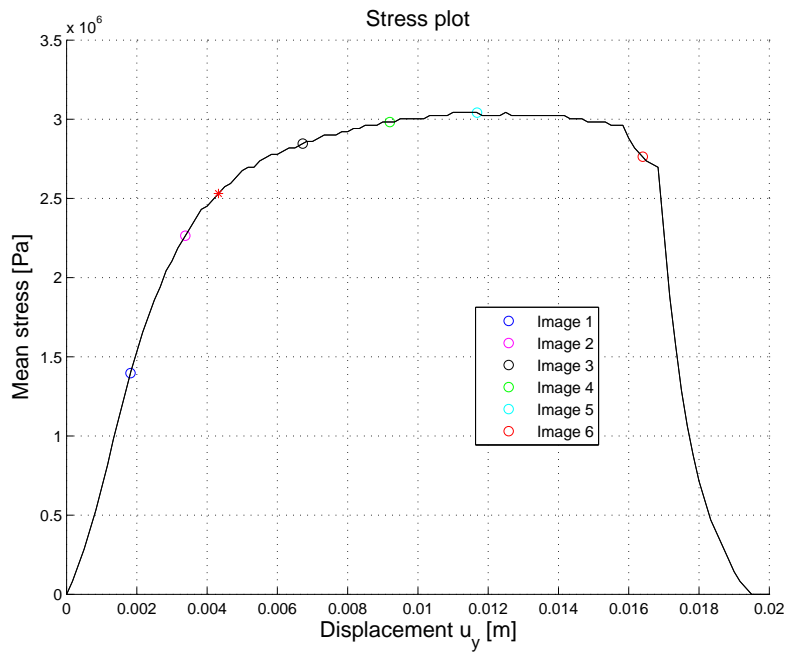
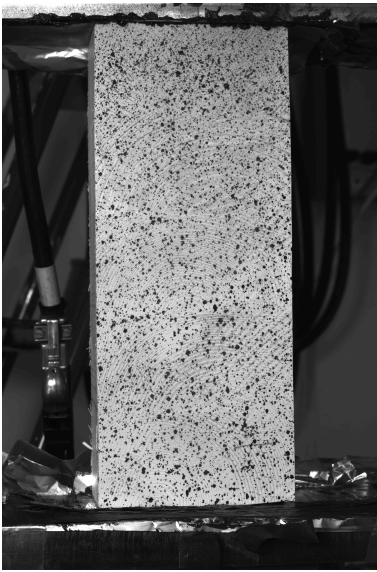


Figure 7.1: Stress- deformation plot, Sample 4, the initial crack is marked by “*”

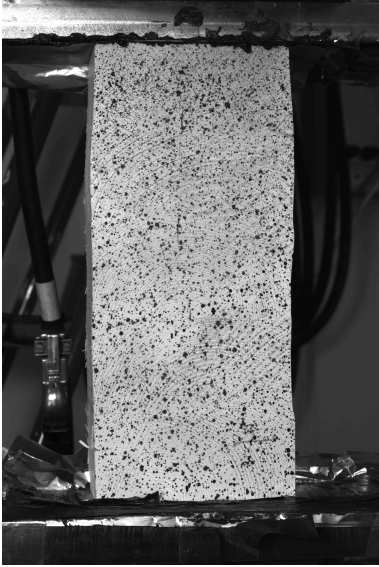


“o”: Image 1

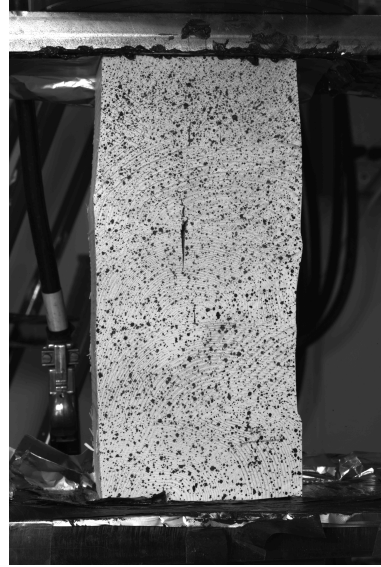


“o”: Image 2

Figure 7.2: Image 1 and Image 2



“○”: Image 3

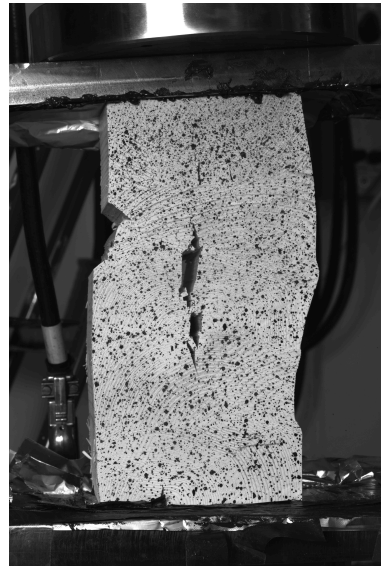


“○”: Image 4

Figure 7.3: Image 3 and Image 4



“○”: Image 5



“○”: Image 6

Figure 7.4: Image 5 and Image 6

The strains computed by the DIC were imported into Matlab. Since the strains from the DIC are computed in random points of the cross-section, the values of the strains were interpolated to a symmetric and evenly distributed grid of points to accomplish a strain plot for the whole cross section. The strains for Sample 4 at an applied compressive stress of approximately 1.8 MPa can be seen in Figure 7.5 - Figure 7.7. Figure 7.8 shows the cross section of Sample 4.

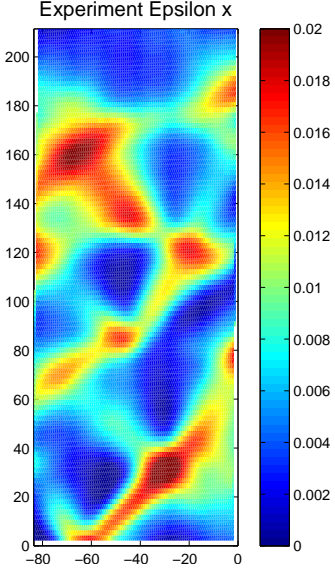


Figure 7.5: Strains in horizontal direction ϵ_x , Sample 4

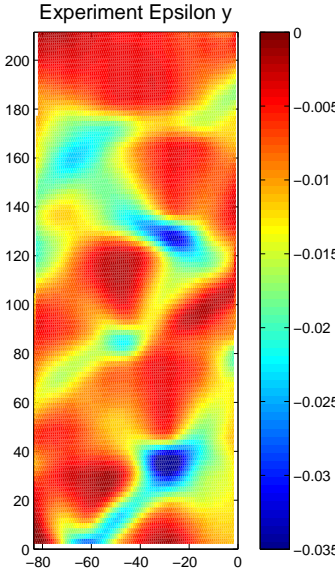


Figure 7.6: Strains in vertical direction ϵ_y , Sample 4

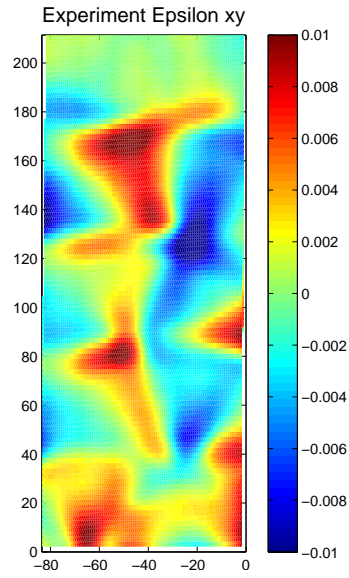


Figure 7.7: Shear strains ε_{xy} , Sample 4



Figure 7.8: The cross section of Sample 4

7.2 Results and analysis

7.2.1 Sample 21 - 3 Lamellae

Images of the cross sections and the sides of the samples are used for detecting imperfections such as cracks, knots, resin pockets etcetera. These imperfections have great impact on the results from the experiments. All sides of Sample 21 can be seen in Figure 7.10.

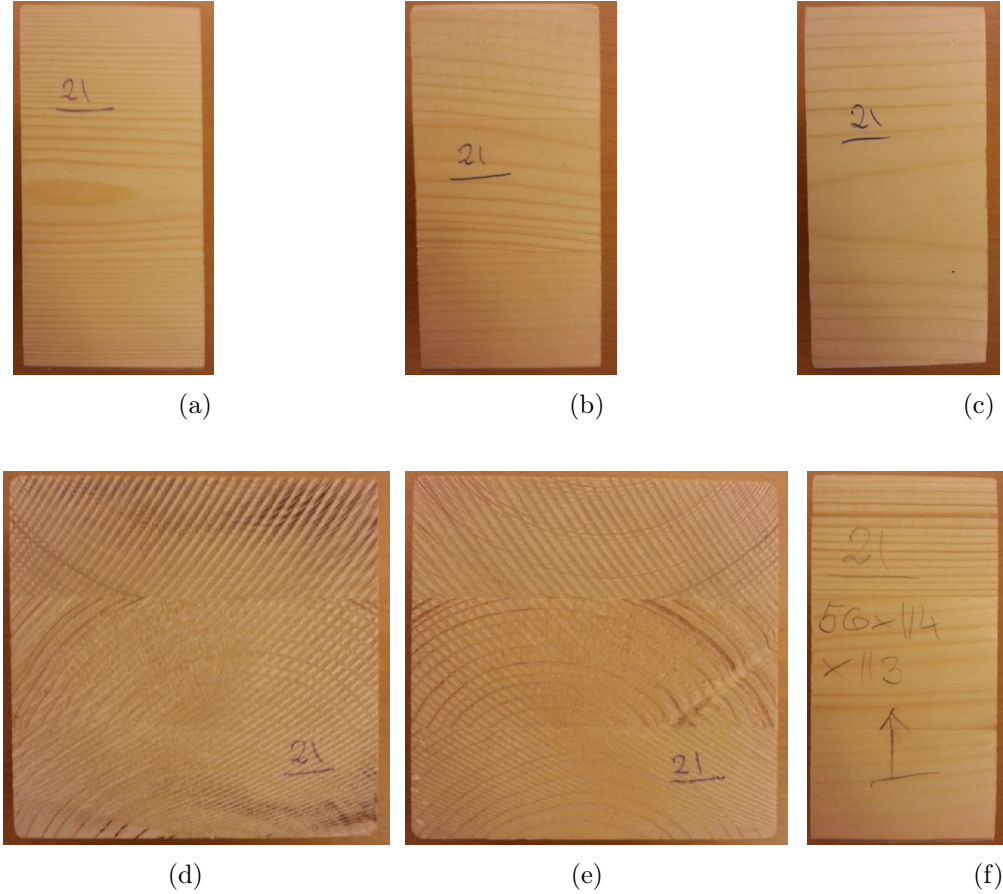


Figure 7.10: Images of the sides of Sample 21. (d): Cross- section used for measurements.

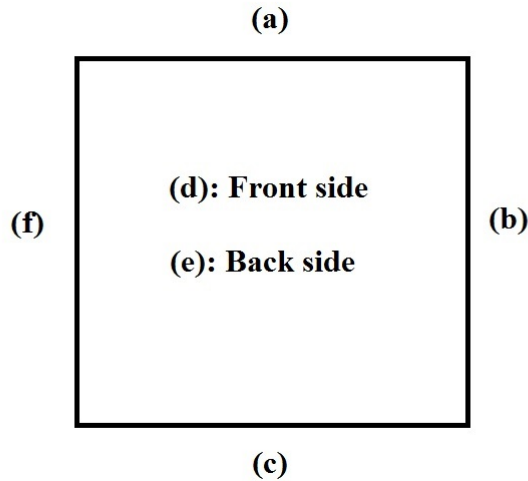


Figure 7.11: Scheme of which image corresponds to which side of the sample as seen by the cameras.

7.2.2 Stress- Deformation plot

Figure 7.12 shows the stress- deformation curve from the experiment and the model. The behavior is fairly linear elastic up until the first crack. This linear part of the material behavior therefore coincides quite well with the linear elastic model. The slope of the curves are similar, they are almost parallel, which indicates that the assumed stiffness parameters in the model seems to be reasonable considering the global stiffness. An obvious difference between the curve of the model and the experimental curve is the offset.

There can be many reasons for the offset seen in Figure 7.12. A finite element model is a numerical method of solving differential equations and the accuracy of the results depends on the size of the elements. The finite element mesh used is 200×200 elements which creates a fairly accurate result, see “cyan” in Figure 6.1. The boundary conditions used in the model is for no friction between the wood surface and the steel plates. In the experiment, graphite grease and aluminum foil was used in an attempt to create the case of no friction. It is, however, not possible to create a scenario that doesn't have any friction at all. The annual rings are simplified as cylindrical, which is not always the case. Knots, resin pockets, existing cracks before loading etcetera are neglected in the model. The stiffness properties are strongly dependent upon the density of the wood and also the distance from the pith. The density is estimated as a mean value for the whole sample, but the density and therefore also the stiffness parameters differ significantly between the different lamellae of the cross sections.

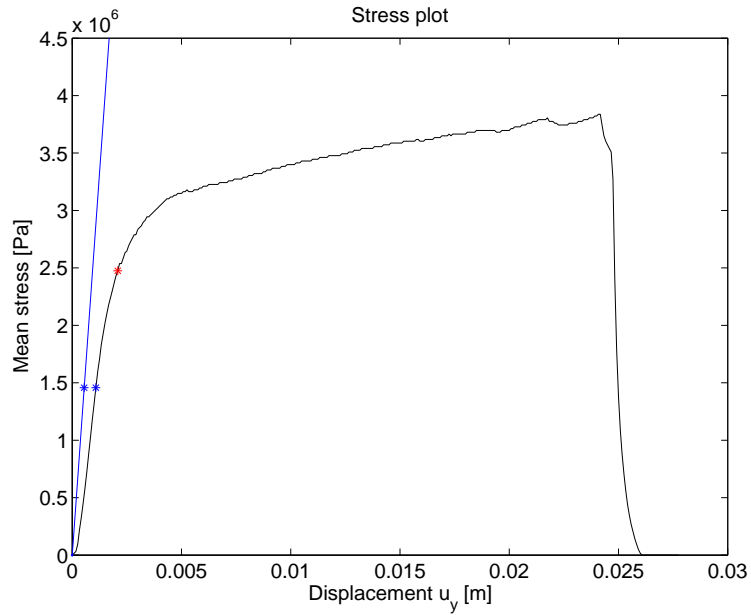


Figure 7.12: Stress- deformation plot, Sample 21. Black: Experiment, Blue: FE- model , “*” marks the initial crack, “*” mark the points for the comparison of the strains.

A close-up of the stress plot, Figure 7.13, reveals a non linear behavior during the first approximately 0.3 mm. This non linear behavior has a large contribution to the offset. The reason for the non linear behavior is non ideal testing conditions such as material settlements and not ideal plane surfaces. All samples show the same initial nonlinear behavior.

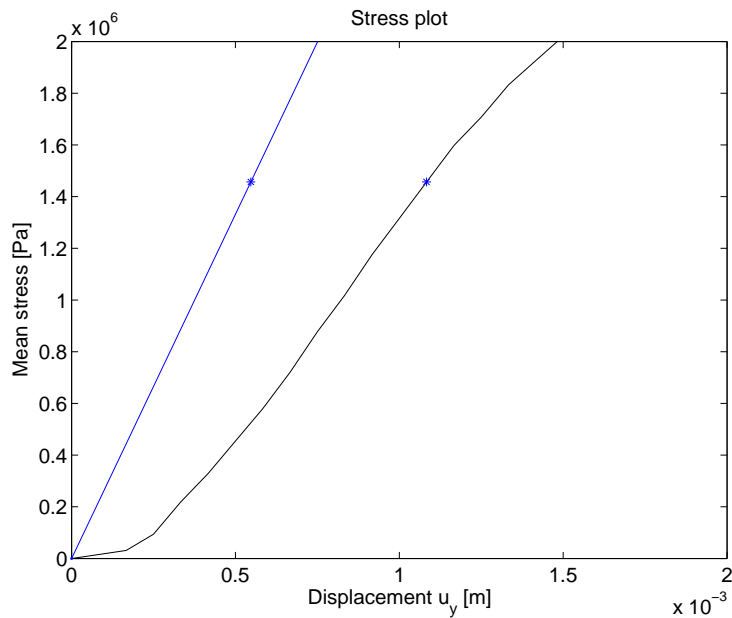


Figure 7.13: Close-up of the initial part of the stress plot

7.2.3 Strains

The comparison between model and experiment regarding the strains can be seen in Figure 7.14. The comparison is made for the mean stress of approximately 1.5 MPa in both the results from the experiment and the model. In Figure 7.12 and Figure 7.13, the points of 1.5 MPa are marked with a “*”.

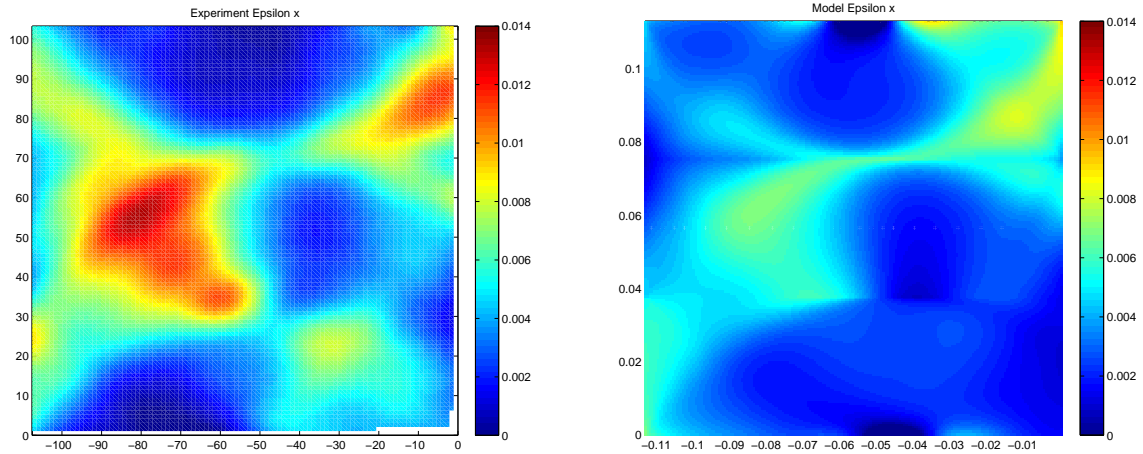


Figure 7.14: Strains in horizontal direction ε_x , Sample 21. Left: Experiment, Right: FE- model

The strains predicted by the model are smaller than the strains from the experiment. The magnitude of the strains are however not the most important aspect in the comparison. The size of the strains depends on the chosen stiffness parameters which varies for each and every sample. Since the stiffness parameters used in the model are mean values for all samples, the magnitude of the strains are fairly inaccurate. It should be noticed that the strains in the horizontal direction are positive. The strains are in tension. For large stresses, the positive strains in horizontal direction may lead to cracks.

An important aspect in the analysis is the distribution of the strains. In the experiment plot, Figure 7.14, the greatest strains are in the middle left side and in the upper right corner. It can also be seen that these two areas with the largest strains almost coincide with each other. In the model plot, Figure 7.14, the largest strains are in a region from middle left side up to the upper right corner. The smallest strains are in the bottom, the middle right side and the middle upper side. In Figure 7.10 (d), it can be seen that the largest strains are in the areas where the annual rings are tilted approximately 45 degrees to the loading direction. Because of the high stiffness in the radial direction and the low shear stiffness, it is likely that the annual rings will, for high stresses, be forced to slide against each other in these areas.

To improve the accuracy of the model one can examine the stiffness parameters for the particular piece of wood. Other error sources are mainly the ones mentioned previously in the discussion of Figure 7.12.

The strains in the vertical direction can be seen in Figure 7.15. The conformance between the model and laboratory result is for the vertical strains not as accurate as for the horizontal strains. An explanation for the difference may be the appearance of knots. Considering compression, knots are in general stiffer than clear wood. On the other hand, considering tension as in the case of Figure 7.14, knots are in general weaker than clear wood pieces.

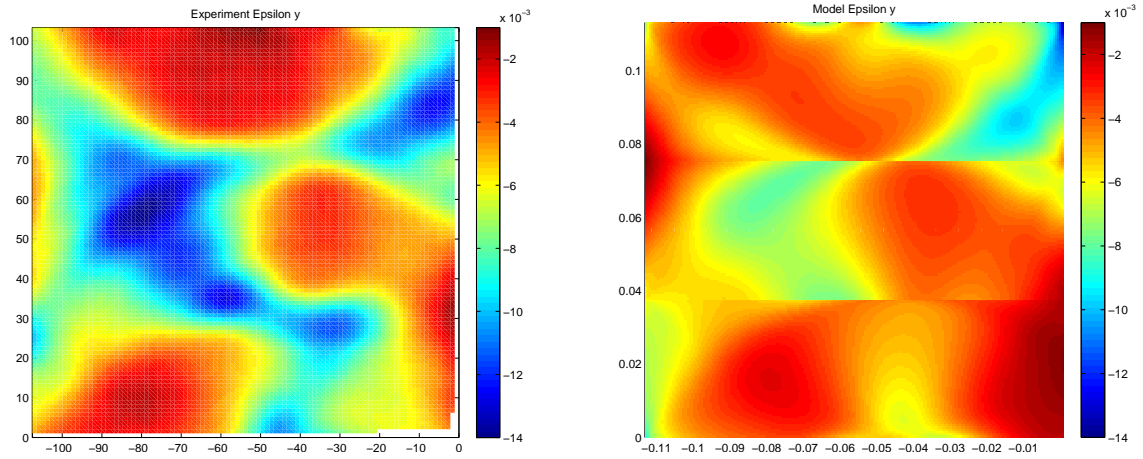


Figure 7.15: Strains in vertical direction ε_y , Sample 21. Left: Experiment, Right: FE- model

The shear strains are shown in Figure 7.16. The magnitudes differ, but the model manages to capture the strain distribution in general. In the two lowest lamellae, the largest strains seem to have some sort of triangular shape. These areas can be seen in the model as well. In the upper part of the plots, the upper lamella, the highest strains from the laboratory work are in the interface between the lamellae. In this region, near the upper right corner, the annual rings differ significantly in the interface of the lamellae, see Figure 7.10 (d). These great differences in the pattern of the annual rings are a probable reason for the high values of strains. These large strains are also present in the result from the model. A difference between the model and the experimental result is the area in the upper left corner. A possible reason for the high strains generated by the model may be that the angle between the curvature of the annual rings and the load direction are near 45 degrees and the boundaries have no friction. In the experiment the annual rings curvature is the same, but the boundaries are not ideal frictionless.

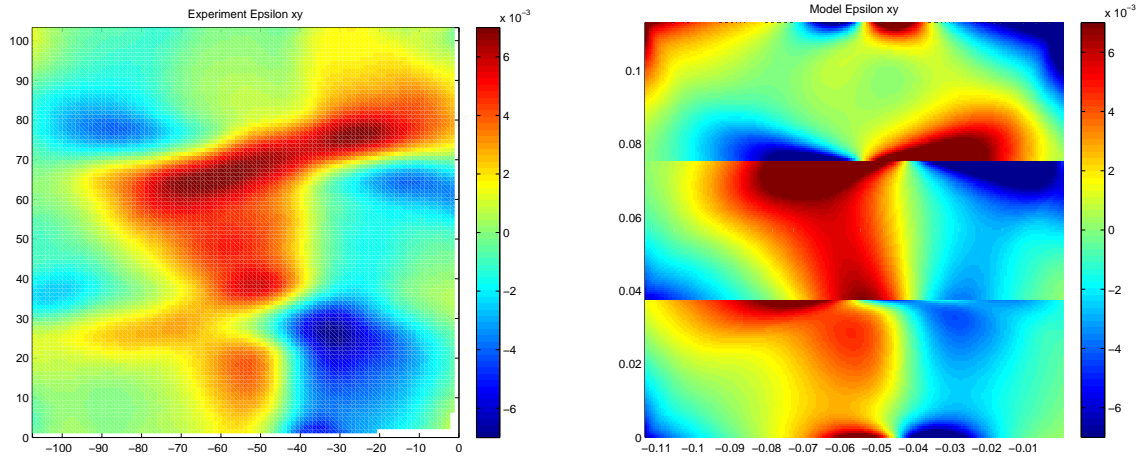


Figure 7.16: Shear strains ε_{xy} , Sample 21. Left: Experiment, Right: FE- model

7.2.4 Norris failure criteria

In order to evaluate where the first crack is to be expected, the Norris failure criteria is used. The strength properties that are used in the criteria can be seen in Table 6.4. The strength properties are estimated values that hold for spruce in general. The strength properties used in the model are mean values corresponding to Spruce at 12% moisture content. Due to the uncertainties of the value of the maximum stress and the uncertainties regarding the chosen strength values, the model can not predict for what load the first crack will initiate. It may instead be used to predict where the first crack could be expected, see Figure 7.17 and Figure 7.18.

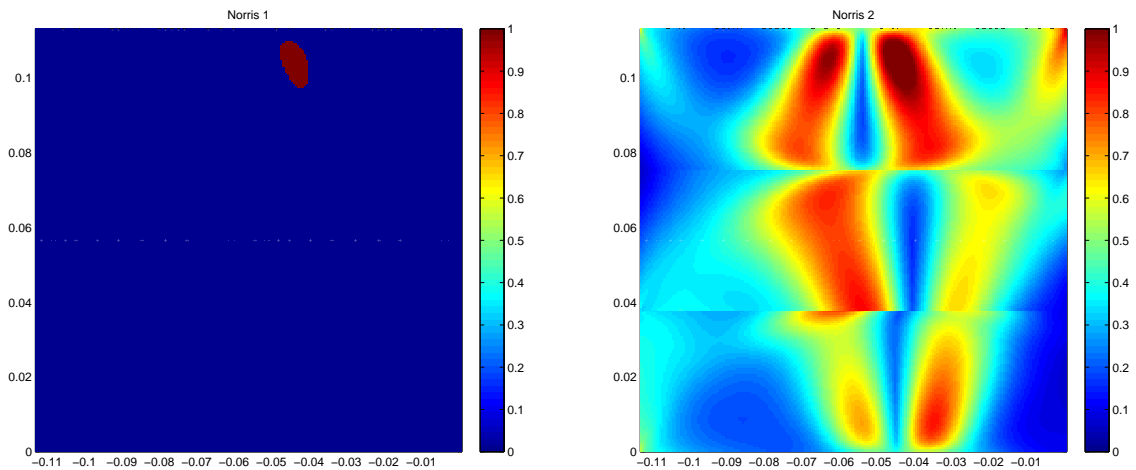


Figure 7.17: Norris failure criteria, Sample 21. Left: Red marks the region where the first crack is predicted by the model, Right: Effective stress based on Norris failure criterion

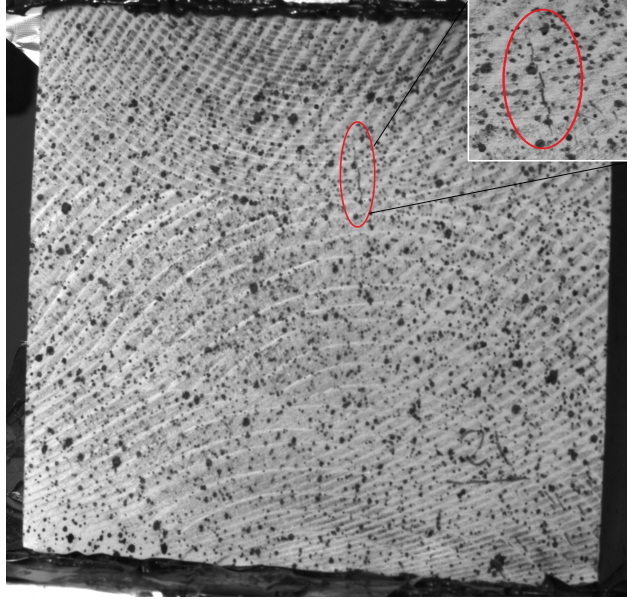


Figure 7.18: Image showing where the first crack occurred during testing, Sample 21

The model predicts that the first crack will initiate in the upper lamella, near the boundary. The real crack initiates in the border between the upper and middle lamella. At this border, annual rings with opposite radial directions coincide. In the spot where the crack initiates the tangential directions of the annual rings of the upper and the middle lamella seem to be parallel. This means that the radial directions of the annual rings in the upper and middle lamella are pointing towards each other. Since the largest stiffness is in the radial direction, large stresses will develop in this spot. The stiffness preventing the annual rings to slide along each other is the shear stiffness and the tangential stiffness. The shear stiffness is much lower than the radial stiffness and the tangential stiffness is roughly half of the radial stiffness. Because of the low stiffness (tangential and shear) in the LT-plane the material starts to slide along the annual rings which leads to a crack in this spot.

An explanation for the difference between the model and experiment may be the boundary conditions in the model. The boundary conditions used in the model are for the case of no friction, in fact there is some friction at the boundaries and this friction prevents the material to expand.

7.3 Sample 11 - 4 Lamellae

Images of Sample 11 can be seen in Figure 7.20. This test specimen has more knots than Sample 21.

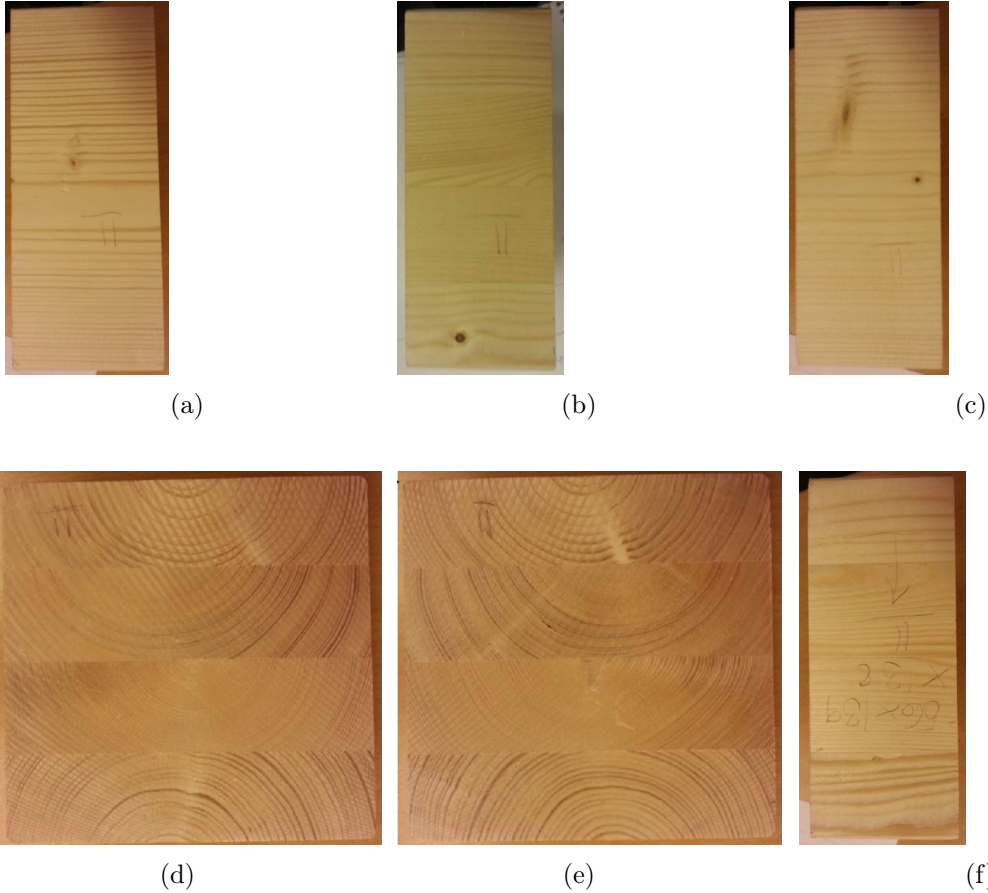


Figure 7.20: Images of the sides of Sample 11. (e): Cross- section used for measurements.

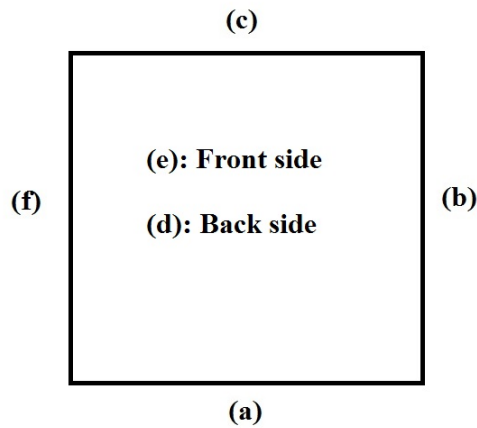


Figure 7.21: Scheme of which image corresponds to which side of the sample as seen by the cameras.

7.3.1 Stress- Deformation plot

Sample 11 is a four lamellae test specimen. Figure 7.22 shows the stress- deformation plot. The experimental curve shows great linearity up to approximately 2 MPa, then the behavior starts to enter the nonlinear zone. The curves are nearly parallel, indicating that the stiffness parameters in the model and in the experiment seem to be in the same range of magnitude. The reasons for the offset are probably the same as for Sample 21.

As seen in Figure 7.22 the first crack initiates far into the nonlinear region. Since the material deforms irreversibly in the plastic zone, the FE-model can no longer predict the behavior in this region. The first crack marked in Figure 7.22 is however the first crack visible by the naked eye. Therefore, the crack may initiate at an earlier state, not visible by the naked eye, and the model could still predict its location.

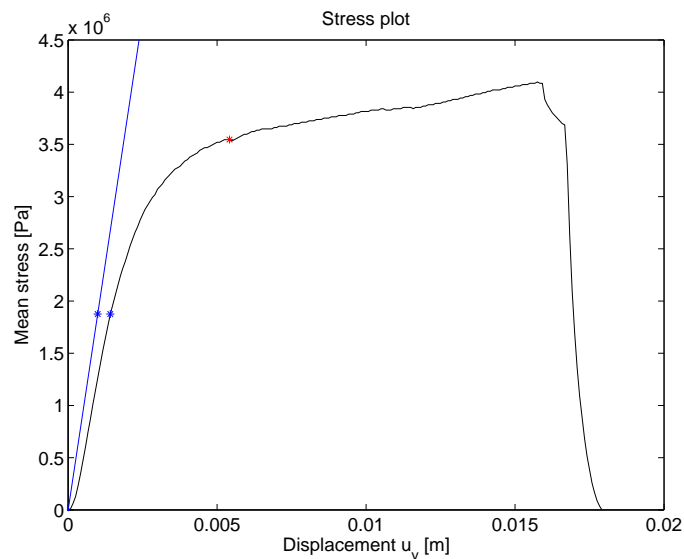


Figure 7.22: Stress- deformation plot, Sample 11. Black: Experiment, Blue: FE -model, “*” marks the initial crack, “*” mark the points for the comparison of the strains.

7.3.2 Strains

The strains in the horizontal direction are positive, i.e. the strains are in tension. Note, the magnitudes of the strains in Figure 7.23 as well as for Figure 7.24 and Figure 7.25 are not accurate because of the estimated stiffness parameters. The most apparent similarities are in the middle region of the plots where most of the strain behavior is captured by the model. The model shows the largest strains in the pith of the second lamella, whereas the experiment shows large strains in the surroundings of the pith. The large strains in the pith, predicted by the model are reasonable. The reason for the large strains from the experiment on the left and the right side of the second lamella pith, may be because of the knots in the cross section. It can be seen in Figure 7.20 (e), that there are two knots in the upper part of the cross section pointing towards the areas where the experiment computes the largest strains. Since these knots may be stiffer than the rest of the cross section, it is possible that these knots increase the stress on the material beneath.

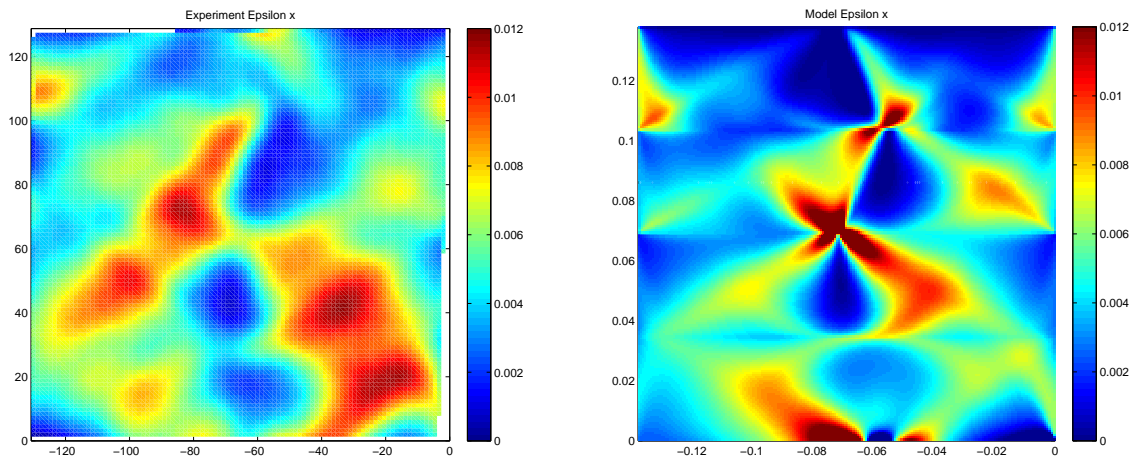


Figure 7.23: Strains in horizontal direction ε_x , Sample 11. Left: Experiment, Right: FE-model

Figure 7.24 shows the vertical strains. Both plots have similar patterns, neglecting the values of the strains. The region with the largest strains in the experimental result is where the annual rings have an angle of approximately 45 degrees to the load direction, see Figure 7.20 (e). The model shows large strains in the same region. This region has a narrow part, seen in the experiment plot, that stretches up to the point where the second lamella has its pith. The plot from the model also shows large strains at the pith of the second lamella. Note that the regions with the largest vertical strains are the same regions as the largest strains in horizontal direction, see Figure 7.23. The large vertical and horizontal strains in these regions are probably because of the knots in the cross section, as mentioned in the discussion of Figure 7.23, and because of the annual rings are tilted roughly 45 degrees to the loading direction. In an area where the annual rings are tilted approximately 45 degrees to the load direction, the stiffness of the shear modulus has a great impact on the stresses and strains.

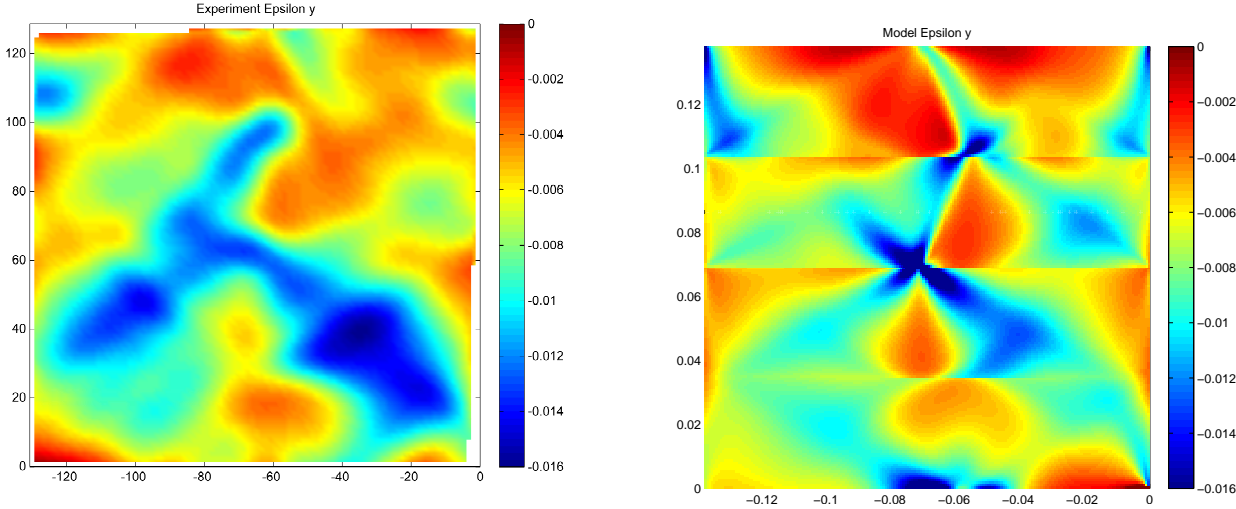


Figure 7.24: Strains in vertical direction ϵ_y , Sample 11. Left: Experiment, Right: FE-model

Finally, the shear strains are illustrated in Figure 7.25. The behavior of discontinuous strains over the interfaces of the lamellae is well simulated by the model. The discontinuity occurs because of the discontinuity in the annual rings. This property is a main difference between glulam and solid timber.

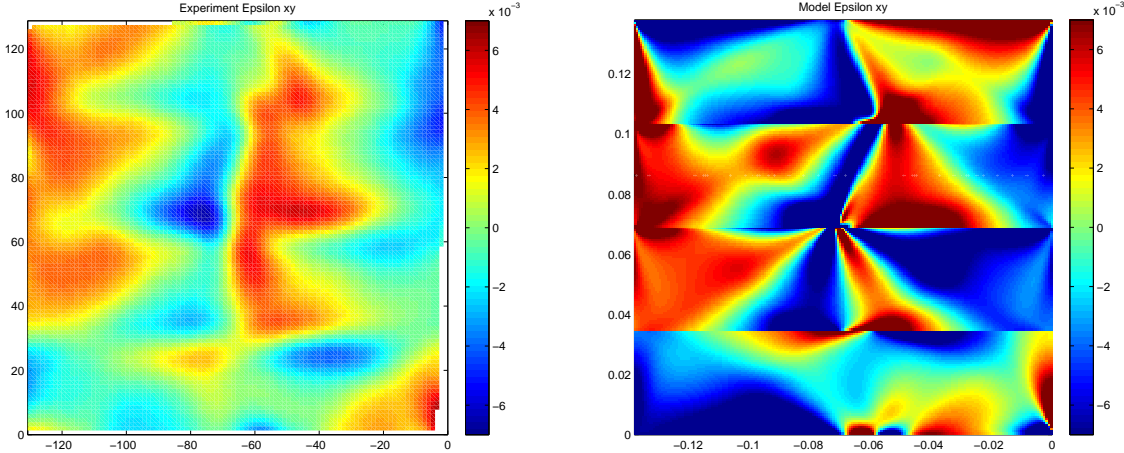


Figure 7.25: Shear strains ϵ_{xy} , Sample 11. Left: Experiment, Right: FE- model

7.3.3 Norris failure criteria

According to the model the first crack will occur in the interface between the lamellae in the middle, see Figure 7.26. The left plot in Figure 7.26 shows that the first region to fail is the one closest to the pith of the third lamella. Near the pith, the global stiffness in the vertical direction is reduced since the annual rings curvature becomes large.

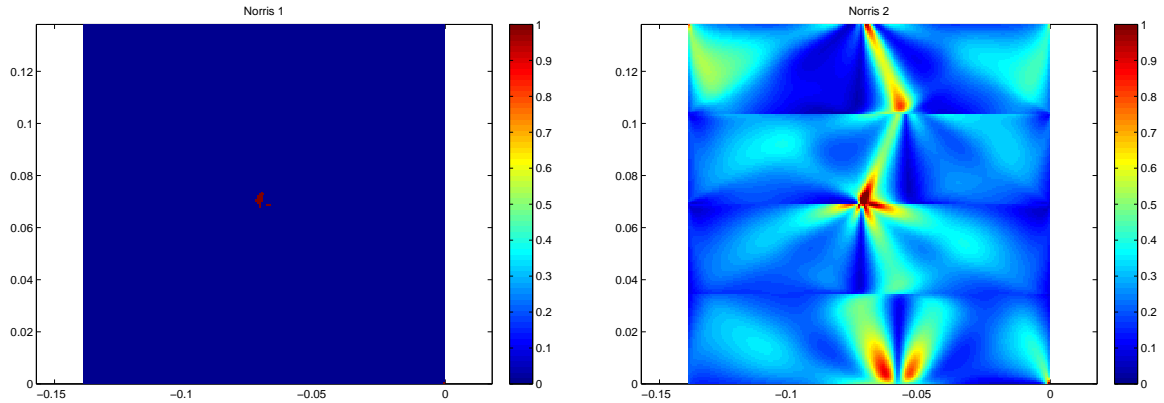


Figure 7.26: Norris failure criteria, Sample 11. Left: Red marks the region where the first crack is predicted by the model, Right: Effective stress based on Norris failure criterion

The point where the first crack initiates is marked in an image of the sample from the experiment, Figure 7.27. Note that the point where the crack occurs is the same as Norris failure criteria predicts in the model.

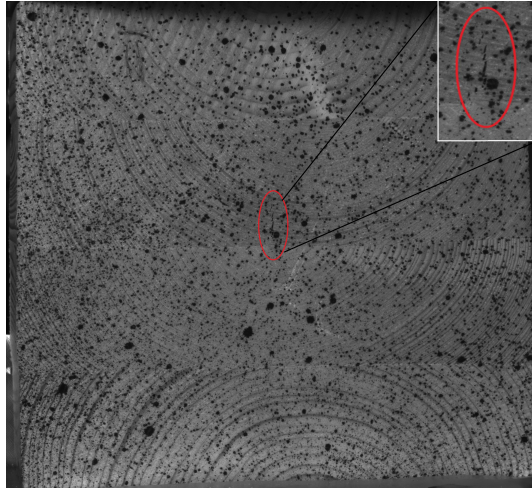


Figure 7.27: Image showing where the first crack occurred during testing, Sample 11

7.4 Sample 16 - 5 Lamellae

Sample 16 is a five lamellae test specimen. Images of the sides, Figure 7.29, reveals that there are some knots in the specimen.



Figure 7.29: Images of the sides of Sample 16. (e): Cross- section used for measurements.

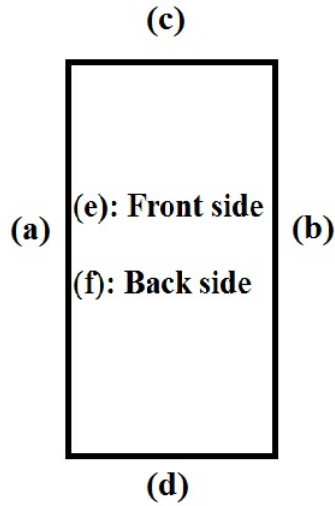


Figure 7.30: Scheme of which image corresponds to which side of the sample as seen by the cameras.

7.4.1 Stress- Deformation plot

The stress- deformation graph, see Figure 7.31, shows a linear elastic behavior of the experiment curve up to approximately 2 MPa. The first crack initiates at 2.6 MPa after some nonlinear behavior. The model curve is almost parallel to the linear elastic part of the experimental curve, indicating that the stiffness in global direction of the model is close to the global stiffness of the sample. The fact that the first crack occurs close to the linear elastic range and the model and experiment have a similar stress- deformation ratios, indicates that the model has some of the conditions needed to predict where the first crack occurs.

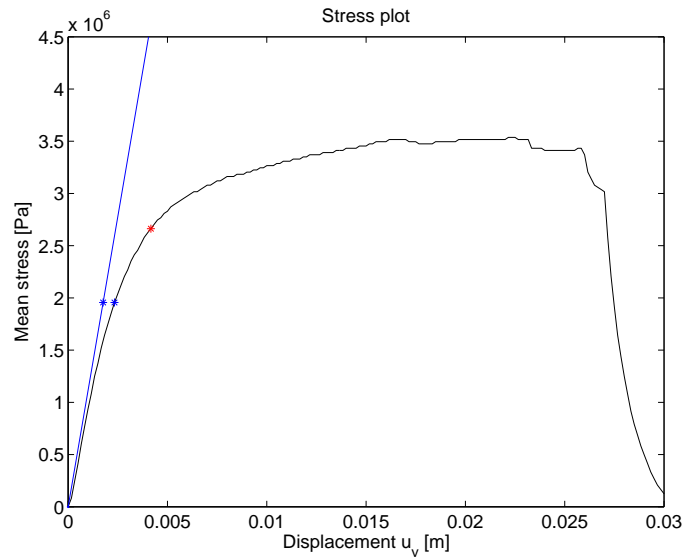


Figure 7.31: Stress- deformation plot, Sample 16. Black: Experiment, Blue: FE- model, “*” marks the initial crack, “*” mark the points for the comparison of the strains.

7.4.2 Strains

Comparison of the strains in horizontal direction in Figure 7.32 shows many similarities between model and experimental results. The model manages to simulate the correct distribution of the strains. Some of the largest differences in the horizontal strains seem to be at the top of the sample. Deviations in the boundaries at the top are possible reasons for the differences. As seen in Figure 7.29, the lamellae of Sample 16 have quite circular annual rings. The circular annual rings in the sample may contribute to the good conformity of model and experimental results. Another possible reason for the similarities may be related to the size of the sample. Since the sample has five lamellae with different annual ring pattern the impact to the strains caused by the annual rings is large. The width and the depth of the sample are small in comparison to the height which may contribute to the impact of the annual rings. Further, the influence of the boundaries is smaller for tall samples. Note that some of the largest strains are beneath the pith of the upper most lamella, the reason for this is discussed further in the analysis of the strains in vertical direction.

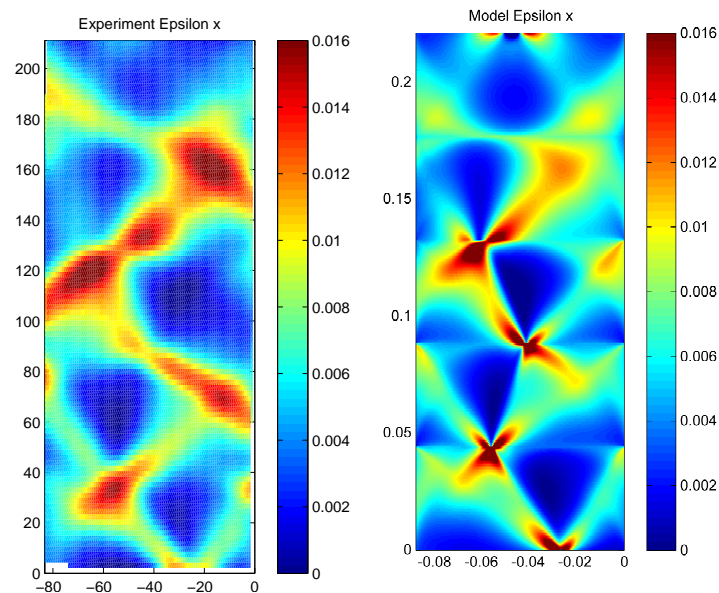


Figure 7.32: Strains in horizontal direction ε_x , Sample 16. Left: Experiment, Right: FE- model

There is also a good conformity regarding the vertical strains, see Figure 7.33. The reasons for the similarities and differences are mainly the same as for the horizontal strains. The areas with the largest strains, the blue regions, are in the areas right beneath the piths of the above lamellae, see Figure 7.29 (e). The reason for the large strains is that the stiffness in the radial direction is greater than in the tangential direction. Figure 7.29 (e), shows that the material directions beneath the pith of lamella 4 and lamella 2 are tilted approximately 45 degrees to the vertical direction. The stiff radial direction above the pith takes much of the loads and leads them into the area beneath the pith where the material is softer due to the change in the material directions. From the experiment plot in Figure 7.33 it can be seen that the area with the largest strains in the bottom of the sample spreads out in four directions. These four directions are in the direction of where the annual rings have a curvature of 45 degrees to the loading direction. This indicates that the global stiffness in the vertical direction is lower where the directions of the annual rings are 45 degrees to the load direction.

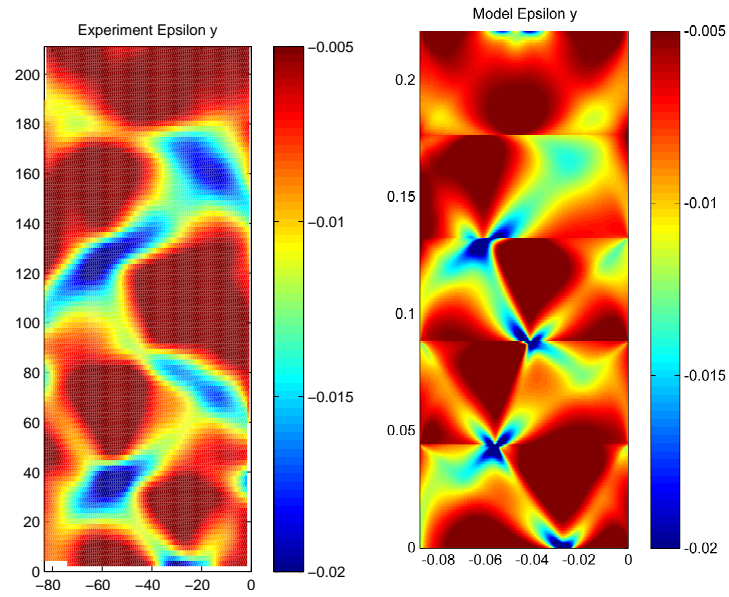


Figure 7.33: Strains in vertical direction ε_y , Sample 16. Left: Experiment, Right: FE- model

The shear strains are presented in Figure 7.34. The shear strains show greater differences than the horizontal and vertical strains. The choice of the stiffness parameters has a larger impact on the shear strains than on the vertical and horizontal strains. The shear strains are acting in the plane and the ratio of the stiffness properties and the Poissons value therefore have a large impact. The discontinuous pattern of the annual rings over the borders of the lamellae also have a larger impact on the shear strains.

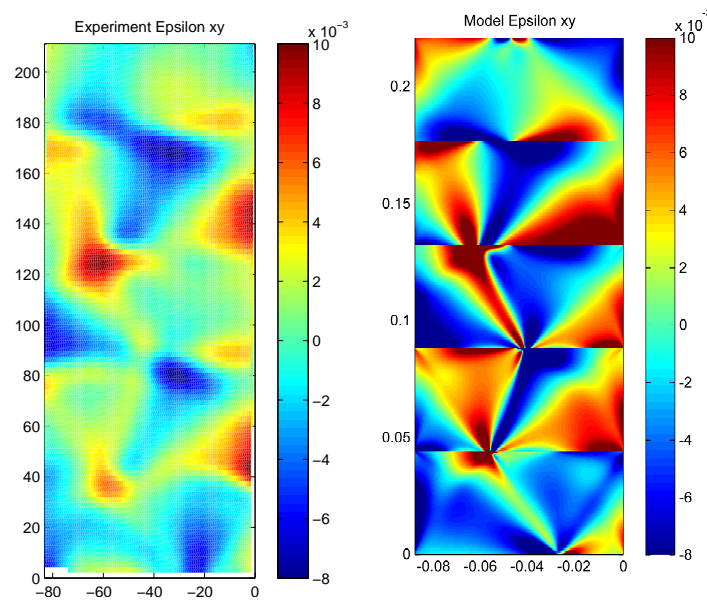


Figure 7.34: Shear strains ε_{xy} , Sample 16. Left: Experiment, Right: FE- model

7.4.3 Norris failure criteria

The model predicts that the first crack will initiate in the bottom boundary of the sample, Figure 7.35. This prediction is wrong according to the experimental result. As seen i Figure 7.36 the first crack occurs between the third and second lamella. The second crack to initiate in the experiment is however in the bottom boundary. The point where the model predicts the first crack is the center of the pith of the bottom lamella. It is reasonable that large strains will occur in this point. If the boundaries in the experiment would be friction free, as the case in the model, it is possible that the crack in the experiment would occur in the point predicted by the model.

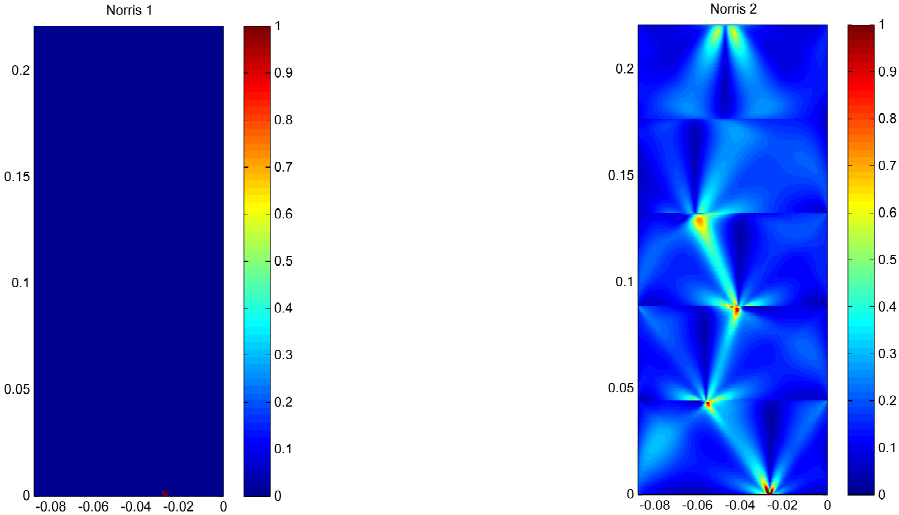


Figure 7.35: Norris failure criteria, Sample 16. Left: Red marks the region where the first crack is predicted by the model, Right: Effective stress based on Norris failure criterion

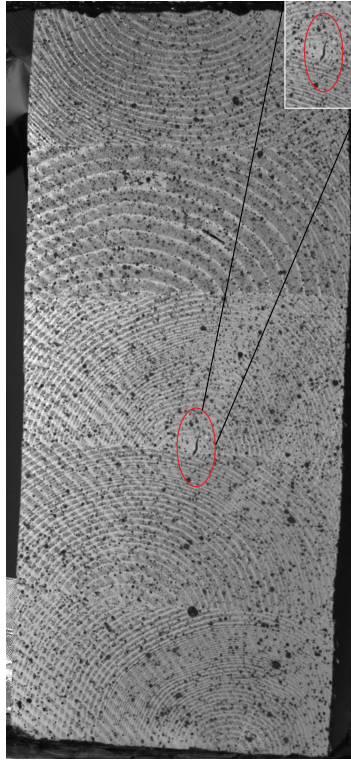


Figure 7.36: Image showing where the first cracks occurred during testing, Sample 16

Chapter 8

Discussion

8.1 Improvements of model

The precision of the model will never be better than the quality of the input data. It is therefore very important to ensure a good accuracy of this data. To improve the precision of the strength and stiffness properties one must know the wood species, the density of the wood, the moisture content, the range of annual rings in the particular piece of wood etcetera. Another improvement of the model is to create boundary conditions that better reflect the real conditions in the experiment. Boundary conditions modeled with springs as an attempt to recreate the scenario of friction may improve the results. The elements in the model are quadrilateral elements which use a linear displacement approximation of the nodal values over the areas of four triangles. One can also use (in the case of plane stress) Melosh elements, Turner- Clough elements or Isoparametric elements which may improve the results. The annual rings are modeled as cylindrical which is not always the case of the annual rings in wood. If the annual ring pattern of the wood differs significantly from the cylindrical shape, another approximation in the model may improve the results.

The model is linear elastic which is a good approximation of the behavior of wood before large deformations. The material behavior is however not ideal linear elastic and a model with a nonlinear approach can improve the results. The largest error sources in the model are because of neglected imperfections in the wood. By taking the imperfections of the wood into account the model will be considerably more accurate.

8.2 The Eurocodes

The design codes for structural timber and glulam, regarding compression perpendicular to the grain, are presented in Chapter 3. One of the aims in this thesis is to discuss how well the Eurocodes describe the behavior of glulam in compression perpendicular to the grain, these being based on the testing procedure of EN 408. From the experimental results, the strength in compression perpendicular to the grain can be calculated. Table 8.1 shows the strength values in compression perpendicular to the grain for all samples. In Figure 8.1, the strength values are plotted in the stress- deformation curves from the experiment. It can be seen that the strength properties are in the nonlinear region of the material behavior. According to (EN 408 : 2010 + A1 : 2012), the strength, $f_{c,90}$, shall utilize some of the remaining strength after the material behavior has entered its plastic deformation.

The initial cracks are also marked in the stress- deformation curves in Figure 8.1. For some samples the calculated strength, $f_{c,90}$, is larger than the stress state for which the first crack

occurs. For other samples the calculated strength is lower than the stress state for the first crack. In the calculation of $f_{c,90}$ as presented in Chapter 4, the risk of crack propagation is not taken into consideration. The calculation of $f_{c,90}$ only says that the maximum strength is reached for a certain deformation. Wood is however an anisotropic material and the strength for an element of wood, for instance the samples in this thesis, depends on how the principal directions are orientated in the element. One can question if the strength tests and the calculation of $f_{c,90}$, according to (EN 408 : 2010 + A1 : 2012), are accurate enough. In design situations it is impossible to know if the strength values will lead to cracks and the size of these cracks. If the wood elements have a poor annual ring pattern with respect to the strength properties, cracks may initiate which probably makes the material weaker. Another uncertainty is whether $f_{c,90}$ is a good assumption of the material strength independent of the loading conditions. For instance, if the samples in this thesis would be a part of a beam, continuously supported in the bottom boundary and loaded in compression at the upper boundary, the conditions for the crack propagation would probably be different.

In the design codes of wood in compression perpendicular to the grain, different loading scenarios are taken into account by the increase factor $k_{c,90}$. For special conditions, presented in Chapter 4, the compressive stress may obtain a larger value thanks to the $k_{c,90}$ - factor. The idea of the factor is to take advantage of different phenomena, for instance the load bearing effect in the surrounding material of the load. Since wood is a complex material and has a large variability in its features, the phenomena taken into account in $k_{c,90}$ are very hard to calculate. For some conditions the factor can be set to 1.5. In equation (3.5), $k_{c,90}$ being 1.5 leads to an increase of the design compressive stress, $\sigma_{c,90,d}$, by 50 %. For the loading condition in the experimental work and from the stress- deformation curves, Figure 8.1, an increase of the compressive stress by 50 % in the region of the strength values, “o” in Figure 8.1, would lead to failure for all samples. Thus, if it is assumed that the approach in Eurocode 5 with $k_{c,90}$ is appropriate, this means that some sort of limitation of the use of $k_{c,90}$ should be defined.

Table 8.1: Strength properties of the Samples

Nr Lamellae	Sample	$f_{c,90}$	$f_{c,90,crack}$	$f_{c,90,max}$
3	3	2.8	3.4	4.4
3	9	2.9	3.0	4.6
3	12	3.1	3.4	4.8
3	21	2.8	2.5	3.8
4	2	3.4	3.6	4.0
4	8	3.5	2.5	4.8
4	11	3.1	3.5	4.1
4	14	2.6	2.2	5.2
4	17	3.4	3.1	4.6
4	18	3.1	3.2	4.2
4	19	3.4	2.5	4.1
4	20	3.8	4.0	5.0
4	22	3.3	2.8	5.0
5	1	2.6	2.5	2.9
5	4	2.5	2.5	3.0
5	10	2.8	3.0	3.4
5	13	2.6	2.5	3.3
5	16	2.5	2.6	3.5
5	27	2.8	2.0	3.4

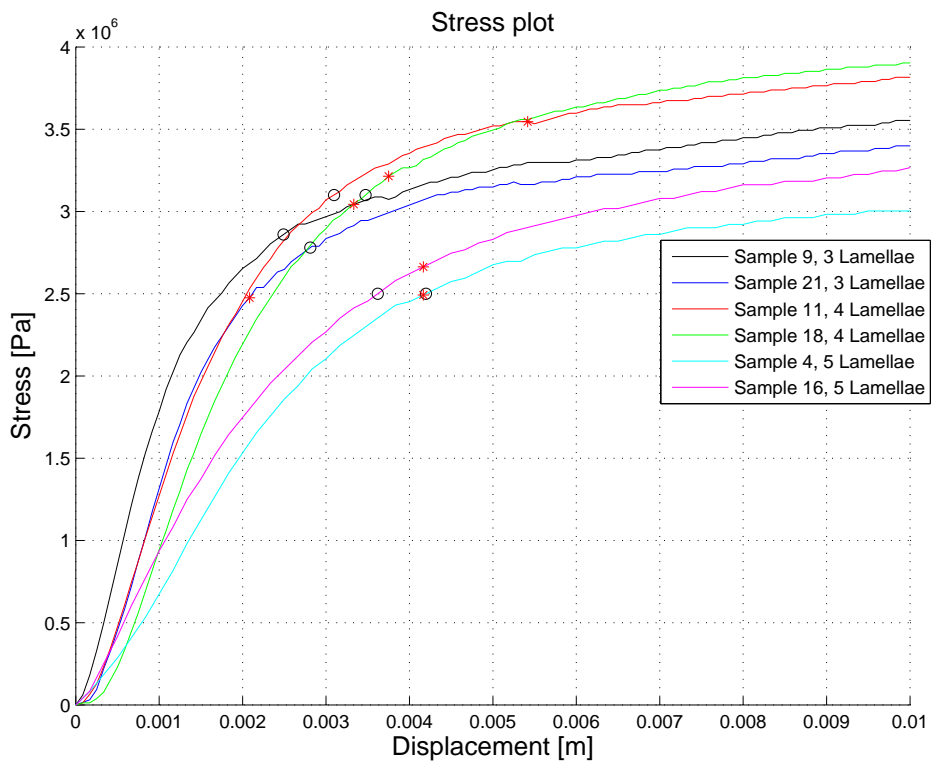


Figure 8.1: Stress- deformation plot of 3, 4 and 5 lamellae specimen. “o” marks the strength properties and “*” marks the initial crack

Chapter 9

Conclusions

As a building material there are a lot of benefits using wood. Thanks to the biological nature of wood, the material has great strength in the fibre direction and a low density which are good properties for building materials. Another good feature of wood, with an increasing importance in the society, is that the material is renewable. But wood being a biological material also makes it anisotropic with large variability in its material properties. This makes wood a complex material, and as a result the calculations of wood requires many simplifications.

One simplification in design situations of wood is neglecting that the strength properties depends on the pattern of the annual rings. The model and the laboratory work in this thesis show that the annual rings have a large impact on the behavior of stresses and strains in a plane perpendicular to the grain. In the determination of the strength properties in (EN 408) the value of the compressive strength only depends on a limit of plastic deformation. In Eurocode 5, different material behavior for different loading scenarios are simplified by the increase factor, $k_{c,90}$. The increase factor may be chosen to 1, 1.5 or 1.75 for glulam depending on support conditions. The contribution to the design compressive stress, thanks to $k_{c,90}$, is large while there are many uncertainties regarding the simplifications. According to the results in this thesis, some sort of limitation in the use of $k_{c,90}$ should be defined.

The finite element model captures most of the material behavior in the glulam cross sections. In the linear elastic range of the material behavior, the model and the results from the experiments show a good conformity in the case of few imperfections in the samples. For many samples the model manages to predict where the first crack will initiate. Especially for the five lamellae samples the model manages to describe the material behavior very well. A reason for the better results of the larger samples may be a smaller impact of the boundary conditions. One way to improve the model is to make the boundary conditions in the model more similar to the real conditions in the experiment.

References

- [1]: Thelandersson, S.: Timber Engineering, John Wiley Sons, Chichester, 2003.
Chapter 1: Timber Engineering- General Introduction
- [2]: Persson, K. (2000): Micromechanical modelling of wood and fibre properties. Doctoral Thesis, Lund University, Division of Structural Mechanics, Lund, Sweden
- [3]: Danielsson, H. (2013): Perpendicular to grain fracture analysis of wooden elements: Models and Applications. Doctoral Thesis, Lund University, Division of Structural Mechanics, Lund, Sweden
- [4]: Limträhandbok, Olle Carling Ingenjörbyrå AB. Svenskt Limträ AB, Stockholm 2002,
<http://www.svensktlimtra.se/sv/limHTML/> (Acc 2015-02-24)
- [5]: Thelandersson, S.: Timber Engineering, John Wiley Sons, Chichester, 2003.
Chapter 12: Design of Structures Based on Glulam, LVL and Other Solid Timber Products.
- [6]: Ottosen, S. N. et al: Introduction to the finite element method, Lund University, Lund, 1992
- [7]: Austrell, P- E et al (2004): Calfem: A Finite Element Toolbox Version 3.4, Lund University, Division of Structural Mechanics, Lund, Sweden
- [8]: Woodworking Industry Information, Montrose, Pennsylvania, USA, 2015
http://www.woodweb.com/knowledge_base/Warp_in_Drying.html (Acc 2015-03-24)
- [9]: Aicher, S., Dill- Langer, G. and Höfflin L.: Effect of Polar Anisotropy Loaded Perpendicular To Grain, Journal of Materials in Civil Engineering, 2001, pp 2-3
- [10]: Gustafsson, P- J., Danielsson, H.: Perpendicular to grain stiffness of timber cross sections as affected by growth ring pattern, size and shape. European Journal of Wood and Wood Products, Springer Verlag Berlin Heidelberg, 2012, pp 3- 6
- [11]: Hoffmeyer, P., Damkilde, L., Pedersen, T. N.: Structural timber and glulam in compression perpendicular to grain. Holz als Roh- und Werkstoff, Springer- Verlag, 2000, pp 4- 6
- [12]: Shipsha, A., Berglund, A. L.: Shear coupling effect on stress and strain distributions in wood subjected to transverse compression. Composites Science and Technology, Science Direct, Elsevier, 2007, pp 1-8

- [13]: Astrup, T., Clorius, C. O., Damkilde, L., Hoffmeyer P.: Size effect of glulam beams in tension perpendicular to grain. Wood Sci Technol, Springer- Verlag, 2006, pp 1-4
- [14]: Department of Mathematics, Oregon State University, Oregon, 1996
<http://math.oregonstate.edu/home/programs/undergrad/CalculusQuestStudyGuides/vcalc/coord/coord.html>
- [15]: Norris, C. B. (1962): Strength of orthotropic materials subjected to combined stresses. Report No. 1816, Forest Products Laboratory, Madison, Wisconsin, USA.
- [16]: EN 14080:2013 Timber structures - Glued laminated timber and glued solid timber - Requirements
- [17]: McCormick, N., Lord J.: Digital Image Correlation. Materialstoday Vol 13 No. 12, National Physical Laboratory, 2006
- [18]: ARAMIS Digital Image Correlation System helps Adidas design the Ultra Boost, Trilion, Philadelphia, USA, 2015,
<http://trilion.com/digital-image-correlation-system-adidas/> (Acc 2015-04-09)
- [19]: EN 1995-1-1:2004 Eurocode 5: Design of timber structures- Part 1-1: General- Common rules and rules for buildings
- [20]: Eurokoder, Swedish Standards Institute, Stockholm,
http://www.sis.se/tema/eurokoder/om_eurokoder/ (Acc 2015-03-29)
- [21]: SS- EN 408 : 2010 + A1 : 2012. Timber structures- Structural timber and glued laminated timber- Determination of some physical and mechanical properties
- [22]: Axelson, M. (2014): Compression perpendicular to grain- a Swedish survey. SP Rapport, Sveriges Tekniska Forskningsinstitut
- [23]: EN 338:2009 Structural timber- Strength classes
- [24]: Gustafsson A. and Eriksson P- E, SP Trä., Engström S., Luleå Tekniska Univeristet., Wik T., Högskolan Dalarna., Serrano E., Linneuniversitetet, (2013): Handbok: för beställare och projektörer av flervånings bostadshus i trä. SP rapport 2012:70, Sveriges Tekniska Forskningsinstitut.
- [25]: Rapport 1999:1, (1999): Reduced emissions of carbondioxide through changed use of materials - a pilot study. Statistiska centralbyrån, Örebro, pp 23- 24

Appendices

Appendix A

Results

Sample 9 - 3 Lamellae

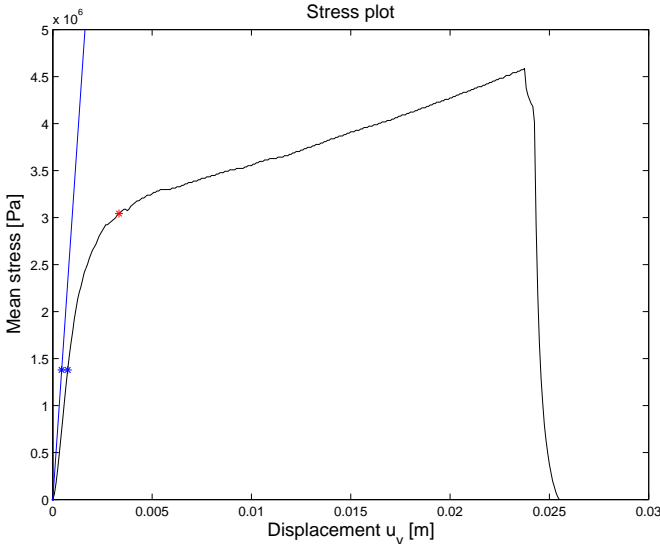


Figure 9.1: Stress- deformation plot, Sample 9. Black: Experiment, Blue: Model, “*” marks the initial crack, “*” mark the points for the comparison of the strains.

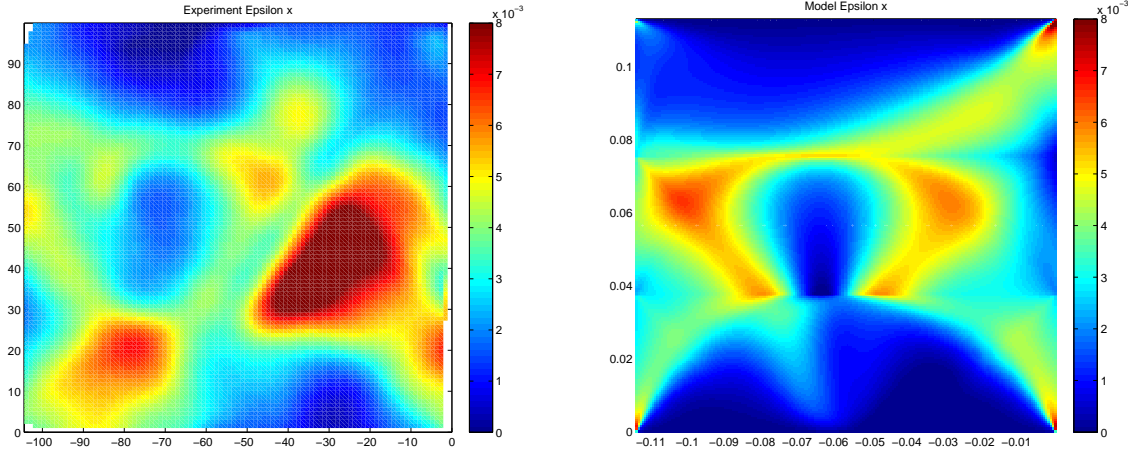


Figure 9.2: Strains in horizontal direction ϵ_x , Sample 9. Left: Experiment, Right: FE- model

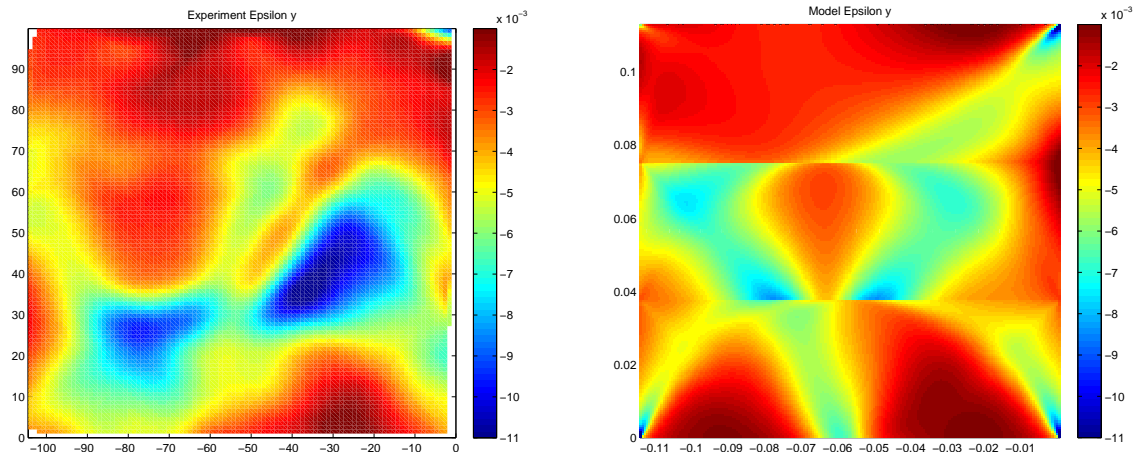


Figure 9.3: Strains in vertical direction ε_y , Sample 9. Left: Experiment, Right: FE- model

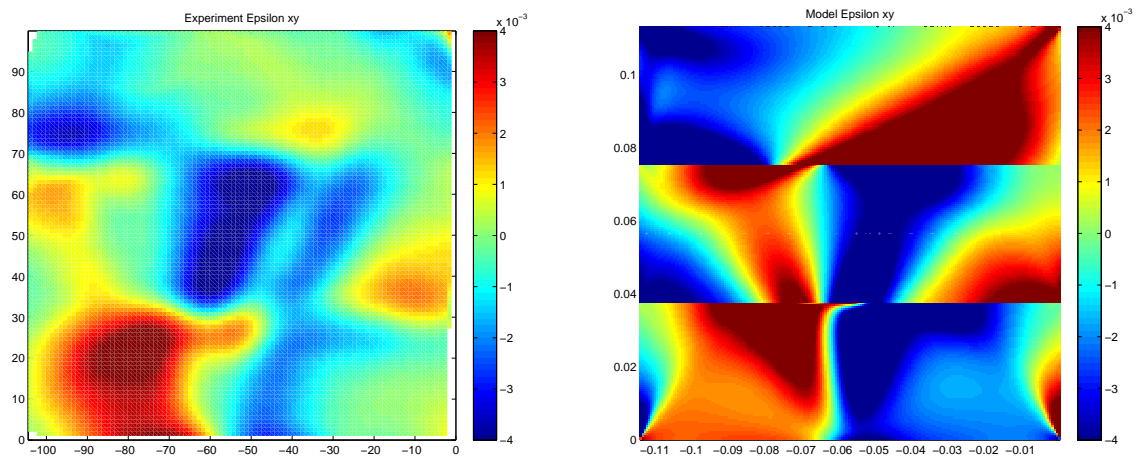


Figure 9.4: Shear strains ε_{xy} , Sample 9. Left: Experiment, Right: FE- model

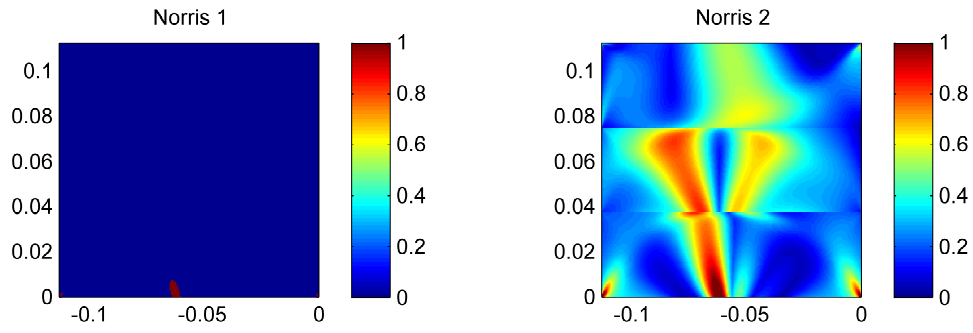


Figure 9.5: Norris failure criteria, Sample 9. Left: Red marks the region where the first crack is predicted by the model, Right: Effective stress based on Norris criterion

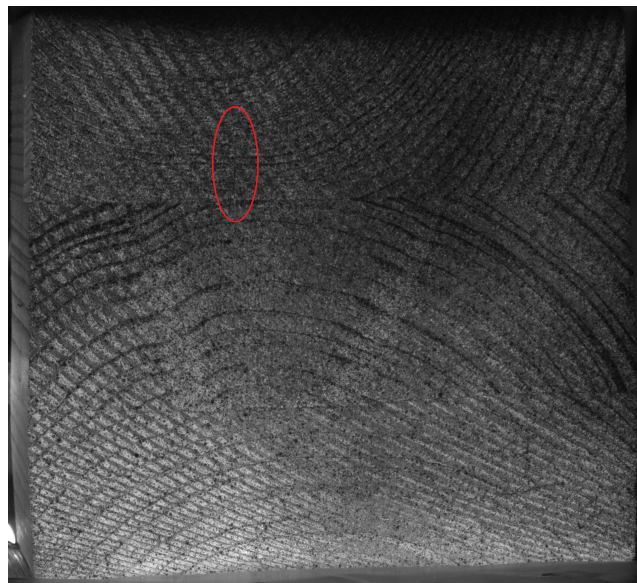


Figure 9.6: Image showing where the first cracks occurred during testing, Sample 9

Sample 21 - 3 Lamellae

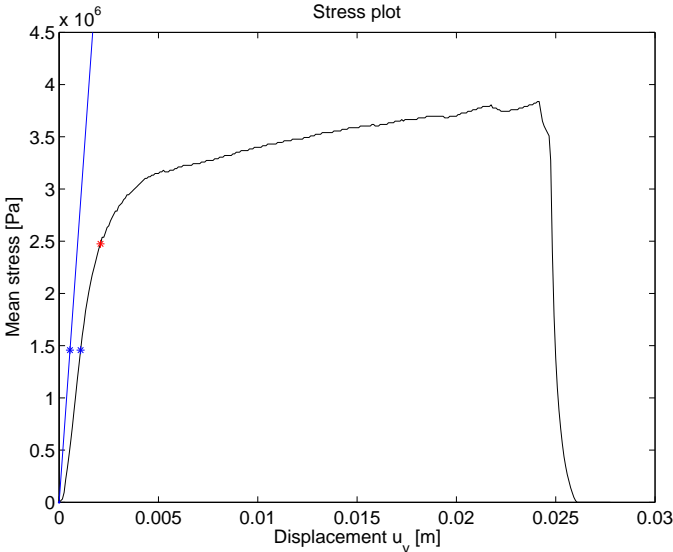


Figure 9.7: Stress- deformation plot, Sample 21. Black: Experiment, Blue: Model, “*” marks the initial crack, “*” mark the points for the comparison of the strains.

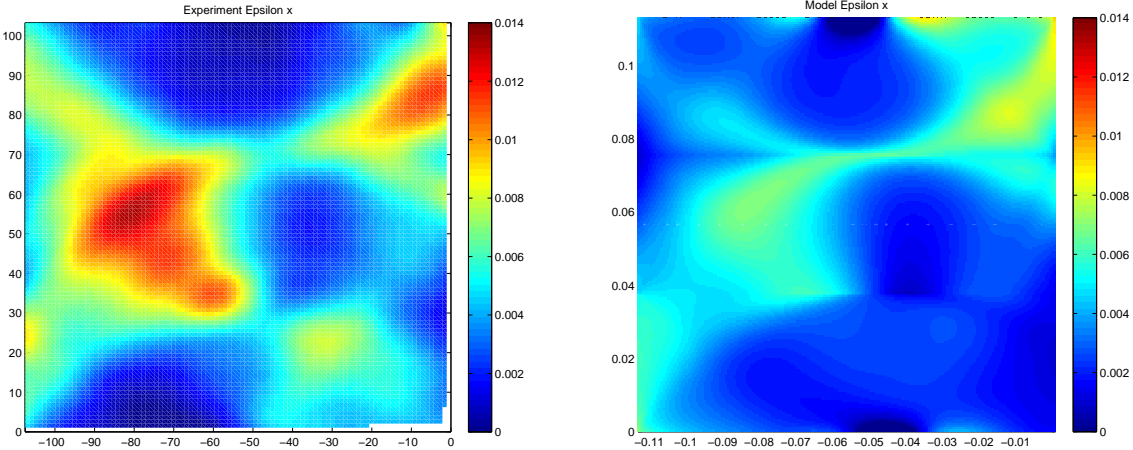


Figure 9.8: Strains in horizontal direction ϵ_x , Sample 21. Left: Experiment, Right: FE- model

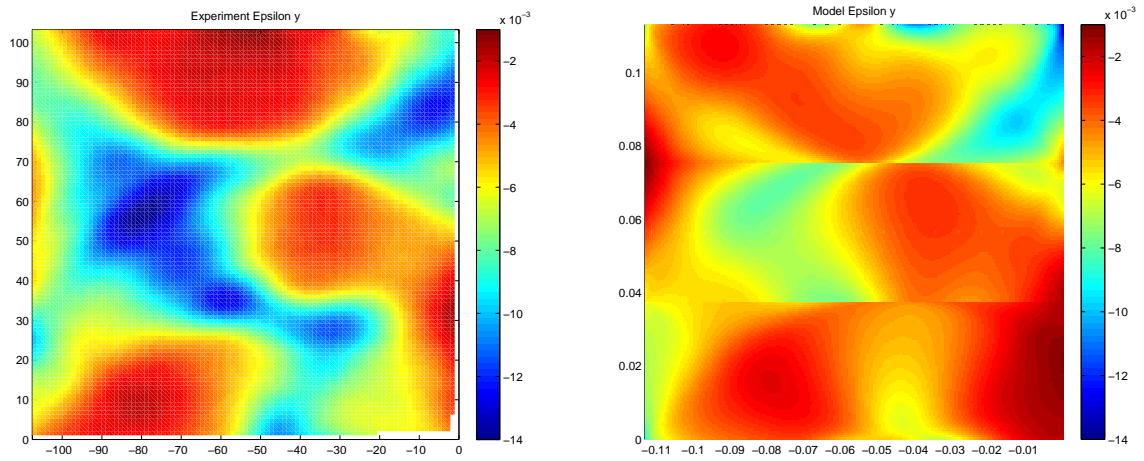


Figure 9.9: Strains in vertical direction ε_y , Sample 21. Left: Experiment, Right: FE- model

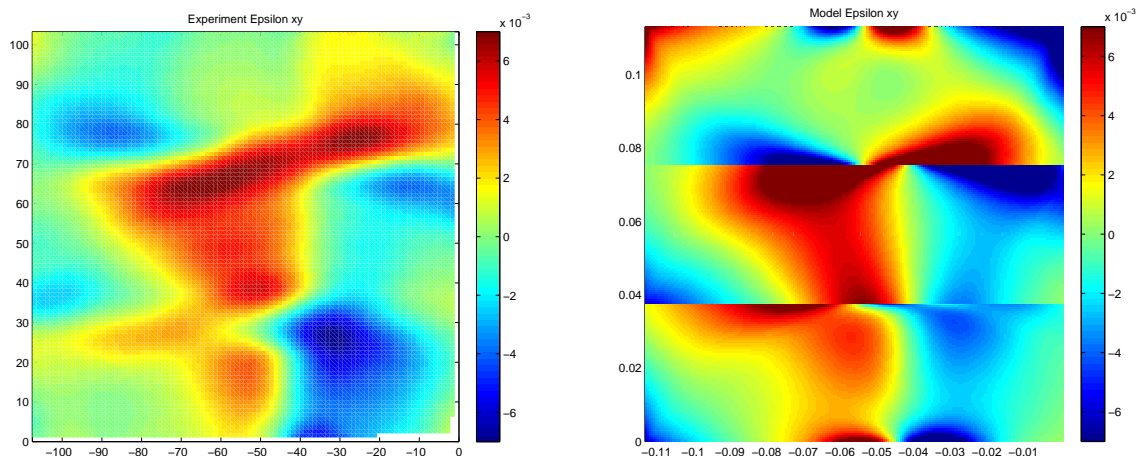


Figure 9.10: Shear strains ε_{xy} , Sample 21. Left: Experiment, Right: FE- model

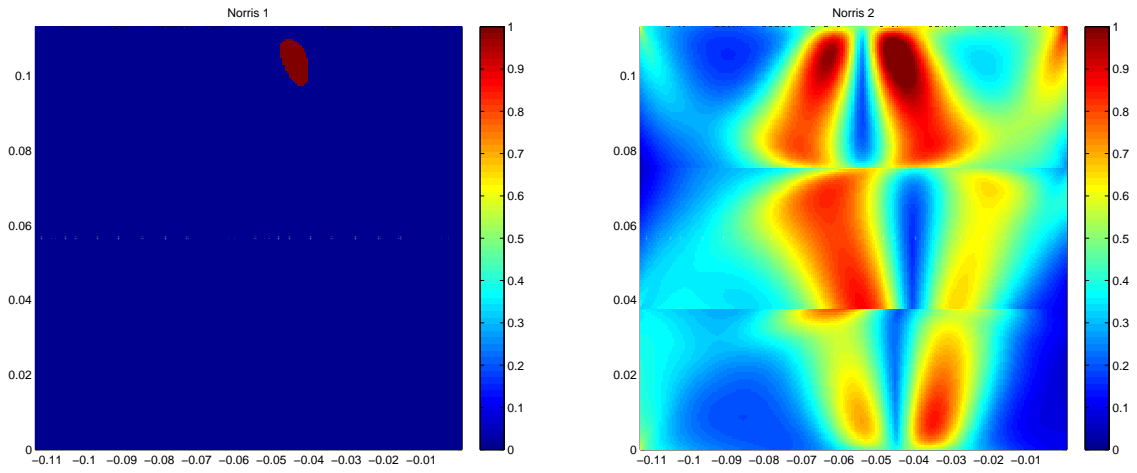


Figure 9.11: Norris failure criteria, Sample 21. Left: Red marks the region where the first crack is predicted by the model, Right: Effective stress based on Norris failure criterion

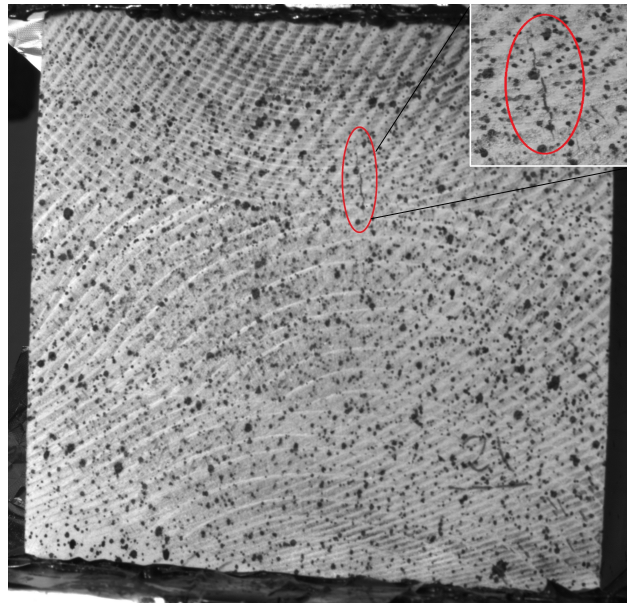


Figure 9.12: Image showing where the first crack occurred during testing, Sample 21

Sample 11 - 4 Lamellae

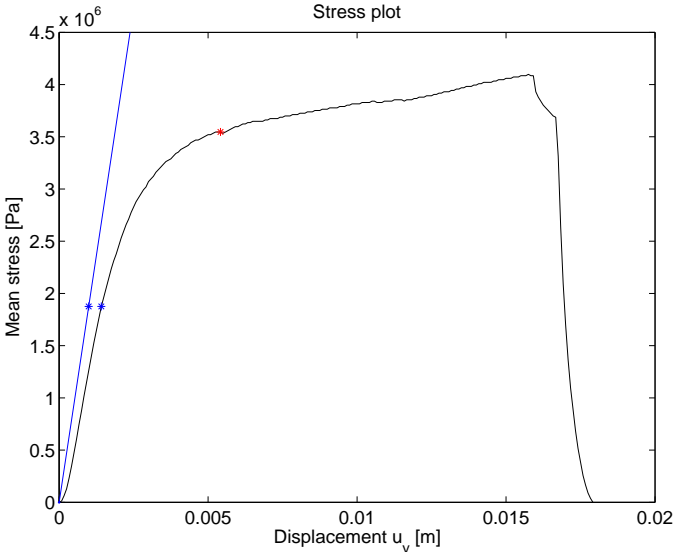


Figure 9.13: Stress- deformation plot, Sample 11. Black: Experiment, Blue: Model, “*” marks the initial crack, “*” mark the points for the comparison of the strains.

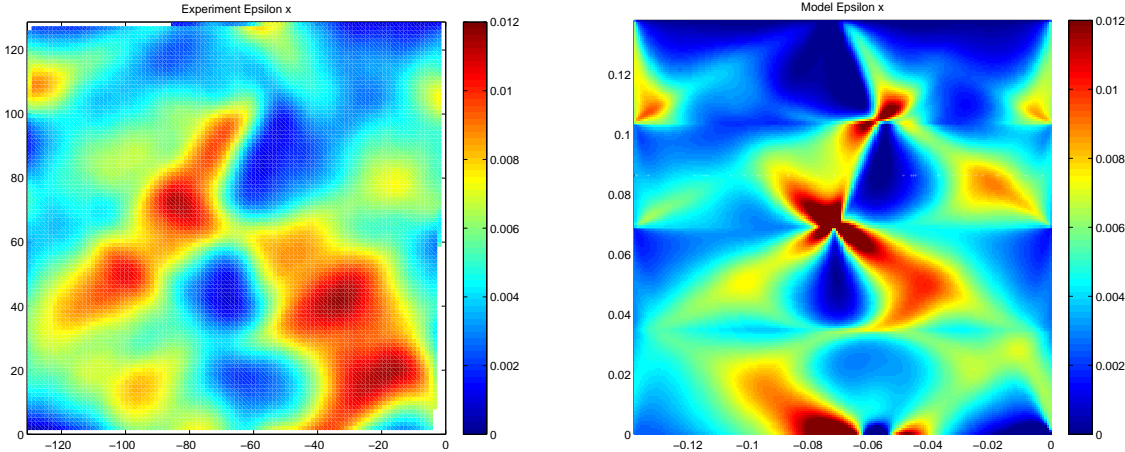


Figure 9.14: Strains in horizontal direction ϵ_x , Sample 11. Left: Experiment, Right: FE-model

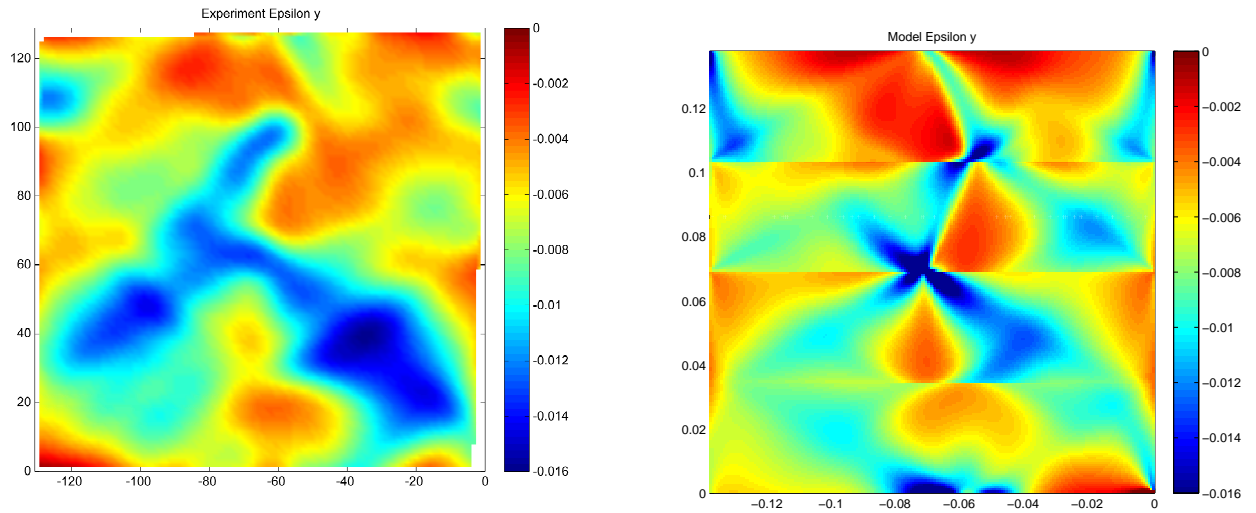


Figure 9.15: Strains in vertical direction ε_y , Sample 11. Left: Experiment, Right: FE-model

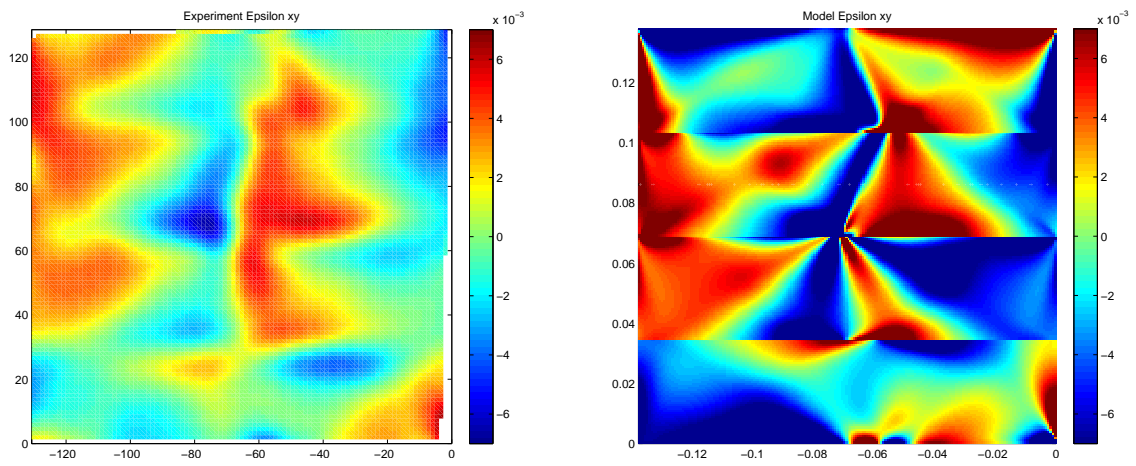


Figure 9.16: Shear strains ε_{xy} , Sample 11. Left: Experiment, Right: FE- model

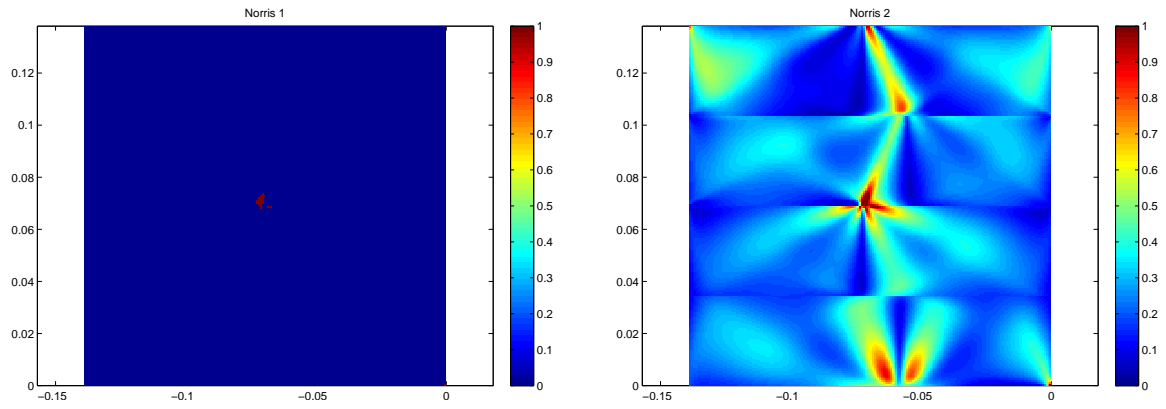


Figure 9.17: Norris failure criteria, Sample 11. Left: Red marks the region where the first crack is predicted by the model, Right: Effective stress based on Norris failure criterion

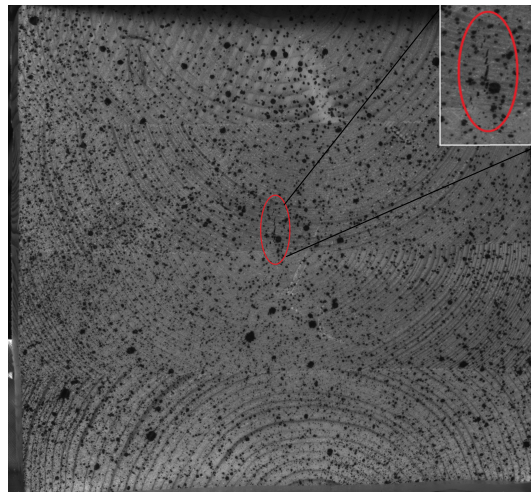


Figure 9.18: Image showing where the first crack occurred during testing, Sample 11

Sample 18 - 4 Lamellae

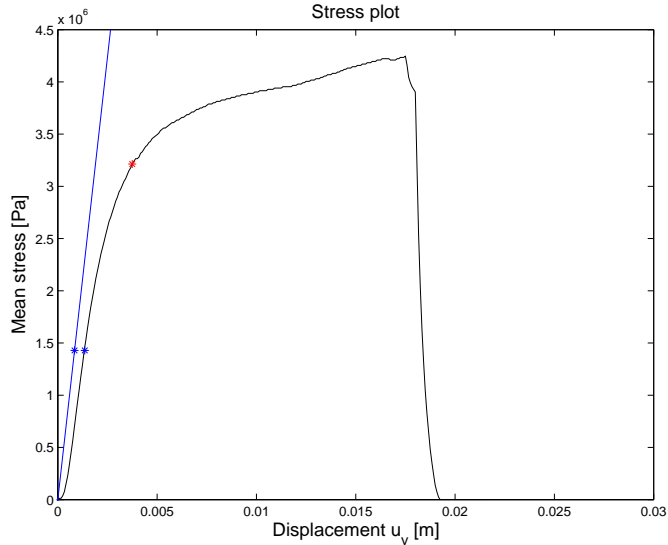


Figure 9.19: Stress- deformation plot, Sample 18. Black: Experiment, Blue: Model, “*” marks the initial crack, “*” mark the points for the comparison of the strains.

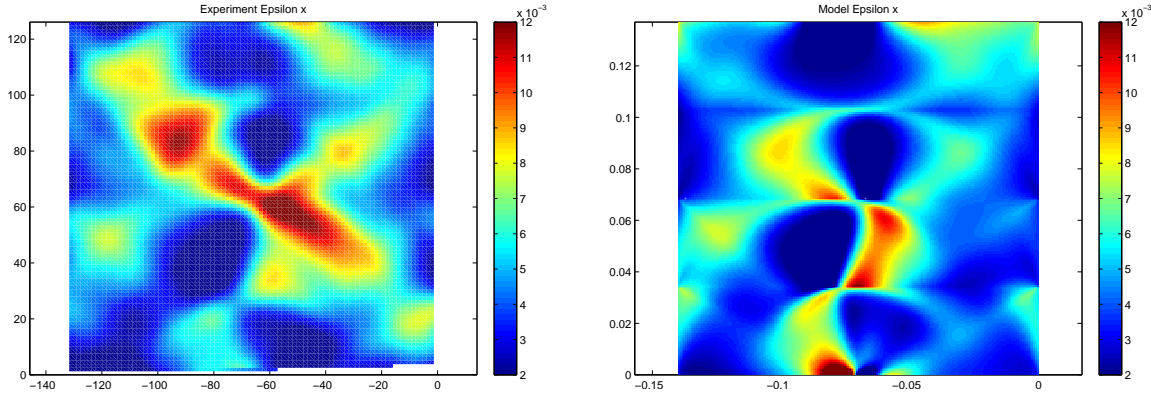


Figure 9.20: Strains in horizontal direction ϵ_x , Sample 18. Left: Experiment, Right: FE- model

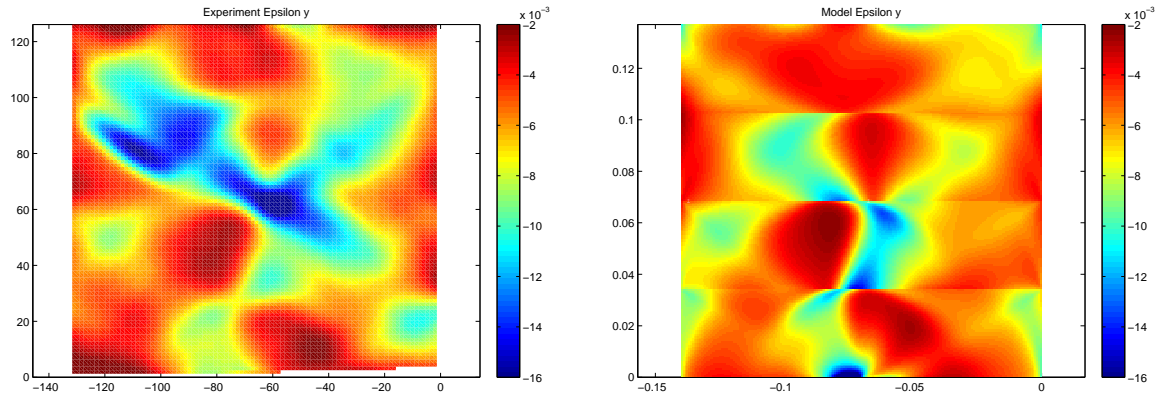


Figure 9.21: Strains in vertical direction ε_y , Sample 18. Left: Experiment, Right: FE- model

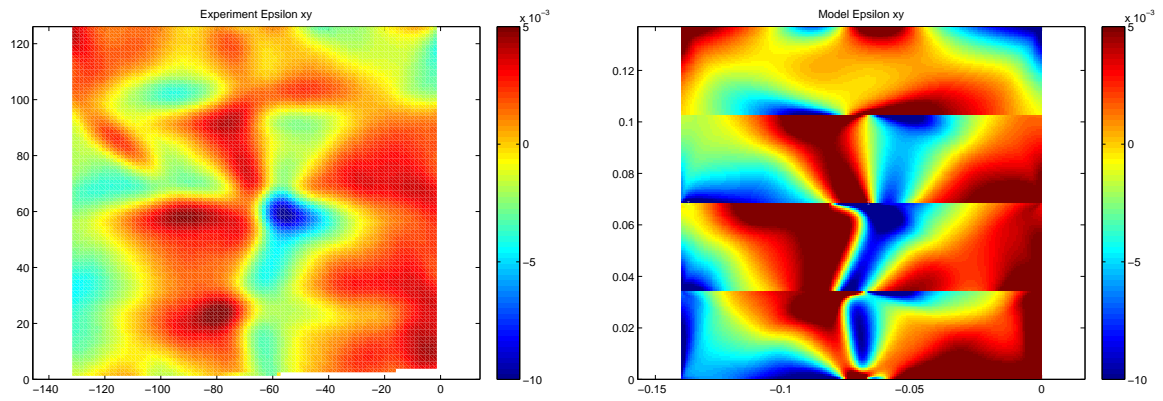


Figure 9.22: Shear strains ε_{xy} , Sample 18. Left: Experiment, Right: FE- model

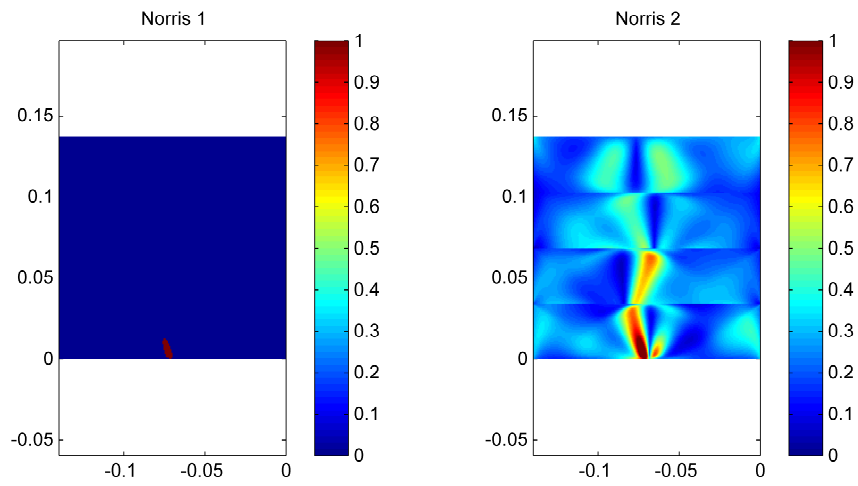


Figure 9.23: Norris failure criteria, Sample 18. Left: Red marks the region where the first crack is predicted by the model, Right: Effective stress based on Norris criterion

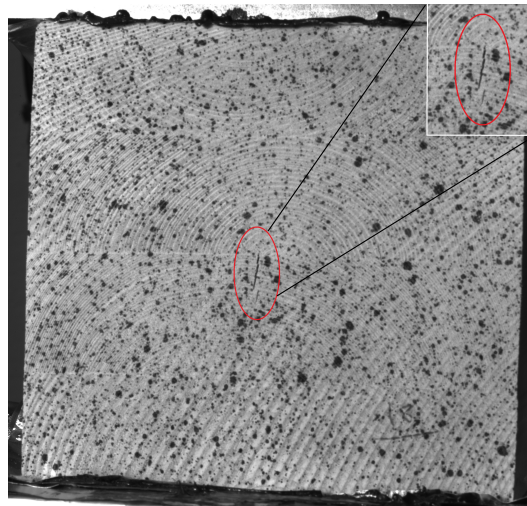


Figure 9.24: Image showing where the first crack occurred during testing, Sample 18

Sample 4 - 5 Lamellae

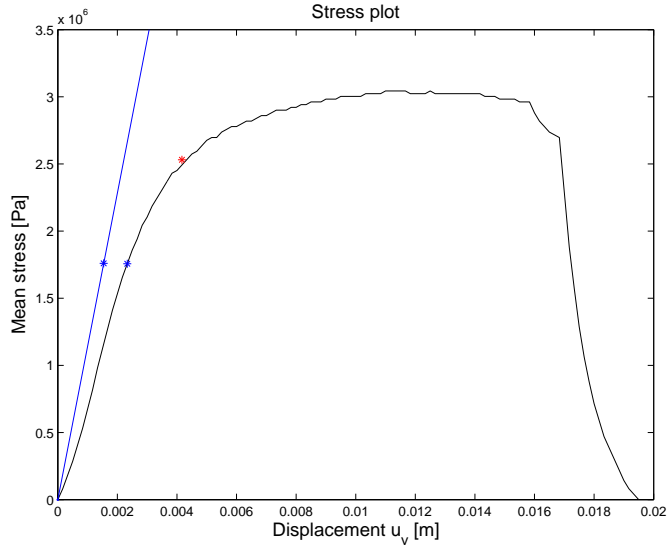


Figure 9.25: Stress- deformation plot, Sample 4. Black: Experiment, Blue: Model, “*” marks the initial crack, “*” mark the points for the comparison of the strains.

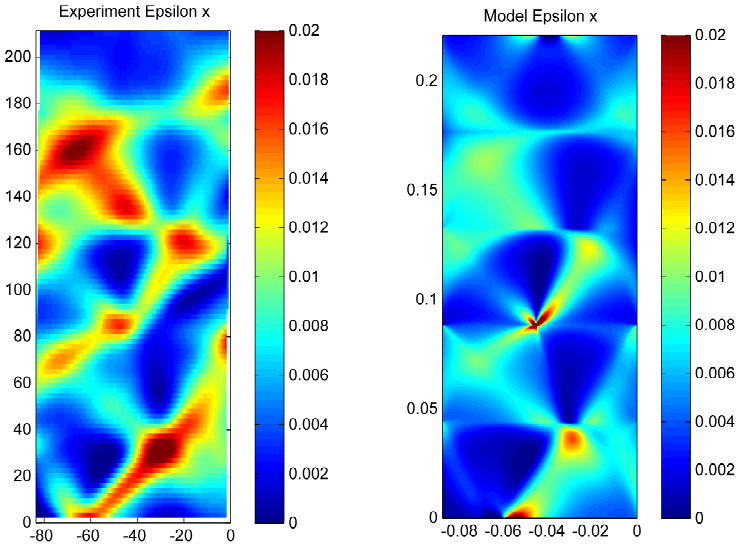


Figure 9.26: Strains in horizontal direction ϵ_x , Sample 4. Left: Experiment, Right: FE- model

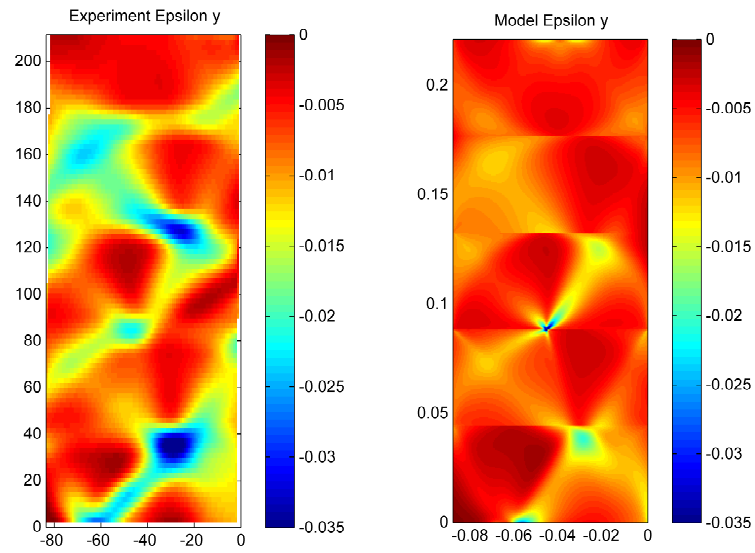


Figure 9.27: Strains in vertical direction ε_y , Sample 4. Left: Experiment, Right: FE- model

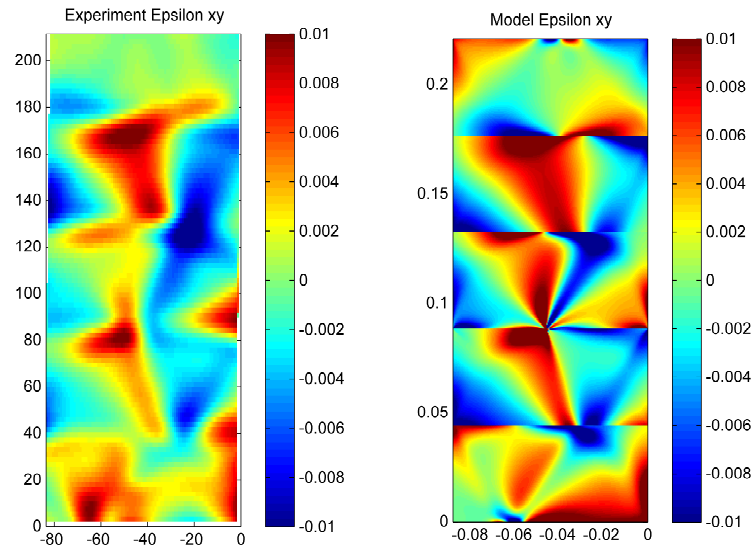


Figure 9.28: Shear strains ε_{xy} , Sample 4. Left: Experiment, Right: FE- model

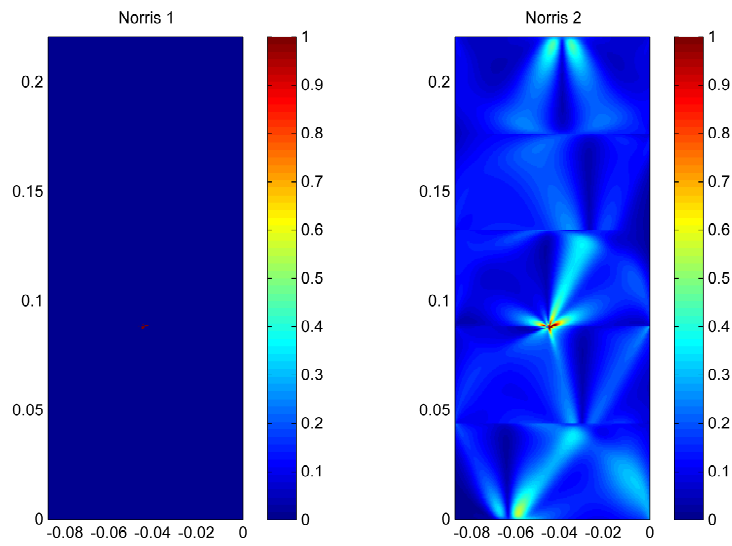


Figure 9.29: Norris failure criteria, Sample 4. Left: Red marks the region where the first crack is predicted by the model, Right: Effective stress based on Norris criterion

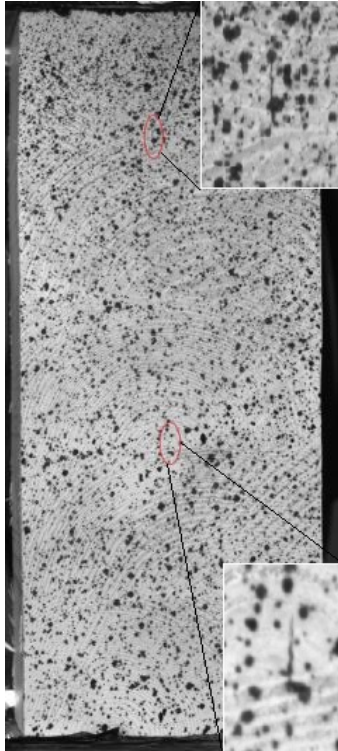


Figure 9.30: Image showing where the first cracks occurred during testing, Sample 4

Sample 16 - 5 Lamellae

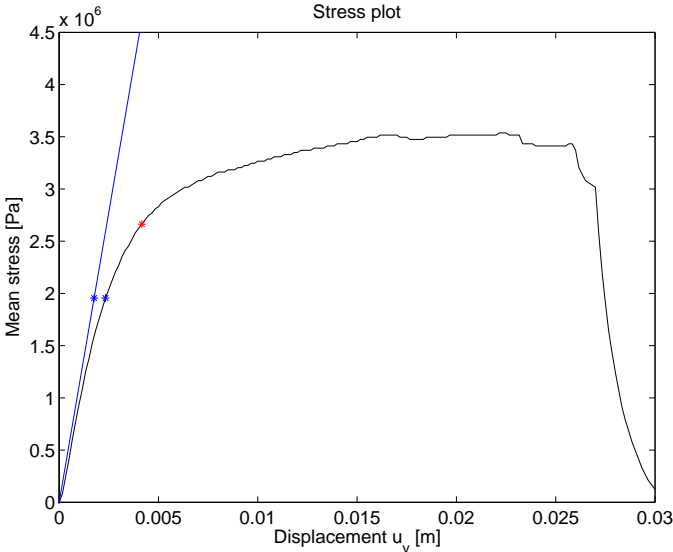


Figure 9.31: Stress- deformation plot, Sample 16. Black: Experiment, Blue: Model, “*” marks the initial crack, “*” mark the points for the comparison of the strains.

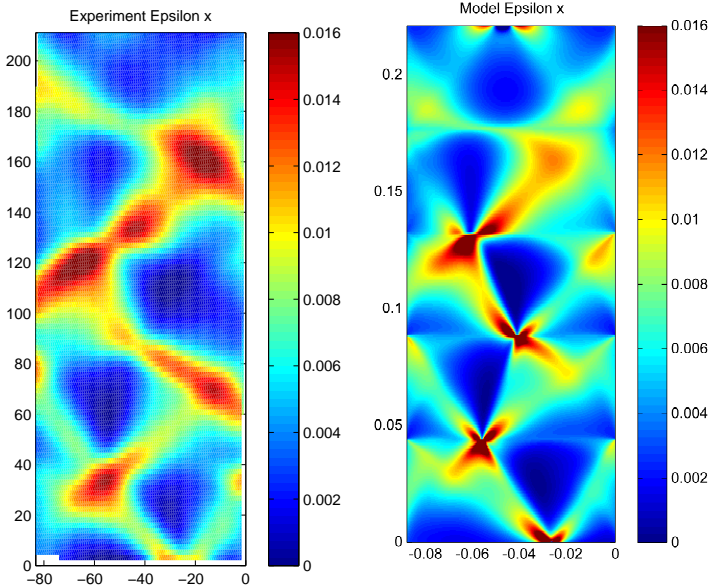


Figure 9.32: Strains in horizontal direction ϵ_x , Sample 16. Left: Experiment, Right: FE- model

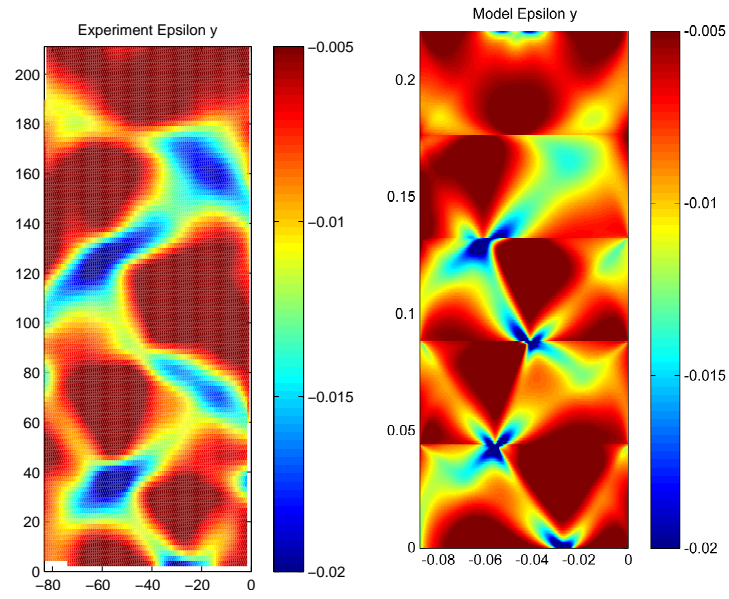


Figure 9.33: Strains in vertical direction ε_y , Sample 16. Left: Experiment, Right: FE- model

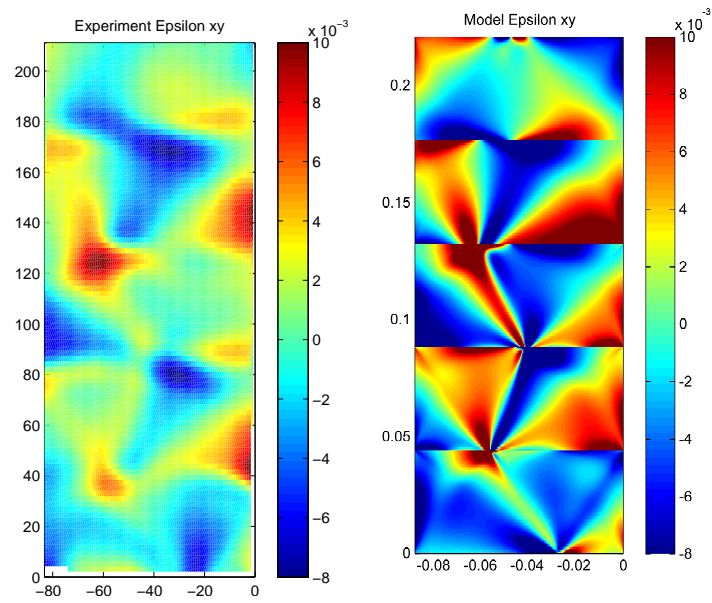


Figure 9.34: Shear strains ε_{xy} , Sample 16. Left: Experiment, Right: FE- model

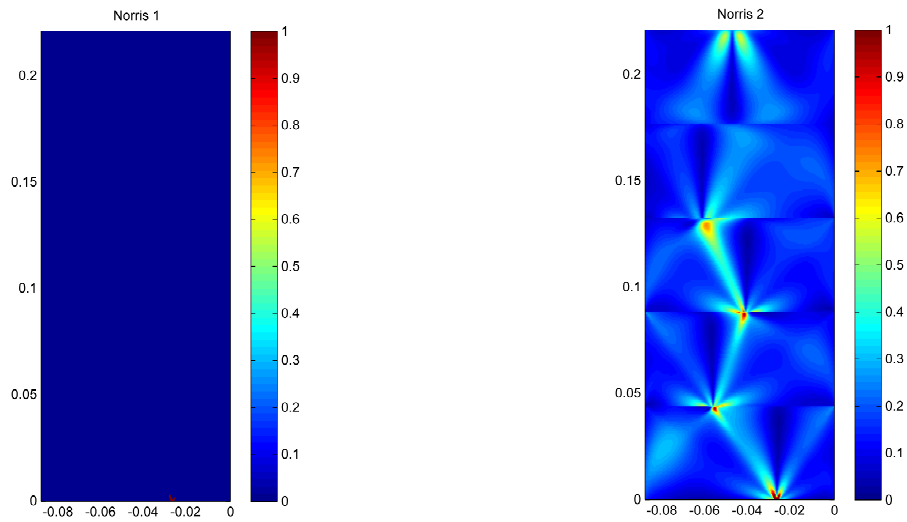


Figure 9.35: Norris failure criteria, Sample 16. Left: Red marks the region where the first crack is predicted by the model, Right: Effective stress based on Norris failure criterion

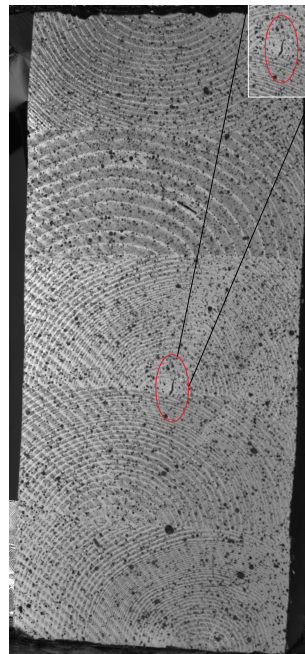


Figure 9.36: Image showing where the first cracks occurred during testing, Sample 16

Appendix B

Laboratory Work

Stress- deformation plot

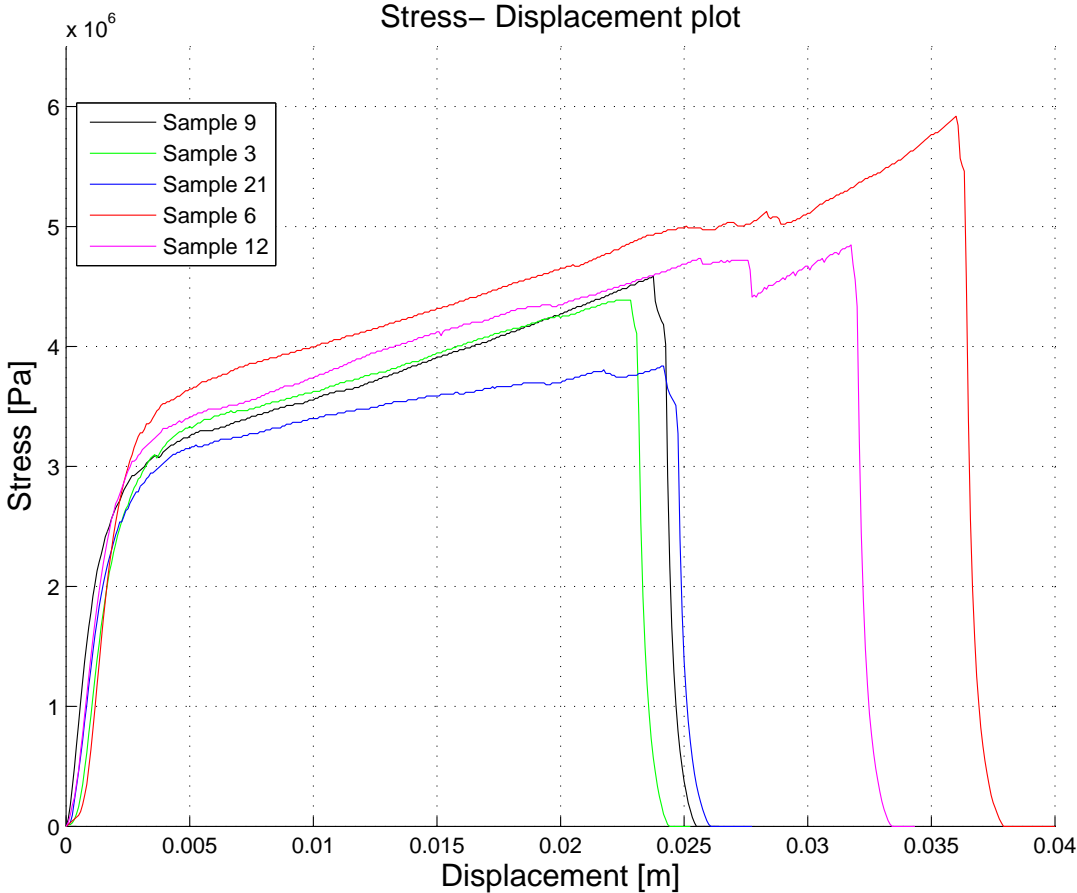


Figure 9.37: Stress- deformation plot, 3 Lamellae

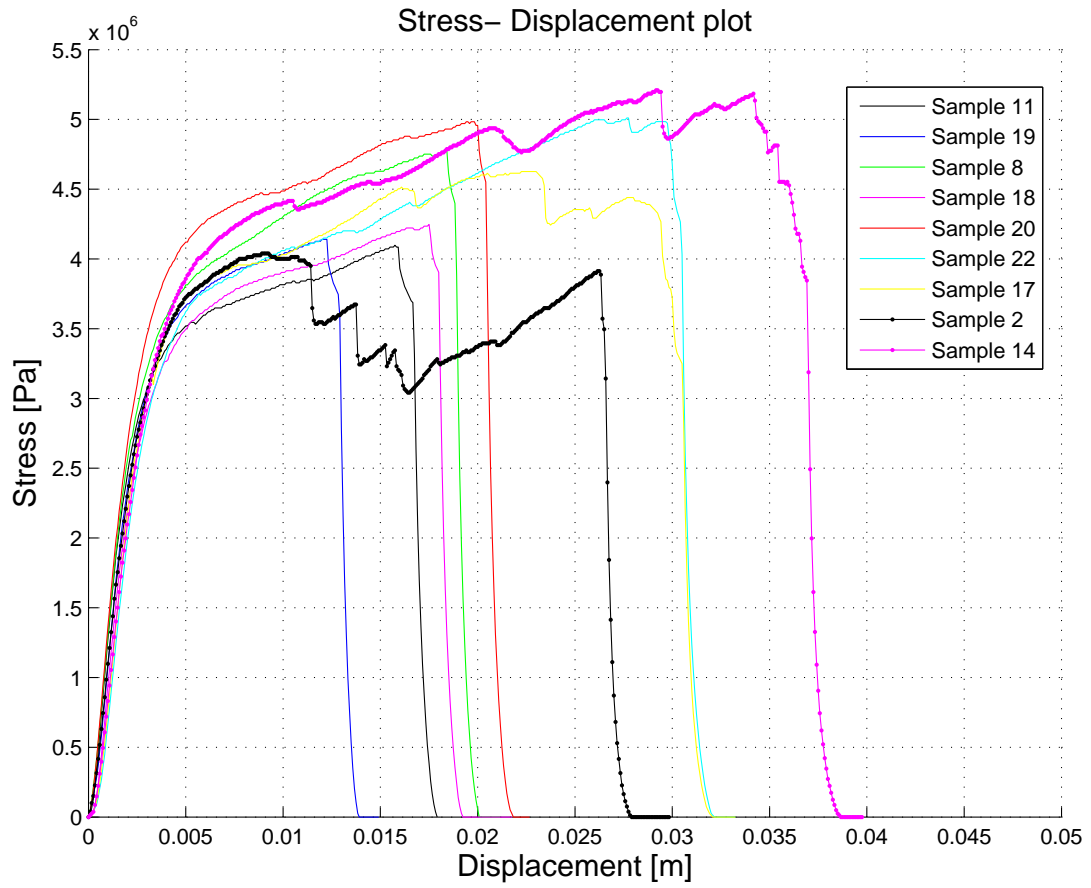


Figure 9.38: Stress- deformation plot, 4 Lamellae

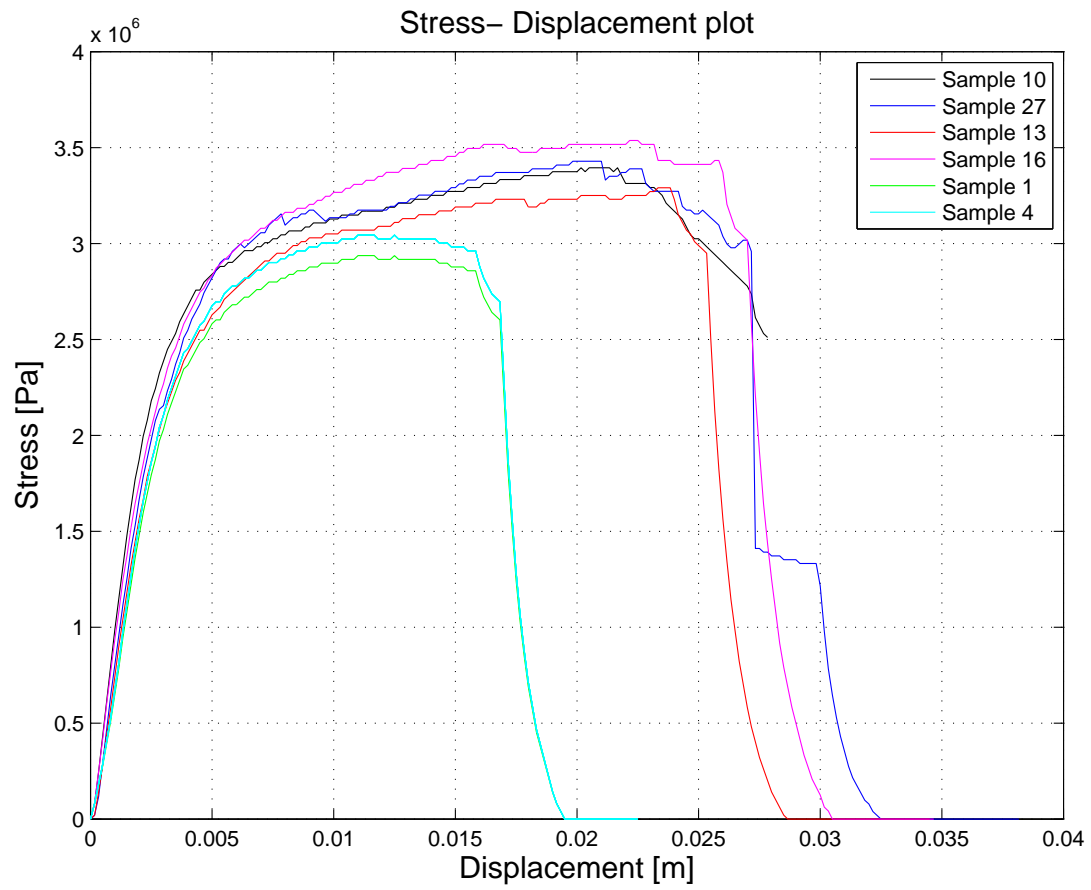


Figure 9.39: Stress- deformation plot, 5 Lamellae

Appendix C

Annual rings

Sample 21

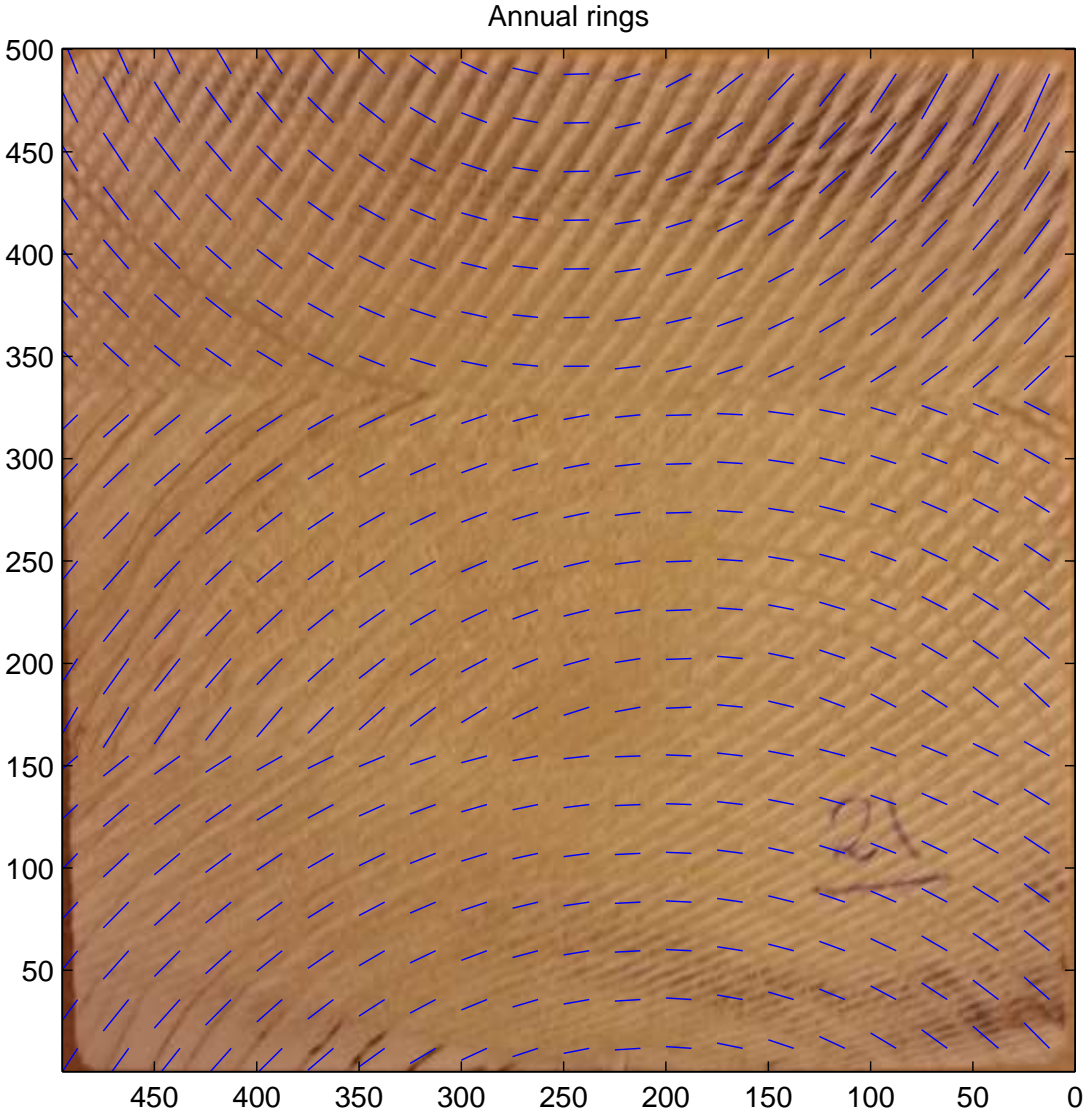


Figure 9.40: Annual rings, Sample 21

Sample 11

Annual rings

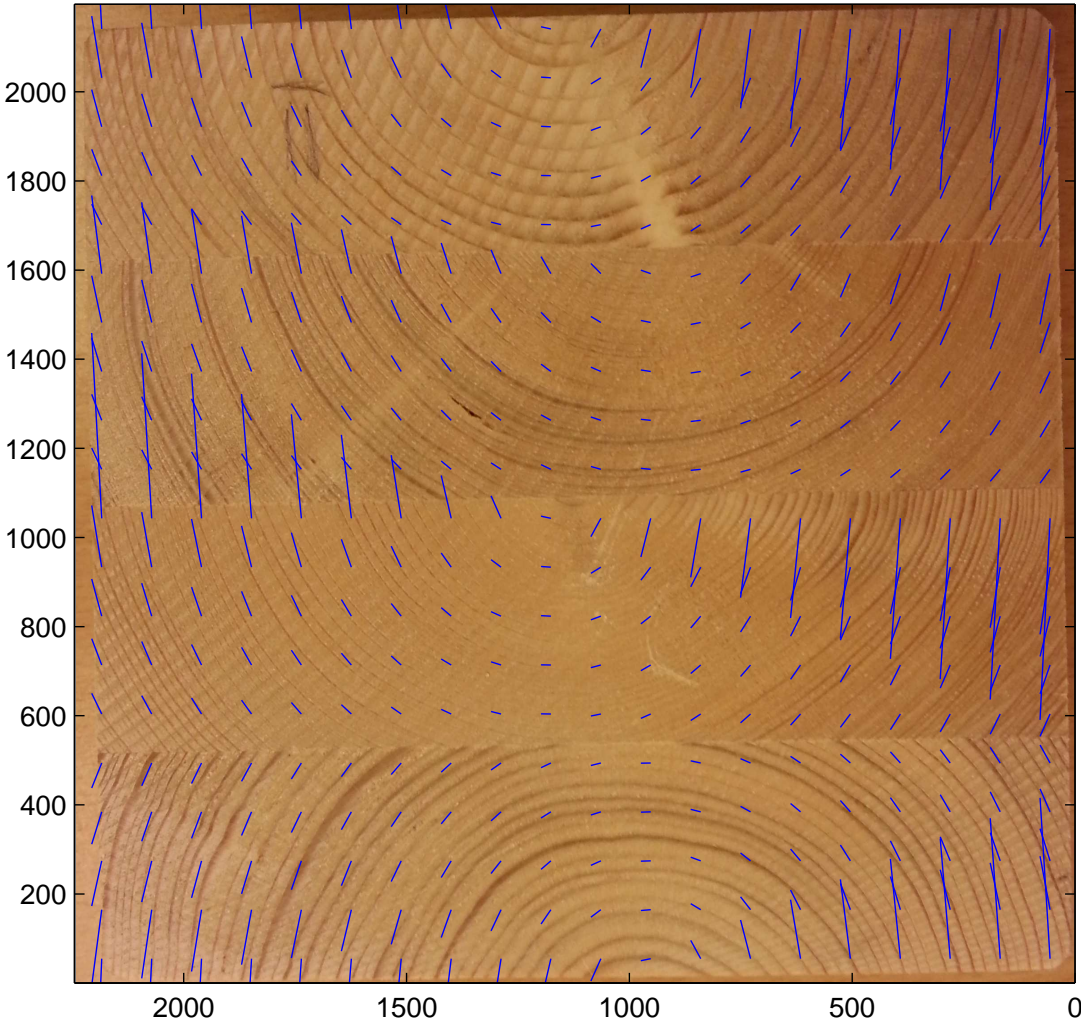


Figure 9.41: Annual rings, Sample 11

Sample 16

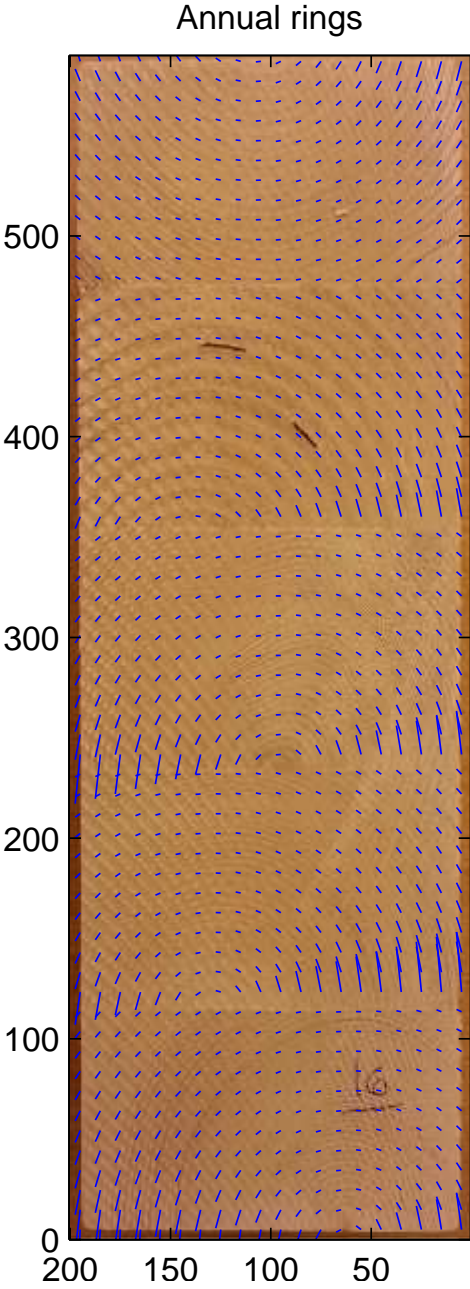


Figure 9.42: Annual rings, Sample 16